CONTROL OF SYSTEMS UNDER THE EFFECT OF FRICTION

A THESIS SUBMITTED TO
THE GRADUATE SCHOOL OF NATURAL AND APPLIED SCIENCES
OF
MIDDLE EAST TECHNICAL UNIVERSITY

BY

BERKAY BAYKARA

IN PARTIAL FULFILLMENT OF THE REQUIREMENTS
FOR
THE DEGREE OF MASTER OF SCIENCE
IN
MECHANICAL ENGINEERING

DECEMBER 2009

Approval of the thesis:

CONTROL OF SYSTEMS UNDER THE EFFECT OF FRICTION

submitted by **BERKAY BAYKARA** in partial fulfillment of the requirements for the degree of **Master of Science in Mechanical Engineering Department, Middle East Technical University** by,

Prof. Dr. Canan ÖZGEN   _____
Dean, Graduate School of **Natural and Applied Sciences**

Prof. Dr. Suha ORAL   _____
Head of Department, **Mechanical Engineering**

Prof. Dr. M. Kemal ÖZGÖREN   _____
Supervisor, **Mechanical Engineering Dept., METU**

Dr. Erdinç N. YILDIZ   _____
Co-Supervisor, **Mechatronics Division, TÜBİTAK-SAGE**

Examining Committee Members:

Prof. Dr. Eres SÖYLEMEZ   _____
Mechanical Engineering Dept., METU

Prof. Dr. M. Kemal ÖZGÖREN   _____
Mechanical Engineering Dept., METU

Prof. Dr. Metin AKKÖK   _____
Mechanical Engineering Dept., METU

Prof. Dr. S. Kemal İDER   _____
Mechanical Engineering Dept., METU

Dr. Bülent ÖZKAN   _____
Mechatronics Division, TÜBİTAK-SAGE

                                        Date: _____

I hereby declare that all information in this document has been obtained and presented in accordance with academic rules and ethical conduct. I also declare that, as required by these rules and conduct, I have fully cited and referenced all material and results that are not original to this work.

Name, Last name : Berkay BAYKARA

Signature   :

ABSTRACT

CONTROL OF SYSTEMS UNDER THE EFFECT OF FRICTION

Baykara, Berkay

M.S., Department of Mechanical Engineering

Supervisor   : Prof. Dr. M. Kemal ÖZGÖREN

Co-Supervisor : Dr. Erdinç N. YILDIZ

December 2009, 175 pages

Precision control under the effect of friction requires an effective compensation of friction. Since friction has a complex and highly nonlinear behaviour, it is generally insufficient to represent the friction in a dynamic control system only with a linear viscous model, which is mostly valid in high-velocity motions. Especially when the control system moves near zero velocity regions or changes the direction of motion, an accurate modelling of friction including the low-velocity dynamic behaviour is a prerequisite to obtain a more complete and realistic dynamic model of the system. Furthermore, the parameters of the friction model should be identified as accurate as possible in order to attain a satisfactory performance. Therefore, the parameters of the friction should be estimated regarding the working conditions. The estimated friction force can then be used to improve the controlled performance of the dynamic system under consideration.

In this thesis, the modelling, identification and compensation of friction in a rotary mechanical system are studied. The effectiveness of the existing friction models in the literature are investigated; namely the classical Coulomb with viscous friction model, the Stribeck friction model, the LuGre friction model, and the Generalized Maxwell-Slip (GMS) friction model. All friction models are applied to

the system together with the same linear, proportional with derivative (PD)-type and proportional with integral and derivative (PID)-type feedback control actions for the sake of being faithful in comparison. The accuracy of the friction compensation methods is examined separately for both the low-velocity and high-velocity motions of the system. The precision of friction estimation is also shown in the case of using both the desired velocity and measured velocity as an input to the friction models.

These control studies are verified in simulation environment and the corresponding results are given. Furthermore, an experimental set-up is designed and manufactured as a case study. The parameters of the aforementioned friction models are identified and the control laws with different friction models are applied to the system in order to demonstrate the compensation capabilities of the models. The results of the experiments are evaluated by comparing them among each other and with the simulation results.

ÖZ

SÜRTÜNME ETKİSİ ALTINDAKİ SİSTEMLERİN DENETİMİ

Baykara, Berkay

Yüksek Lisans, Makina Mühendisliği Bölümü

Tez Yöneticisi   :   Prof. Dr. M. Kemal ÖZGÖREN

Ortak Tez Yöneticisi :   Dr. Erdinç N. YILDIZ

Aralık 2009, 175 sayfa

Sürtünme etkisi altında hassas denetim, sürtünmenin etkin bir biçimde telafisini gerektirir. Sürtünmenin karışık ve son derece doğrusal olmayan bir davranışa sahip olmasından dolayı, dinamik bir sistemdeki sürtünmeyi sadece, çoğunlukla yüksek hızlı hareketlerde geçerli olan doğrusal bir viskoz sürtünme modeli ile temsil etmek genellikle yetersiz kalır. Denetim sistemi, özellikle hızın sıfır olduğu bölgelere yakın hareket ediyor veya hareket yönünü değiştiriyorsa, düşük hızlardaki dinamik davranışı kapsayan doğru bir sürtünme modelinin kullanımı, sistemin daha eksiksiz ve gerçekçi bir dinamik modelini elde etmek için bir önkoşuldur. Dahası, sistemden tatmin edici bir başarım elde etmek için, sürtünme modeli parametreleri mümkün olduğu kadar doğru bir biçimde belirlenmelidir. Bu yüzden belirtilen parametreler, çalışma koşulları dikkate alınarak kestirilmelidir. Bahsedilen kestirim sonucunda elde edilen sürtünme kuvveti, göz önüne alınan dinamik sistemin denetim başarımını iyileştirmekte kullanılabilir.

Bu tezde, dönel bir mekanik sistemdeki sürtünmenin modellemesi, tanımlaması ve giderilmesi hususu ele alınmıştır. Literatürde var olan sürtünme modellerinin, özellikle klasik Coulomb ve viskoz sürtünme modeli, Stribeck sürtünme modeli, LuGre sürtünme modeli ve genelleştirilmiş Maxwell-Kayma

sürtünme modelinin etkinliği araştırılmıştır. Karşılaştırmanın tutarlılığını sağlamak adına, göz önüne alınan bütün sürtünme modelleri; özdeş, doğrusal, oransal ve türevsel (PD) tip ve oransal, tümlevsel ve türevsel (PID) tip geribesleme denetim işlemleri ile birlikte sisteme uygulanmıştır. Sürtünme giderilmesi için önerilen yöntemlerin doğruluğu, sistemin hem düşük hem de yüksek hızlı hareketlerini içeren durumlarda ayrı ayrı incelenmiştir. Sürtünme kestiriminin hassasiyeti, istenen ve ölçülen hız değerlerinin sürtünme modellerinde girdi olarak kullanıldığı durumlarda da gösterilmiştir.

Bu çalışmada, ele alınan denetim sistemi çalışmaları benzetim ortamında gerçeklenmeye çalışılmış ve ulaşılan sonuçlar verilmiştir. Ayrıca, örnek bir çalışma olarak bir deney düzeneği tasarlanmış ve imal edilmiştir. Bahsi geçen sürtünme modellerinin parametreleri kestirilmiş ve modellerin sürtünme giderme yeteneklerini göstermek için, değişik sürtünme modellerini içeren denetim kuralları sisteme uygulanmıştır. Deneyler sonunda elde edilen sonuçlar, birbirleri ve benzetim sonuçları ile karşılaştırılarak değerlendirilmiştir.

Anahtar Kelimeler: Sürtünme, sürtünme modelleri, sürtünme telafisi, sürtünme altında denetim, sabit parametreli sürtünme telafisi.

To My Parents

ACKNOWLEDGEMENTS

TABLE OF CONTENTS

LIST OF TABLES

LIST OF FIGURES

LIST OF ABBREVIATIONS

3D   :   Three-dimensional

DC   :   Direct current

DOF   :   Degree of freedom

FRF   :   Frequency response function

GMS   :   Generalized Maxwell-Slip

I/O   :   Input/Output

LIP   :   Linear in parameter

PC   :   Personal computer

PD   :   Proportional with derivative control action

PI   :   Proportional with integral control action

PID   :   Proportional with integral and derivative control action

PMDC   :   Permanent magnet direct current

PPR   :   Pulse per revolution

PR   :   Proportional with rate feedback control action

PWM   :   Pulse width modulation

VDC   :   Volts of direct current

LIST OF SYMBOLS

Basic Latin letters:

C :   Attraction parameter of the GMS friction model

C_C :   Attraction parameter of the GMS friction model used in friction compensation simulations

$D(s)$:   Ideal characteristic equation of the closed loop control system

$D_{CLS}(s)$:   Normalized characteristic equation of the closed loop control system

DV :   Velocity threshold for Karnopp friction model

F_C :   Coulomb friction force / torque

F_E :   Applied external force

F_f :   Friction force

F_{fss} :   Steady-state friction force

$F_h(z)$:   i. Hysteresis function of the Leuven friction model

                       ii. Output of the Maxwell-Slip model

F_i :   Individual force of an element in the Maxwell-Slip model and the GMS friction model ($i = 1,\ldots,N$)

F_N :   Normal force

F_S :   Static friction or break-away force / torque

F_v :   Linear viscous friction coefficient

F_{v2} :   Nonlinear viscous friction coefficient

$G_{CLS\_PD}(s)$:   Closed loop transfer function of the system without friction and with PD control action

$G_{CLS\_PID}(s)$:   Closed loop transfer function of the system without friction and with PID control action

$G_{CLS\_PR}(s)$	:	Closed loop transfer function of the system without friction and with PR control action
$G_P(s)$	:	Transfer function of the open loop system without friction
J	:	Total moment of inertia of the system
k	:	Stiff slope for the implementation of the Stribeck friction model
k_d	:	Derivative gain of linear PD/PID/PR controllers
k_i	:	i. Integral gain of linear PD/PID controllers ii. Linear spring constant of an element in the Maxwell-Slip model and the GMS friction model ($i = 1,\ldots,4$)
k_{ic}	:	Linear spring constant of an element in the GMS friction model used in friction compensation simulations ($i = 1,2,3$)
k_p	:	Proportional gain of linear PD/PID/PR controllers
N	:	Maximum number of elements in the Maxwell-Slip model and the GMS friction model
s	:	Laplace operator
$s(v)$	:	Curve of the Stribeck effect
$sign(.)$	:	Signum function
$s_m(v)$	:	Modified curve of the sliding region of friction in the grease-added friction case
t	:	Time variable
T_f	:	Actual friction torque in computer simulations
$\hat{T}_f$	:	Estimated friction torque in computer simulations
T_{linear}	:	Linear part of the controller
T_{linear_pd}	:	Time domain representation of PD control action
T_{linear_pid}	:	Time domain representation of PID control action
T_{linear_pr}	:	Time domain representation of PR control action
T_m	:	Motor torque in computer simulations
v	:	Velocity variable

v_i	:	Stribeck velocities for the modified curve of the sliding region of friction in the grease-added friction case ($i = 1,2$)
v_s	:	Stribeck velocity
W_i	:	Maximum force of an element in the Maxwell-Slip model ($i = 1,\ldots,N$)
x	:	Displacement variable
z	:	i. Internal state variable in the LuGre friction model
		ii. Common position input variable in the Maxwell-Slip model

Greek letters:

α_i	:	Constant fractional parameter of an element in the GMS friction model ($i = 1,\ldots,4$)
α_{ic}	:	Constant fractional parameter of an element in the GMS friction model used in friction compensation simulations ($i = 1,2,3$)
β_i	:	Parameters for the modified curve of the sliding region of friction in the grease-added friction case ($i = 1,\ldots,5$)
δ	:	Shape factor of the nonlinear viscous friction
δ_d	:	Shape factor of the hysteresis curve of the Dahl friction model
δ_l	:	Shape factor of the Leuven friction model
δ_s	:	Shape factor of the Stribeck friction model
ε	:	Sliding velocity threshold of the continuous Stribeck friction model
ξ_i	:	Individual position output of an element in the Maxwell-Slip model ($i = 1,\ldots,N$)
μ_C	:	Coefficient of the Coulomb friction
ω_n	:	Bandwidth value of a closed loop control system
σ_0	:	i. Initial stiffness of the contact in the Dahl friction model

          ii. Stiffness of the bristles in the LuGre friction model

σ_1	:	Micro-viscous damping coefficient in the LuGre and Leuven friction models
σ_2	:	Linear viscous friction coefficient
θ	:	Angular position of the shaft (assuming rigid)
$\dot{\theta}$	:	Angular velocity of the shaft (assuming rigid)
$\ddot{\theta}$	:	Angular acceleration of the shaft (assuming rigid)
θ_d	:	Desired, or reference, angular position signal of the closed loop control system
$\dot{\theta}_d$	:	Desired, or reference, angular velocity signal of the closed loop control system
ζ	:	Damping value of a closed loop control system

CHAPTER 1

INTRODUCTION

1.1 General background

Friction is a natural phenomenon resulting from the complex interaction between the surface and near-surface regions of two interacting bodies or materials [1]. From the theoretical point of view, friction can be described as a tangential reaction/resisting force between the contacting bodies having relative motions or tendency to such motions. Since it can be due to the solid-solid contact or solid- fluid contact in the case of using fluid lubricants, it exists in all mechanical, hydraulic, and pneumatic systems that encounter relative motions. The fact that friction depends on various factors in micro and macro levels such as surface texture/roughness, environmental conditions (dirt, temperature etc.), and normal load etc. makes the friction phenomenon variable/time-dependent and highly nonlinear.

In the literature, when dealing with friction analysis, friction can be considered as composed of mainly two regions which are called pre-sliding, or micro-slip, region and sliding, or gross-sliding, region. To make the definitions of friction regimes more understandable, a microscopic view of the contact surface of the two contacting bodies is given in Figure 1.1. Actually, the bodies touch each other at different contact points which are called asperity junctions. Friction occurs due to the variable roughness of the contacting surfaces by means of these asperity junctions. These asperity junctions deform elasto-plastically in the pre-sliding regime, which results in a nonlinear hysteretic spring-like behaviour in friction force. Because of this deformation, adhesive forces are dominant and the friction force happens to be a predominant function of displacement instead of the relative velocity. In this regime, the system is called 'in stick' because not all asperity

junctions break away and the displacement of the system until the system leaves the presliding regime is very small, that is in the level of micron or milliradian. As the tangential external force on the bodies increases, this displacement also grows up and more junctions will break away eventually putting the system into the sliding regime. In contrast to pre-sliding regime, friction force is a predominantly function of velocity in the sliding regime where all asperity junctions are broken apart.
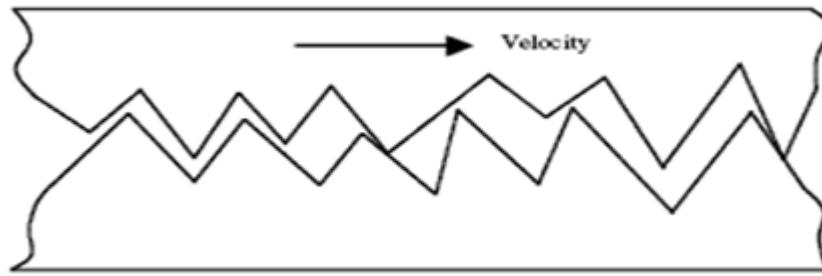
Figure 1.1. A microscopic view of friction phenomenon [2]

In general, friction has both desirable and undesirable effects on the mechanical systems. Since friction has a dissipative characteristic, it puts an additional damping into the system where it exists. This property of friction is generally preferred and used in brake/clutch systems and applications where high vibration exists. In high-precision control systems; however, it can cause control problems such as tracking errors, steady-state errors, limit cycles, and stick-slip motions which strictly deteriorate the performance of the control system under consideration. Moreover, its nonlinear behaviour makes the control law synthesis more difficult and requires nonlinear and complex control strategies to compensate the undesired effects of it satisfactorily. Because of these facts, friction should be understood well and need to be accurately compensated in a convenient manner.

As far as the friction compensation is considered, two methods are generally mentioned in the literature: Model-based friction compensation technique and non-model-based friction compensation technique. In model-based friction compensation technique, an explicit model of friction is used in order to instantaneously estimate the real frictional behaviour in the system and the output of this explicit model is

added to the control input signal, which is used to track the changes in the reference signal of the closed loop control system, in order to make the performance of the system higher. To apply the model-based techniques, accurate modelling and identification of friction characteristics are necessary. In this respect, friction models with different complexity levels ranging from simple static Coulomb model to very complex dynamic models such as the LuGre and the Generalized Maxwell-Slip (GMS) models are encountered in the literature. These complexity levels change model by model depending on the accuracy of the friction model in approximating the real frictional behaviour and easiness of obtaining the parameters of the models by identification. In the literature, the explicit friction models are separated into two groups, which are static friction models and dynamic friction models. Both models are stated as a function of velocity. The static friction models only reflect the steady-state constant velocity behaviour of friction whereas the dynamic friction models give, in addition to the steady-state friction characteristics of the static models, the transient and time-dependent behaviour of friction which was found experimentally. These models will be explained in detail in Chapter 2. It should be noted that the friction model structure is very important for the accuracy of the friction estimation, and the accuracy of the friction model parameters, i.e. the accuracy of the identification process used to find the model parameters, are as important as the friction model structure since the inaccurate model parameters make the friction estimation worse and diminish the system performance even if the friction model structure perfectly matches to the real friction characteristics.

On the contrary of model-based friction compensation techniques, non-model-based techniques do not require certain friction model structures to model the real friction. The friction force in the system is treated as a disturbance on the system. For the compensation tasks, high gain proportional with integral (PI), proportional with derivative (PD) or proportional with integral and derivative (PID) control actions can be used alone both to track the changes in the reference signal of the closed loop control system and to suppress the negative effects of friction on the system. However, the usage of high gains increases the sensitivity of the controller to the measurement noise as well as controller saturation [3] and is limited by the

hardware used. Moreover, the integral gain in PI and PID strategies may cause the system to have slower response, enter a limit cycle or exhibit stick-slip phenomenon whereas in PD action, the system may exhibit higher steady-state errors due to the lack of integral gain [4]. Except these strategies, the compensation in non-model-based friction compensation approach are generally done by applying a disturbance observer which uses the system input-output data to estimate the friction. Then, by adding the output of the disturbance observer to the control input signal, as in model-based friction compensation, the system performance is improved.

When the model-based friction compensation is considered in detail, the friction estimation signal added to the control input signal can be produced by means of using either the desired velocity profile in the case of tracking tasks or measured velocity of the closed loop system as an input to the friction model. However, both of them require a careful treatment in terms of compensation. In the case of using the desired velocity as an input to the friction model, which is called model-based feedforward friction compensation, the model might give inaccurate estimation of friction when the actual velocity cannot follow the desired one satisfactorily; for example, lagging behind the reference velocity, or has jumps especially near zero velocity region or oscillates with high frequency. On the other hand, if the measured velocity will be used as an input to the friction model, which is called model-based feedback friction compensation, the resolution of velocity measurement should be high enough for the application and measurement noise should be low to estimate the friction accurately and to avoid instability issues.

1.2 Review of the literature on friction models and friction compensation approaches

There is a number of friction compensation approaches in the literature including fixed parameter model-based compensation (using standard static and dynamic friction models or neural-network models), friction model-based observer compensation, model-based adaptive compensation, model-based robust adaptive compensation, and non-model-based compensation (using disturbance observer or high gain linear PI, PD, or PID controller) techniques. In general, all of them

improve the performance of a control system with friction where it is used. Here, the model-based compensation approaches in the literature will be mentioned actually since the friction compensation methods will be limited to the model-based ones in this study as will be explained later.

In [5], [6], [7], [8], the model-based feedback friction compensation works are done regarding the linearized form of the Stribeck friction model whose shape factor is equal to 1. In all of them, the low and high-velocity portions of the Stribeck curve are described by two lines and the compensation model is translated into a form which is linear in parameter (LIP). In [5], the PD action are combined with the fixed parameter LIP friction model whereas the adaptive and robust algorithms based on the LIP models are added to the PD law in [6] and [7]. The simulations show an improvement on the performance of the system. In [8], both fixed parameter friction compensation and robust adaptive compensation based on LIP model are applied to the considered system. The improvement of the response with the addition of the fixed parameter friction compensator to the PD action, and the effectiveness of the robust adaptive algorithm different from [7] over the well-tuned PID controller are shown experimentally. In [9], the dynamic effects are also modelled as if it was bounded by a curve which has the LIP form in addition to the LIP model of static Stribeck curve. The boundedness of the dynamic effects is derived from LuGre model. According to these, a robust adaptive algorithm is designed and the improvement of the response over the well-tuned PID controller is shown in the same experimental set-up [8].

In [10], a time delay friction model representing the frictional lag in sliding region is used for modelling friction and to derive an adaptive algorithm using neural network radial basis function based on this model. The PD control action is again used as the linear part of the controller, and the advantage of the algorithm is demonstrated in a convenient simulation environment.

In [11], the friction model includes the different form of the Stribeck friction model, stiction, and position-dependent friction. As a controller, the PD action is used with two adaptive friction estimator, one of which is also a sliding-mode based

robust controller. The perfectness of the tracking is shown by relevant computer simulations.

In [12], a different form of the Stribeck friction model which is continuous in nature is derived in order to be applied in continuous controller synthesis in contrast to the original Stribeck friction model, which is discontinuous near zero velocity.

When [13] is examined, one can see that the dynamic LuGre model, the first model combining the pre-sliding and sliding regions without switching, is introduced here. This paper mentions about the properties of the LuGre model and proposes a condition for the control law structure including a friction observer based on this model which guarantees good tracking performance. In [14], an identification method for the LuGre model is proposed and applied on an experimental set-up. In this paper, the control law structure in [13] is used here with a linear PID control action for friction compensation task. Also, the adaptive algorithm based on the LuGre model observer is derived. Experimentally, it is verified that the performance of the adaptive law is better than the fixed parameter friction compensation, which in turn is better than the PID action without any friction compensation term in a tracking task, particularly the zero-velocity crossing regions. In [15], the static and dynamic friction models in the literature including lastly the LuGre model are described. The friction compensation algorithms with Coulomb and LuGre models added to a linear PI controller are compared in velocity tracking simulations, and the LuGre models overperforms the Coulomb model compensation. By referring [14], some experimental results are also repeated. In [2], using the LuGre model as the actual friction in the simulations, PD action with the adaptive friction compensation terms based on the different LIP forms of the Stribeck model whose shape factor is equal to 1 are mentioned.

In [1], the Leuven model which is a new dynamic model and an improved version of the LuGre model in terms of pre-sliding behaviour is proposed. After the properties of the model are given, the identification and implementation of the model are described on an industrial robot. According to the low-velocity tracking experiment conducted, the PI control action with Leuven model-based feedforward friction compensation leads to much better response characteristics than the PI with

Coulomb model and only PI control action. In [16], Leuven model in [1] is modified to solve some implementation problems and more practical formulation of it is obtained. In [17], more general description of friction models in the literature than the ones in [15] including the Leuven model also is given. An experimental comparison of Stribeck, Dahl, LuGre, and Leuven friction model feedforward compensation approaches together with a weak PD feedback control action is given in [18]. The identification of models is done considering the cogging effect of the motor. The pre-sliding and sliding region experiments show that Leuven model yields higher performance in both cases whereas the Stribeck model gives the lowest one even lower than the no compensation case due to its discontinuity at zero velocity. Moreover, the Dahl model is better than LuGre model in pre-sliding region [18].

In [19], the GMS model is introduced to the literature based on the generic model which is able to simulate all experimentally observed low-velocity behaviour of friction. The properties of the GMS model and the comparison of its properties with the generic, LuGre, and Leuven models are submitted in this work. In [20], again the properties of the GMS model is simulated and it is concluded that the GMS model is the model most closest to the experimental results. In [21], fixed parameter feedforward friction compensation methods based on four dynamic models, Dahl, LuGre, Leuven, and GMS models, are compared at low velocities on a machine tool table system. To see the effects of the models, a weakly-tuned PD action is added to these compensation models. As a result, the GMS model gives better results than its Leuven counterpart, which in turn gives more accurate responses than Dahl and LuGre model, respectively. Also, a suitably-designed disturbance observer not based on a friction model and its combination with the friction models are explained in this paper. In [22], the friction identification and compensation tasks in a DC motor are described. The model-based feedforward fixed parameter friction compensation in combination with a PD control action is applied by using Coulomb, LuGre, and GMS models. The advantages of the GMS model over the LuGre model, the LuGre model over the Coulomb model, and all of the models over without friction compensation case are indicated in both pre-sliding and sliding region experiments. In [23] and

7

[24], the velocity tracking simulations based on a proportional velocity control together with an adaptive feedback friction compensator based on a linearly-parameterized GMS model are also demonstrated. Here, the linearly parameterized GMS model is obtained by defining the Stribeck effect in a new, linearly-parameterized polynomial form. Then, the simulations show the performance increase in velocity tracking. In [4], the results in [22] is repeated, and moreover, the two nonlinear controllers based on Coulomb and Maxwell-Slip models without feedforward friction parts are compared with a model-based compensation. It is observed that not an important improvements are present among them. In [25], a robust adaptive friction compensator based on a linearized GMS model is described and applied in simulations together with a PD controller. According to the comparison of this robust adaptive law with conventional PD and PID controllers for random step and ramp position inputs, the robust adaptive law based on GMS model gives much better tracking results than the PD and PID-type controllers, and prevents the limit cycle tendency of PD and PID controllers in response to ramp input. In [26], the friction compensation task is achieved by using a PD control action and an observer based on a fixed parameter GMS model. The parameter identification of the GMS model is explained here, and is applied on a two degree of freedom (DOF) robot. The results of the identification and the response of the system to the sinusoidal and polynomial trajectories are experimentally demonstrated with and without the friction observer. Finally, in [27], the static and dynamic friction models frequently used in system modelling and including the most recent GMS model are explained briefly as an overview of models.

1.3   Scope of the thesis

In order to design a control system with satisfactory performance under the effect of friction, one requires the knowledge of friction and the implementation techniques of friction compensation. Then, by using this knowledge, an effective control law can be synthesized for the compensation of the undesired effects of friction on a control system, such as steady-state errors, tracking errors, limit cycles, and stick-slip motions. In this respect, the aim of this study can be stated as follows:

The design and comparison of the model-based fixed parameter friction compensators for the precise position tracking task of a control system under the effect of friction.

In this thesis, the friction characteristics between the interacting bodies in surface contact will be studied experimentally. This type of frictional contact actually exists in many mechatronic systems including power screws, worm gears, hydraulic and pneumatic actuators. Such elements are widely used in precise position control applications such as attitude control of rocket launchers.

The position tracking task will be done in computer simulation environment using the MATLAB$^®$ SIMULINK$^®$ and then, conducted on an experimental set-up established for this purpose in order to reach the accuracy of the friction compensators in real conditions. In this respect, the works done in this study are outlined below:

In Chapter 2, the general friction characteristics found by experimental studies conducted for decades are mentioned first in order to get an insight into the friction phenomenon. Then, the friction models derived in the literature in order to represent the real frictional behaviour with different possible aspects are described and their mathematical formulations are given.

The simulation activities for the friction compensation task of this study are done in Chapter 3. Four different friction models are used in the design of model-based friction compensators, and the produced compensators are compared in terms of both the feedforward and feedback compensation approaches. Then, the responses of the system with different friction compensators are examined in order to find which compensator is the best in tracking the reference position signals.

In Chapter 4, the experimental studies performed are mentioned. Firstly, the experimental set-up established is described, and then, the identification of the plant is explained. After the plant identification, the two case studies with different friction characteristics are performed on the experimental set-up. In each case study, the specific frictional behaviour is deduced, the parameters of the four friction compensation models are identified, the position tracking experiments are conducted

on the set-up, and the experimental results of the different friction compensation methods are given comparatively in order to see the performance characteristics of the four friction compensation models. Furthermore, some comments on the experimental findings and on the comparison of the experimental results with the simulation results are given. At the end of the chapter, a repeatability analysis done for some experimental results and a simple flexibility analysis of the system are mentioned.

Finally, discussions and conclusions about the findings in this thesis are given and future works which can be done are mentioned in Chapter 5.

CHAPTER 2

NOTABLE FRICTION MODELS FOUND IN THE LITERATURE

To analyze the dynamic systems with friction and make the controller synthesis more accurately, a number of friction models have been proposed in the literature. According to the behaviour in response to the velocity and position, and also modelling capacity of frictional behaviour, these models have been separated into two groups in the literature as *static friction models* and *dynamic friction models*.

As far as the literature is examined, there are a lot of static models, such as classical friction models which can be formed as a different combination of the static friction, or stiction, Coulomb friction, and viscous friction, Stribeck friction model, Karnopp model, and Armstrong model. Moreover, additional terms can be added to these models or friction characteristics can be adapted to make the simulations in an easier manner. Formerly, these static friction models were used extensively. However, as the friction characteristics become more understandable, the experiments showed that friction in control systems exhibits some phenomena which affect the performance of control systems considerably and cannot be modelled by static friction models. Hence, a number of dynamic friction models were developed in practical sense. Among these models, only the most preferred and updated ones will be mentioned in this thesis, which include Dahl model, LuGre model, Leuven model, and Generalized Maxwell-Slip model. Although both of the static and dynamic kinds are often used for simulation purposes, dynamic models can have a tendency to be preferred since they include more empirical phenomena about friction and thus, simulating friction more accurately. In this respect, the empirical findings

that characterize the friction and cause it to be separated as static and dynamic friction models should be understood well.

2.1 Friction phenomenon by experimental findings

It has been experimentally [17] shown that friction has some characteristics which should be modelled as accurate as possible if good control performance and high precision, especially at low velocities, are desired in a control system. These behaviours include *varying break-away force, pre-sliding displacement, frictional lag or hysteresis, realistic stick-slip behaviour, time dependency, position dependency, direction dependency, and continuity of friction force*.

2.1.1 Varying break-away force

When the system is in 'stick', the friction is called static friction. The force required to overcome the static friction, or stiction, and initiate the motion is called *break-away force*. The dependency of the breakaway force on the rate of change of applied external force is called *varying break-away force*. According to the experimental results [15], the magnitude of the break-away force decreases and saturates to some level when the rate of change of force is increased in both negative and positive directions. This behaviour is shown in Figure 2.1.
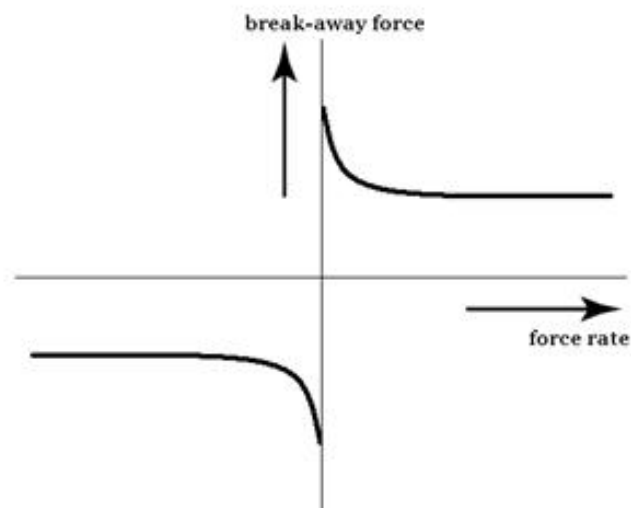
Figure 2.1. Varying break-away force [17]

2.1.2 Pre-sliding displacement

In the pre-sliding regime, since the friction force behaves like a nonlinear spring, the system exhibits small displacements, which are called *pre-sliding displacement* or *Dahl effect* when the applied external force is gradually increased and decreased below the level of break-away force [17]. As previously mentioned, the asperity junctions deform elasto-plastically in this regime. Because of the plastic deformation of junctions, the change of friction force due to the applied external force do not follow the same curve for the cases of increasing and decreasing pre-sliding displacement, thereby resulting in frictional hysteresis [17]. This behaviour is demonstrated in Figure 2.2. This motion is important especially in applications including velocity reversals.
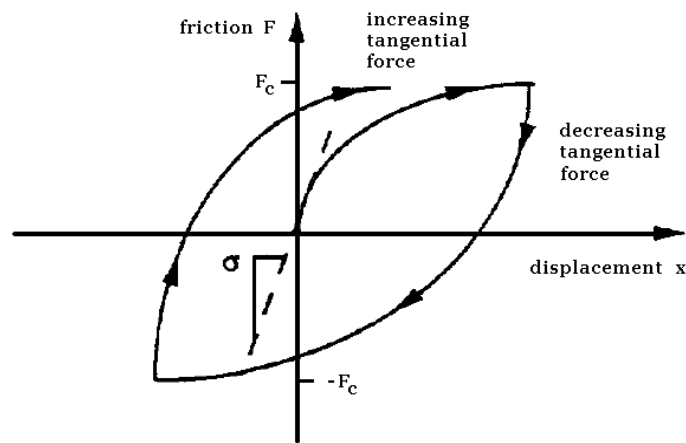
Figure 2.2. Pre-sliding displacement and hysteresis behaviour in pre-sliding region of friction [17]

2.1.3 Frictional lag

Frictional lag, frictional hysteresis or *frictional memory,* is the delay between the change of friction force and the change in velocity. Because of this, friction can not respond instantaneously to a change in unidirectional velocity and a hysteresis loop occurs between the friction force and velocity *at the low-velocity portion of the sliding regime* as shown in Figure 2.3. From Figure 2.3, one can see that the friction

13

force is larger for increasing direction of velocities than decreasing direction of velocities. Moreover, although it is not shown in Figure 2.3, it has been found that the width of this hysteresis loop increases when the frequency of velocity variation or the rate of change of the velocity, i.e. acceleration, increases [15], [17].
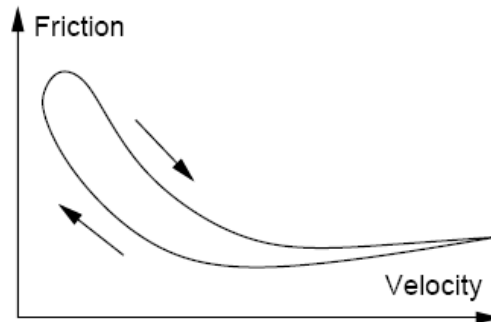
Figure 2.3. Frictional lag [15]

2.1.4 Realistic stick-slip behaviour

Stick-slip behaviour is a phenomenon caused by the fact that the break-away force is higher than the friction during motion. In this respect, when the break-away force is exceeded, the motion accelerates suddenly and when the stiction zone is approached, the motion stops again. The repetition of these motions successively cause velocity fluctuations and control problems that should be compensated, especially when the system works at the low-velocity region. Thus, there is a need for friction models displaying this effect accurately.

2.1.5 Time dependency

Experimental conditions [17] show that friction force changes in time in an unknown manner due to the dirt, temperature changes, wear of surface materials etc.

2.1.6 Position dependency

Again it is experimentally observed [17] that friction force also changes with position due to some inhomogeneities in the material surface or non-uniform distribution of normal load that compresses the material surfaces each other.

2.1.7 Direction dependency (Asymmetric behaviour)

It is experimentally verified [17] that different levels of static, Coulomb, and viscous friction components can be obtained in the positive and negative velocity directions because of the geometrical properties of rubbing materials.

2.1.8 Continuity of friction force

In literature, it is observed that the change in friction force is continuous when the system alters direction of motion and also passes through the pre-sliding regime to sliding regime, or vice versa.

2.2 Static friction models

Static friction models are the models that only describe the constant velocity steady-state friction characteristics of the friction as a function of velocity and sign of velocity. Although static models do not exhibit most of the empirical phenomena about friction, they are still used as a simulation tool because of their simplicity in mathematical modelling. In this section, classical models, Stribeck model, Karnopp model, and Armstrong model will be investigated as the static friction models mentioned in the literature.

2.2.1 Classical models

The classical models which are typically preferred in simulation studies due to their simplicity and ease of application are composed of three elements, each of which models different behaviour of friction. These elements are Coulomb friction, viscous friction, and static friction as described below.

2.2.1.1 Coulomb friction

Coulomb friction is the opposing force when the relative velocity is different from zero. Its magnitude is constant independent of the magnitude of velocity, and only changes with sign of velocity and normal load on the rubbing surfaces. In this respect, the formula for the friction force (F_f) is given as below:

$$F_f = \left| F_C \right| sign(v) \tag{2.1}$$

where, as $\left| F_C \right| = \mu_C F_N$; μ_C and F_N are the coefficient of Coulomb friction, or kinetic friction, and normal load on surfaces, respectively. Also, v stands for the velocity quantity.

In (2.1), signum function [$sign(.)$] is also described for any function $f(x)$ in the following manner:

$$sign(f(x)) = \begin{cases} -1 & if \ f(x) < 0 \\ 0 & if \ f(x) = 0 \\ 1 & if \ f(x) > 0 \end{cases} \tag{2.2}$$

From this formulation, one can see that the Coulomb friction model is only defined for non-zero velocities. At zero velocity, the model is discontinuous and attains infinite number of values for friction force which is actually the problem for all classical models. The velocity dependency of the model can be seen in Figure 2.4a.

2.2.1.2 Viscous friction

Viscous friction is the result of fluid lubrication between the contacting surfaces. In general, it is assumed to change linearly with velocity and its formulation is given below:

$$F_f = F_v \, v \tag{2.3}$$

where F_v is the linear viscous friction coefficient.

In the experiments which are carried out to define the friction characteristics in viscous region, some nonlinear relationships can be fitted to the measurements better, for example, as given in (2.4) below [15]. In practical applications; however, the linear relationship is generally preferred because of its linearity and simplicity.

$$F_f = F_{v2} |v|^\delta sign(v) \tag{2.4}$$

where F_{v2} is the nonlinear viscous friction coefficient and δ is the shape factor depending on the geometry.

The velocity dependency of the viscous friction and the Coulomb with viscous friction are also given in Figure 2.4b and Figure 2.4c, respectively.

2.2.1.3 Static friction

Static friction, or stiction, is the opposing force at rest. It prevents the system from moving by resisting the external applied force below the break-away force limit. The magnitude of the static friction is typically known to be greater than Coulomb friction level. In contrast to the Coulomb and viscous friction components, static friction cannot be described as a function of velocity alone since it represents the friction at zero velocity. Additionally, the external force is used for defining the stiction as shown in (2.5) [15], [17]:

$$F_f = \begin{cases} F_E & if \ v = 0 \ \ and \ \ |F_E| < F_S \\ F_S \ sign(F_E) & if \ v = 0 \ \ and \ \ |F_E| \geq F_S \end{cases} \tag{2.5}$$

In (2.5), F_E and F_S are the applied external force and break-away force, respectively. Again the combination of static friction with Coulomb friction and the combination of static, Coulomb, and viscous terms are illustrated in Figure 2.4d and Figure 2.4e, respectively.

As can be seen from Figure 2.4, one can use the different combinations of frictional behaviour and all these combinations are referred to as *classical models*. These combinations can be constructed depending on which frictional behaviour is dominant in the system. However, the discontinuity of the classical models at zero velocity can limit their applications and cause instabilities in practical applications.
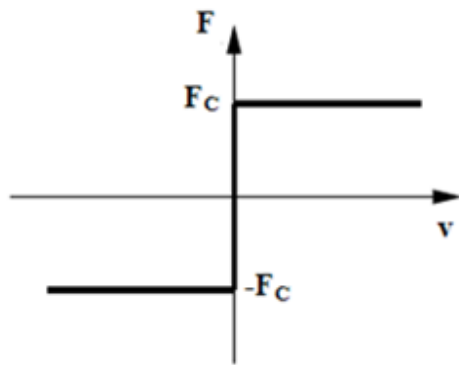
a) Coulomb friction
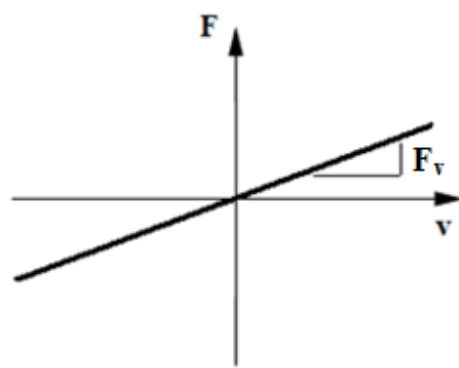
b) Viscous friction
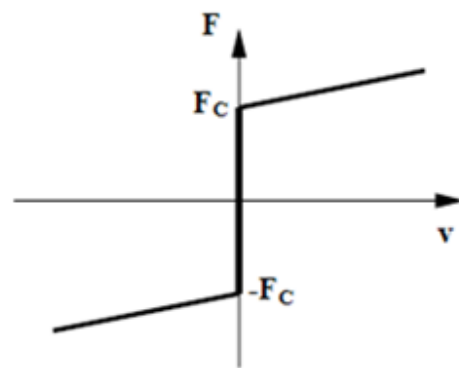
c) Coulomb + viscous friction
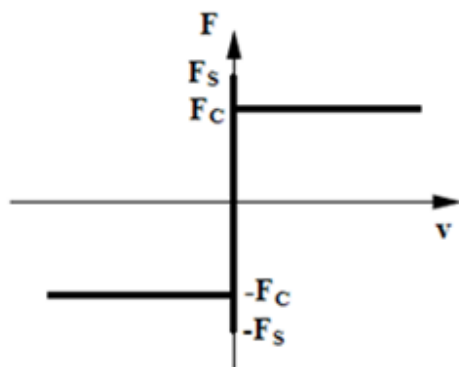
d) Stiction + Coulomb friction
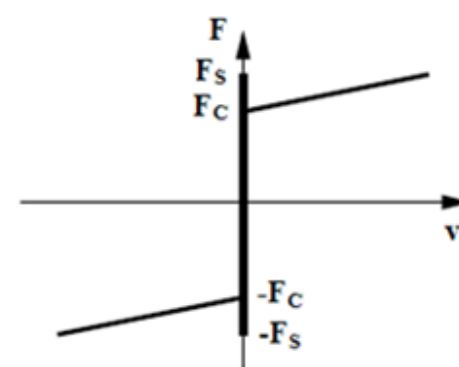
e) Stiction + Coulomb + viscous friction

Figure 2.4. Classical approaches within static friction models [15]

2.2.2 Stribeck model

Stribeck model is the friction model which is based on the experimental observations done by Stribeck that friction force does not change discontinuously from static friction level to the Coulomb friction level as in Figure 2.4e [15]. Instead, it *decreases with increasing velocity at the low-velocity* portion of the sliding regime in a continuous manner [17]. This is known as the *Stribeck effect* in the literature. In Figure 2.5, where F and v stand for the friction force and relative velocity respectively, the *Stribeck effect* is shown as a function of the sliding velocity. A careful inspection of Figure 2.5 shows that the curve representing the *Stribeck effect* is bounded by an upper limit of the static friction force F_S at zero velocity and a lower limit of the Coulomb friction force F_C [17], [19], [21].
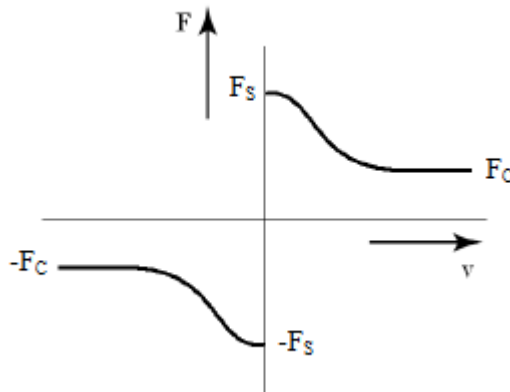
Figure 2.5. Stribeck curve showing Stribeck effect [17]

The *Stribeck effect* is actually resulting from the fluid lubrication between the contacting surfaces, and it should be contained in a friction model in addition to the viscous friction for the accuracy of the stick-slip motion and frictional behaviour. In Figure 2.6, the Stribeck friction model is demonstrated as a combination of the *Stribeck effect* and classical viscous friction. In this respect, the decay in the *Stribeck effect* is generally modelled exponentially and a common form of the Stribeck friction model is given by (2.6) [18].
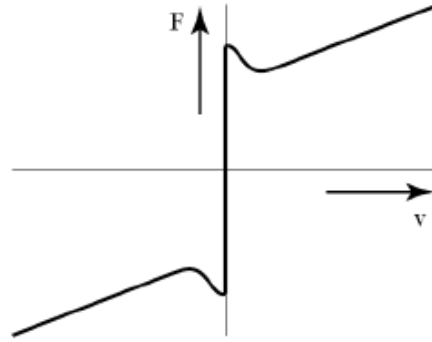
Figure 2.6. Stribeck friction model [17]

$$F_f(v) = sign(v)(F_C + (F_S - F_C)e^{-\left|\frac{v}{v_s}\right|^{\delta_s}}) + F_v v \qquad (2.6)$$

In the above equation, v_s and δ_s are known as the Stribeck velocity and the Stribeck shape factor since it adjusts the shape of decay and gives flexibility to the friction model in order to fit the friction model parameters to the experimental data, respectively. Again, the discontinuity of the Stribeck model at zero velocity does not reflect the reality of friction and causes some control problems. However, to overcome this jump at zero velocity and to provide the continuity of frictional behaviour in simulations, the discontinuity can be replaced by a line of steep slope up to a very small threshold sliding velocity, i.e. $v = \varepsilon$, as in Figure 2.7. In this case, there will be a need for switching function to pass through between regions before and after the threshold value ε.
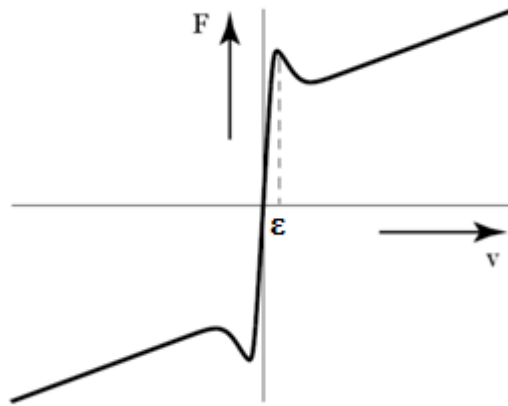
Figure 2.7. Continuous friction curve of Stribeck model [17]

2.2.3 Karnopp model

The basic issue encountered in the simulation of friction phenomenon which is generally modelled as in (2.6) by Stribeck friction is the detection problem of zero velocity. To overcome this detection problem and avoid switching between different state equations of sticking and sliding, Karnopp defines a zero velocity region, i.e. $|v| < DV$ threshold region, in the model he developed [15], [17]. Because of this dead-zone in velocity, even if the internal state of the system, i.e. velocity, is non-zero, the velocity is assumed to be zero by the model within this velocity interval.

Although the Karnopp model solves the detection problem, it has some disadvantages that it is strictly coupled with the rest of the system and external force becomes an input to the model, which unfortunately is not always given explicitly. Moreover, the zero velocity interval does not agree with the real frictional behaviour, thereby limiting its usage despite the fact that some variations of Karnopp model are used extensively since they allow efficient simulations [15], [17].

2.2.4 Armstrong model

Armstrong proposed a new model which is known as his name by adding some experimental observations about friction to the classical models [15], [17]. In this model, the pre-sliding and sliding regimes are modelled by two different

equations requiring a switching to pass through each other. While the pre-sliding displacement is modelled by a stiff spring, the hysteresis behaviour in pre-sliding cannot be obtained with this model. In the sliding regime; however, the static friction is modelled with the Stribeck friction except that a time-delayed version of velocity is used to model the frictional lag. To capture the varying break-away force, time-dependency is given to the force representing stiction level. Although it includes the dynamics of friction, Armstrong model is not much appropriate for simulation purposes due to the difficulties in its implementation. Details and formulation of this model can be reached in the literature [15], [17].

2.3 Dynamic friction models

The major disadvantage of the static friction models is the inaccuracy of the models due to the discontinuous behaviour at zero velocity and also lack of showing empirical behaviours. Thus, to model friction more accurately and overcome some control issues, Armstrong [15] and others modified static models to include the dynamic effects by adding delays and making some parameters time-dependent. However, the approach of introducing an extra internal state variable to the friction model is an efficient way to include dynamics of friction. Therefore, the dynamic models formed in this way will be explained in this study. In this sense, four dynamic friction models including Dahl, LuGre, Leuven, and Generalized Maxwell-Slip models will be investigated respectively.

2.3.1 Dahl model

The Dahl model, which is a comparatively simple dynamic model and the first approach that models the hysteresis behaviour of pre-sliding regime, was used extensively to simulate the bearing friction in control systems and has been utilized in aerospace industry [21]. The model captures neither stiction nor the Stribeck effect; however, it produces a smooth transition near zero velocity. The Dahl model is actually the extension of classical Coulomb friction and it attains the Coulomb friction in steady-state. Since Dahl started the formulation of model from the stress-strain curve, the formulation is stated as the first order generalized differential

equation of friction force F_f with respect to displacement x, and the model is actually valid in the pre-sliding regime only. In this respect, the Dahl model formula for F_f is given in (2.7) as follows [17]:

$$\frac{dF_f}{dx} = \sigma_0 \left| 1 - \frac{F_f}{F_C} sign(v) \right|^{\delta_d} sign(1 - \frac{F_f}{F_C} sign(v)) \tag{2.7}$$

where F_C, σ_0 and δ_d determine the Coulomb friction level, the initial stiffness of the contact near zero velocity and the shape of the hysteresis curve, respectively whereas x represents the displacement variable. In applications, the shape factor, δ_d, is usually considered to be equal to 1. For its larger values, the hysteresis curve has sharper bends. As a matter of fact, the hysteresis behaviour of the Dahl model in (2.7), i.e. the friction output of the model, is figured out as a function of position in Figure 2.8.
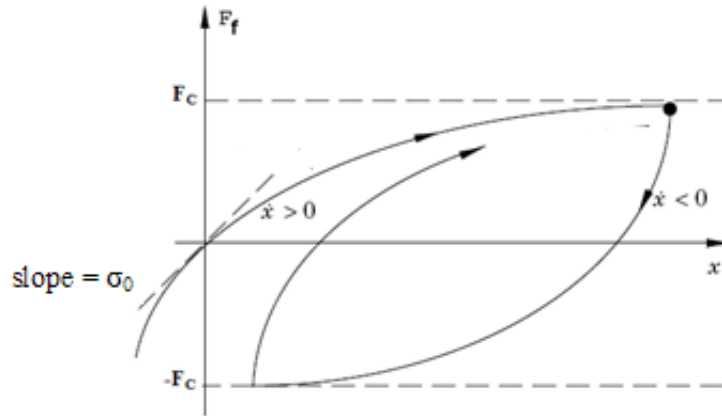
Figure 2.8. Dahl friction model output [15]

2.3.2 LuGre model

The LuGre model [13] is the dynamic friction model developed by the researchers from both the Lund and Grenoble universities [19]. It includes the

dynamic behaviours of friction, i.e. pre-sliding displacement, varying break-away force, and frictional lag. Mainly, this model combines the pre-sliding behaviour of the Dahl model (with a shape factor equal to 1) with an arbitrary steady-state friction characteristic in sliding regime such as the Stribeck friction curve in a single formulation. In this respect, this is the first model in the literature that provides smooth transition between the pre-sliding and sliding regimes without requiring a switching function.
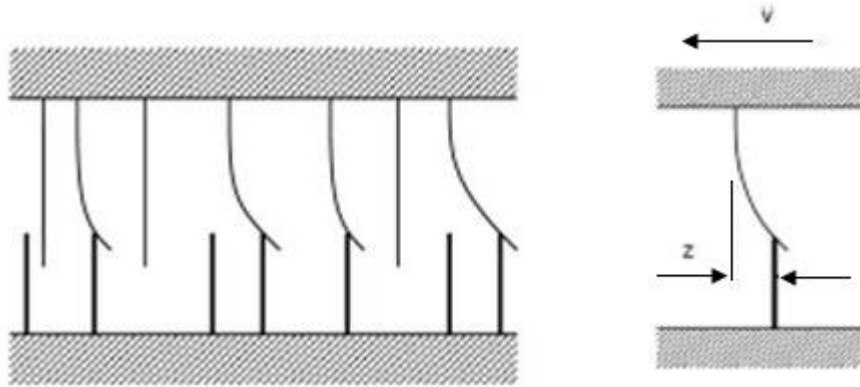
Figure 2.9. Bristle interpretation of friction [17]

From the theoretical point of view, the LuGre model is based on the bristle interpretation of friction as mentioned in [15] and as can be seen in Figure 2.9. Here, the contacting bodies are thought to be rigid and the asperity junctions are considered to be as elastic bristles. From the point of understanding, one can consider the lower bristles as rigid as in Figure 2.9. When the bodies move with respect to each other, bristles are bent and the bending force produced is visualized as friction force. Instead of regarding the random nature of bristle deflections as in the Bristle model in the literature [15], [17], the LuGre model is derived according to the average behaviour of bristles. In this respect, the friction force is defined as a function of the state variable z and the velocity v as in (2.8) and the dynamics of the z variable is given in (2.9) as follows [13], [18]:

24

$$F_f = \sigma_0\, z + \sigma_1 \frac{dz}{dt} + \sigma_2\, v \qquad (2.8)$$

$$\frac{dz}{dt} = v - \sigma_0 \frac{|v|}{s(v)} z \qquad (2.9)$$

where z, σ_0, σ_1, σ_2, and $s(v)$ represent the average bristle deflection (internal state of the system), stiffness of the bristles, micro-viscous damping coefficient, viscous friction coefficient, and the Stribeck effect, respectively. Also, t stands for the time parameter. Here, the $s(v)$ function is given in a common form of the exponential decay in (2.10) [18], [24], [25].

$$s(v) = F_C + (F_S - F_C)e^{-\left|\frac{v}{v_s}\right|^{\delta_s}} \qquad (2.10)$$

As implied by (2.8) through (2.10), when the system is in steady-state at a constant relative velocity, i.e. $\frac{dz}{dt} = 0$ and $v = constant$, the steady-state friction force converges to (2.11), which is simply the Stribeck friction model given in (2.6), which is an arbitrary steady-state friction force of velocity (F_{fss}) in sliding regime.

$$F_{fss} = s(v)\,sign(v) + \sigma_2\, v \qquad (2.11)$$

Although the LuGre model is very useful in the control area because of its simplicity and requiring no switching function between the friction regimes, it suffers from the inaccurate modelling of dynamic behaviours such as hysteresis in pre-sliding regime, transition behaviour between the regimes, and drifting of position

25

in pre-sliding regime. However, these properties are considered in the Leuven model, which will be explained next.

2.3.3 Leuven model

The Leuven model [1] is a modification of the LuGre model in order to fit the experimental findings in the pre-sliding region to the LuGre model such that more precise tracking results near zero velocity can be obtained. The original Leuven model proposed by [1] was so complicated that it was modified and improved by [16] for practical implementations and for solving some discontinuity problems. In this thesis, the modified Leuven model [16] will be investigated.
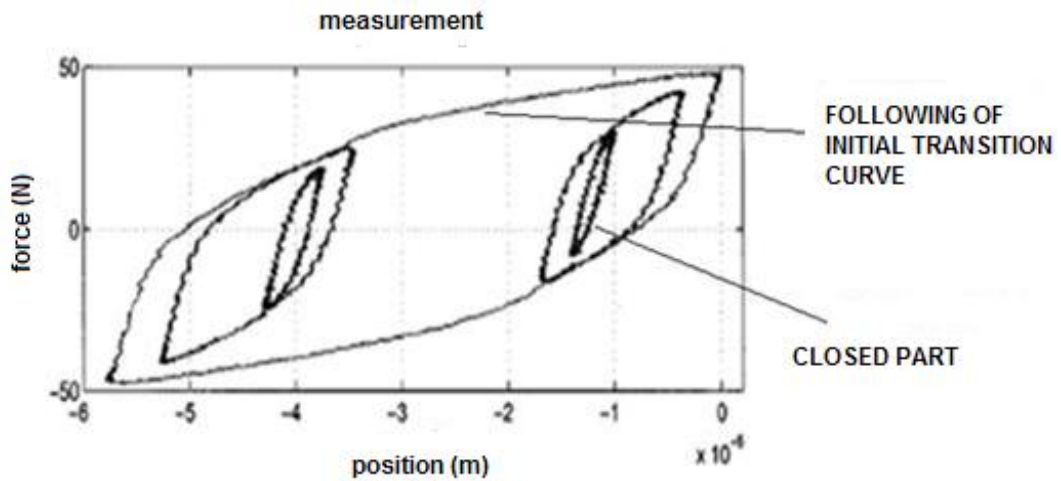
Figure 2.10. An experimental result on a linear slide-way showing the behaviour of hysteresis with non-local memory [1].

Experiments revealed that friction in the pre-sliding region represents *hysteresis with non-local memory*. The experimental data indicating this behaviour are shown in Figure 2.10. These curves are obtained by ramping up and down the external applied force below the break-away limit. Here, the friction curve forms internal closed loops when the external force attains the same value while increasing and decreasing. Furthermore, after the internal loops are closed, friction curve follows the first outer transition curve from the place where it left before it entered

26

the internal loop. These two properties are the main characteristics of the *hysteresis with non-local memory*. To adapt this behaviour into the LuGre model and obtain more accurate results, formulation of the LuGre model was modified in the Leuven model without changing the fact that formulation still requires no switching function in transition between friction regimes. In this respect, the mathematical representation of the Leuven model is given in (2.12) and (2.13) [16], [21]:

$$\frac{dz}{dt} = v(1 - sign(\frac{F_h(z)}{s(v)\,sign(v)}) \left| \frac{F_h(z)}{s(v)} \right|^{\delta_l})$$

(2.12)

$$F_f = F_h(z) + \sigma_1 \frac{dz}{dt} + \sigma_2 v$$

(2.13)

where z, σ_1, σ_2 parameters represent the same meaning as in LuGre model, δ_l is the Leuven shape factor, $s(v)$ again represents the Stribeck effect and given by equation (2.10), and $F_h(z)$ is the term representing the behaviour of hysteresis with non-local memory as a function of internal state variable z. Again, if the steady-state behaviour of friction at constant velocity in sliding regime is desired, i.e. for $\frac{dz}{dt} = 0$ and $v = constant$, one can find that Leuven model gives the same arbitrary steady-state curve of Stribeck friction in sliding region as in the LuGre model in equation (2.11) and also in (2.6).

The $F_h(z)$ function, which is one of the differences between the original and modified Leuven model, is implemented with the Maxwell-Slip model [16] due to its ease of implementation. The Maxwell-Slip model is a distributed element model composing of parallel connection of N different elasto-slide elements as shown in Figure 2.11.
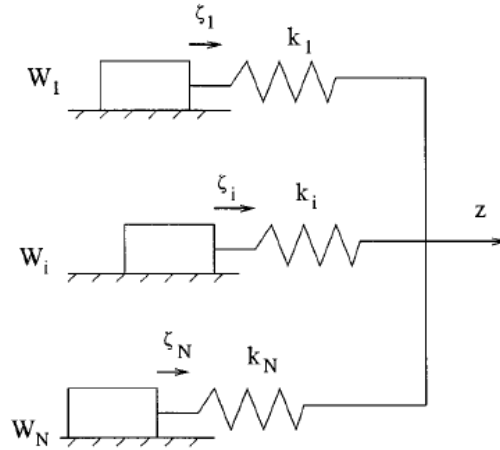
Figure 2.11. Maxwell-Slip model of N elements [16]

In this model, each element, or block, has one common input z and one output force F_i where $i = 1,\ldots,N$. Furthermore, each element is characterized by its own linear spring constant k_i, maximum force W_i, and state variable ξ_i which represents the position of the element. Since the elements are assumed to be massless, a static relationship is obtained between the friction force F_i and relative displacement $(z - \xi_i)$. This relationship for each element is given in (2.14) for $i = 1,\ldots,N$ [16], [21]:

$$
F_i = \begin{cases}
\begin{cases}
F_i = k_i\,(z - \xi_i) \\
\xi_i = constant
\end{cases} & \text{if } |z - \xi_i| < \dfrac{W_i}{k_i} \\[4ex]
\begin{cases}
F_i = sign(z - \xi_i)W_i \\
\xi_i = z - sign(z - \xi_i)\dfrac{W_i}{k_i}
\end{cases} & \text{if } |z - \xi_i| \geq \dfrac{W_i}{k_i}
\end{cases}
\tag{2.14}
$$

Then, the total hysteresis force of the Maxwell-Slip model is equal to the sum of these individual forces as given in (2.15) [16], [21].

$$F_h = \sum_{i=1}^{N} F_i \qquad (2.15)$$
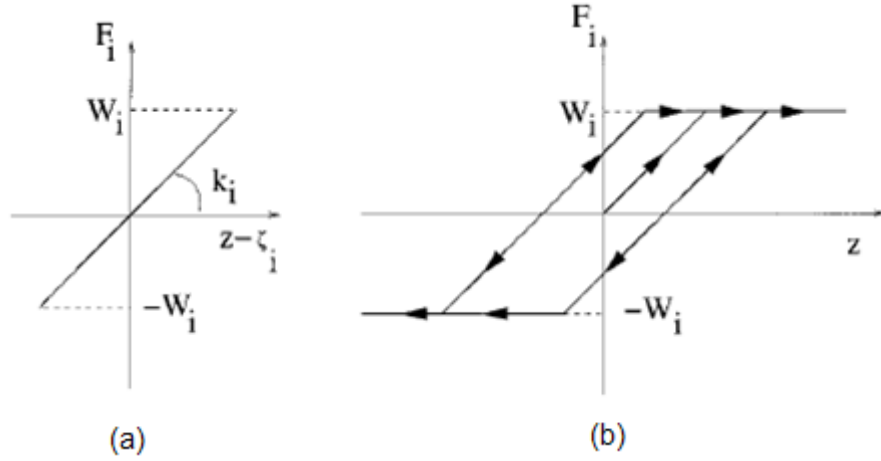
Figure 2.12. The hysteretic behaviour of an element of Maxwell-Slip model [16]

As a better understanding, the output of a block is given graphically in Figure 2.12. Note that the saturated behaviour of the friction force of an element by its own maximum force W_i (Coulomb law), and the linear hysteretic behaviour of an element are demonstrated in Figure 2.12b. Since the spring constant and the maximum force of each element in the Maxwell-slip model are different from each other, i.e. at least two of them are different, a nonlinear hysteresis curve is obtained by using the N of these blocks as in Figure 2.10.

As a result, the total output of these blocks defined in (2.15) is used in the Leuven model to represent the hysteresis with nonlocal memory. Although the Leuven model represents the friction phenomenon more accurately than the LuGre model, identification of its model parameters, especially for the hysteresis curve, is not straigthforward since this hysteresis curve depends on the internal state z which is actually unmeasurable and unknown. In practical, instead of using z, the displacement variable x can be used to find the hysteresis curve; however, this gives

a deformed hysteresis curve $F_h(z)$ because of the nonlinear transformation between x and z in (2.12). In this respect, the Generalized Maxwell-Slip model makes the parameter identification of the hysteresis curve easier although it needs switching functions for the transitions between the friction regions.

2.3.4 Generalized Maxwell-Slip (GMS) model

The Generalized Maxwell-Slip model is an asperity-based description of friction phenomenon and developed from the physically motivated friction model in the literature [19], [20]. Actually, it is a different formulation of the Maxwell-Slip model with a rate-state approach applied [4], [20]. While the GMS model keeps the original structure of the Maxwell-Slip model, i.e. parallel connection of N elementary blocks, it differs from the Maxwell-Slip model in that the Coulomb law of each block is replaced by the steady-state curve of the Stribeck effect to account for sliding dynamics. Then, the total friction force of the GMS model is given as the summation of the output forces of N different, single-state friction blocks, each of which represents the generalized asperity contact at the contacting surface, in addition to the viscous friction term lumped into a parameter for the whole asperities. This formulation is stated in (2.16) as follows [19], [21], [26]:

$$F_f = \sum_{i=1}^{N} F_i + \sigma_2 v \tag{2.16}$$

where F_f, F_i, σ_2, $i = 1,...,N$ represent the total friction force, individual friction force of each elementary block, viscous friction coefficient same as in the LuGre and Leuven models, and the number of elementary blocks used in the GMS model, respectively. Here, each block can either be in sticking mode or slipping mode. Thus, the dynamic behaviour of each block is determined by two differential equations. Then, the differential equations of the individual friction force F_i of each block are given in a following manner according to the mode a block attains [19], [24], [25]:

- If a block is sticking, then the state equation of it is given as:

$$\frac{dF_i}{dt} = k_i\, v \qquad (2.17)$$

and the elementary block remains sticking until $\left| F_i \right| > \alpha_i\, s(v) = W_i$.

- If a block is slipping, then the state equation of it is given as:

$$\frac{dF_i}{dt} = C\left(\alpha_i\, sign(v) - \frac{F_i}{s(v)}\right) \qquad (2.18)$$

and the block remains slipping until its velocity goes through zero.

In these formulations, k_i stands for the elementary linear spring constant, α_i is the constant fractional parameter which determines the maximum force of each elementary block in sticking region, C is the attraction parameter that determines the convergence rate of the total friction force to the Stribeck curve in sliding regime, $s(v)$ is the Stribeck effect same as in the LuGre and Leuven models and given by equation (2.10), and W_i can be said to represent the individual Stribeck effect of each element.

According to the equation in (2.18), if the individual element is slipping, the steady-state value of the friction force of each block at constant velocity, i.e. for $\frac{dF_i}{dt} = 0$ and $v = constant$, is equal to the $\alpha_i\, s(v)\, sign(v)$. Then, if the condition in (2.19) is satisfied and all blocks are slipping at steady-state constant velocity, the total friction force will become equal to the steady-state curve of the Stribeck friction in sliding regime [19], [26]. This curve is the same as the one in the LuGre and Leuven models and given by the equations (2.6) and (2.11).

$$\sum_{i=1}^{N} \alpha_i = 1 \qquad\qquad (2.19)$$

From the practical point of view, the GMS model exhibits the experimental findings on friction phenomenon and it is derived regarding explicitly the following three conditions:

1) The arbitrary steady-state friction curve of Stribeck friction for constant velocities in sliding region.
2) Hysteresis with non-local memory in pre-sliding region.
3) Frictional lag in sliding region.

All of these properties are available in the LuGre (except for the 2nd property), Leuven, and GMS models. However, the GMS model represents the frictional behaviour more accurately than the others since the 3rd property is used directly in the derivation of the GMS model whereas it is obtained implicitly in the LuGre and Leuven models. Moreover, since the dynamics of each block in the GMS model is expressed in terms of the velocity in sticking region, the hysteresis curve in the pre-sliding region can be obtained and identified as a function of measurable position more correctly than the Leuven model. The only disadvantage of the GMS model is that it needs two different switching functions to pass through the friction regimes. However, it is superior in modelling the pre-sliding friction while not losing the accuracy in the sliding regime and it is easy to identify the parameters. For these reasons, the GMS model is suitable for simulations and practical applications.

CHAPTER 3

MODELLING AND CONTROL UNDER FRICTION

Modelling and control of a system including nonlinear effects in itself, especially friction phenomenon, is a challenging problem. Because of its complex behaviour, the existence of friction also makes the controller design more difficult. Although the existence of the friction provides some desirable damping effects on the control system, it generally affects the system accuracy in a negative way by introducing tracking and steady-state errors. In this manner, the most commonly used linear controllers in the control system design, i.e. proportional with integral and derivative (PID), and proportional with derivative (PD) strategies, remain inadequate in reducing the undesired effects of friction in high precision control. The usage of a PID controller in the system with dominant frictional effects may cause the system to enter a limit cycle, exhibit an oscillatory behaviour, show a stick-slip behaviour and even a slower response although it exhibits a good steady-state behaviour due to the existence of integral action [4]. In contrast to the PID controller, the PD strategy yields higher steady-state errors although the high derivative gain can minimize the stick-slip effect on the system [4]. Thus, to analyze a control system accurately and obtain a high performance, one should understand the frictional behaviour and compensate it.

As mentioned in the first chapter, friction compensation can be done regarding an explicit friction model which is based on the data acquired by the system identification process or implicitly by treating the friction as an observable disturbance not based on any explicit model. However, it is a good way to reduce the effects of friction on a control system based on an explicit model if an accurate model of friction is available. Therefore, both the structure of the friction characteristics in the system can be examined and more structured control laws are

synthesized based on the known structure of the disturbance due to the friction. Then, the strategy is to eliminate the negative effects of friction by adding the estimated friction force output of the explicit friction model, which is assumed to be instantaneously equal and opposite to the real friction force in the system, to the control input. However, this strategy is not enough for accurate friction compensation. As mentioned in the second chapter, the explicit friction models all have the same input as velocity, thereby requiring a velocity knowledge of the system for the friction estimation. This information can be derived from the desired velocity profile during tracking tasks, or can be measured directly. Note that very high resolution velocity sensor, which is rarely used in servo applications, is needed for the direct measurement solution. Thus, the model-based friction compensation can be done in two different way, which are

- Model-based feedforward friction compensation based on the desired, or reference, velocity
- Model-based feedback friction compensation based on the measured velocity of the system

In both of the two strategies, the produced friction force is added to the control input of the system. Each technique has some advantages and disadvantages. For the model-based feedforward technique, if the velocity response of the system does not follow the desired velocity profile sufficiently, then the friction estimation will not be satisfactory to cancel the undesired effects of the real frictional behaviour in the system. On the other hand, for the model-based feedback friction compensation, the velocity measurement should be accurate enough. The measurement lag and noise should be as low as possible to yield a good estimation of friction and to decrease coping with the stability problems.

As far as the model-based friction compensation methods in the literature are considered, the applied friction compensation strategies might be fixed parameter friction compensation [1], [4], [5], [14], [15], [18], [21], [22], [26]; observer-based friction compensation [13], [14], [15], [26]; adaptive friction compensation [6], [10], [14], [15], [23], [24]; and robust adaptive friction compensation [2], [7], [8], [9],

[11], [25]. Both static and dynamic friction models have been used with these techniques as an explicit model of friction. In most of these papers, the linear part of the controllers has been composed of the classical PD action.

In this chapter, four model-based fixed parameter friction compensation techniques will be examined in simulation environment. While doing this, all friction models will be added to the same **linear PD feedback control strategy**, and these overall control algorithms will be compared to the **same bandwidth PD and PID linear control strategies only.** In this respect, both model-based feedforward and feedback friction compensation techniques will be applied. As explicit friction models, two static friction models including the **Coulomb with viscous friction model** and the **Stribeck friction model,** and two dynamic friction models including the **LuGre friction model** and the **Generalized Maxwell-Slip friction model** have been selected for friction compensation. Since the classical Coulomb and viscous friction levels have been seldomly used together in the literature, and the Stribeck friction model has been one of the most accurate representation of the sliding regime so far, these two static models are used in simulations. For the dynamic friction models, since the LuGre model includes both regimes of friction and is a popular, relatively simple model among the other dynamic models, and the GMS model is the most recent model in the friction modelling, these two models are selected with the aim of comparison. Moreover, **the actual frictional behaviour is assumed to be reflected by the GMS friction model** since it is the most recently developed model that reflects the friction characteristics in both regimes in a better way from the other dynamic models [19], [20]. As will be mentioned in detail in successive sessions, three inputs emphasizing the different dominant behaviours of friction regions will be applied to the system and the system will be run in three different cases of actual friction in order to see the system responses in the cases of undercompensation and overcompensation of friction during the simulations.

In the simulations, the dynamic system is considered to be a rotary system since the experimental set-up which will be used to verify the results of the simulations and described in the next chapter is designed as a rotary mechanical system.

In the subsequent sessions, firstly the open loop and closed loop dynamic system models will be derived. After the linear parts of the control laws are derived, the friction model used to reflect the actual friction in the system and the friction compensation models will be explained. Some significant points on the parameter identification of the friction models will be presented. Finally, the simulation results of the closed loop system with friction will be investigated.

3.1 Dynamic system with friction

The objective of this thesis is based on the position control of a system under the severe frictional effects. In this respect, the schematic of the experimental set-up prepared for this task is shown in Figure 3.1. Here, the plant is considered to be a 1-DOF rotary system without any elastic mode. Then, the equation of motion of the system to be controlled, i.e. plant, is given in (3.1) in the following manner:
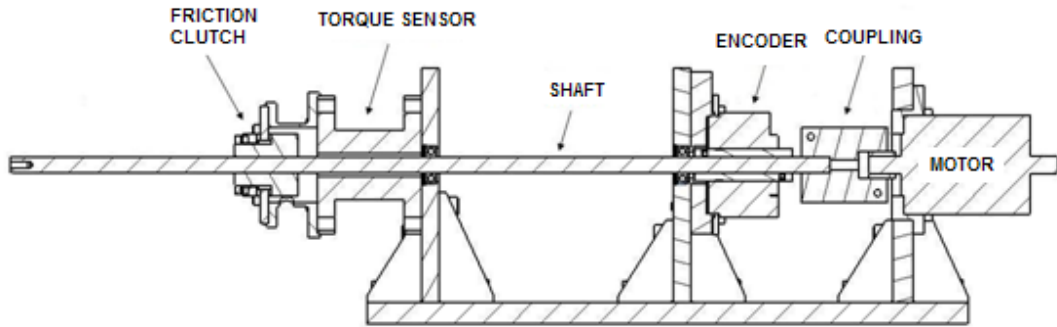
Figure 3.1. The schematic of the experimental set-up

$$J\ddot{\theta}+T_f = T_m \tag{3.1}$$

where J is the total moment of inertia of the system which is reduced to the motor rotor and includes the inertia of the motor rotor, coupling, encoder's rotor, shaft and the friction clutch, T_f is the actual friction torque on the system including viscous terms, T_m is the motor torque applied, θ, $\dot{\theta}$, and $\ddot{\theta}$ are the angular position, velocity

and acceleration of the shaft (assuming rigid), respectively. According to (3.1), the open loop transfer function of the plant without friction, where θ is the output of the plant and T_m is the input to the plant, is given in (3.2).

$$G_P(s) = \frac{\theta(s)}{T_m(s)} = \frac{1}{J s^2} \qquad (3.2)$$

where s is the Laplace operator.

According to (3.1) and (3.2), the block diagram of the open loop system with friction is shown in Figure 3.2.
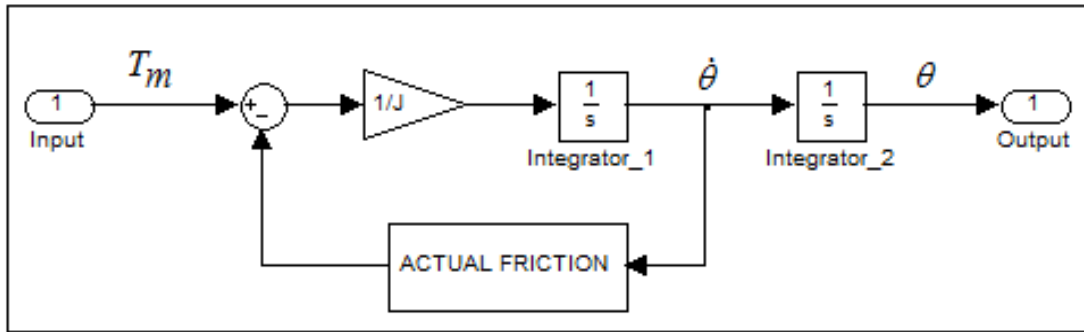
Figure 3.2. Block diagram of the open loop system with friction

For the precise positioning of the system, the control algorithm composed of the linear and nonlinear parts is added to the plant to form a closed loop position control system. This control input for the plant is given in equation (3.3) as follows:

$$T_m = T_{linear} + \hat{T}_f \qquad (3.3)$$

where T_{linear} and $\hat{T}_f$ stand for the linear part of the controller and estimated friction torque with caret denoting the estimated quantity, respectively.
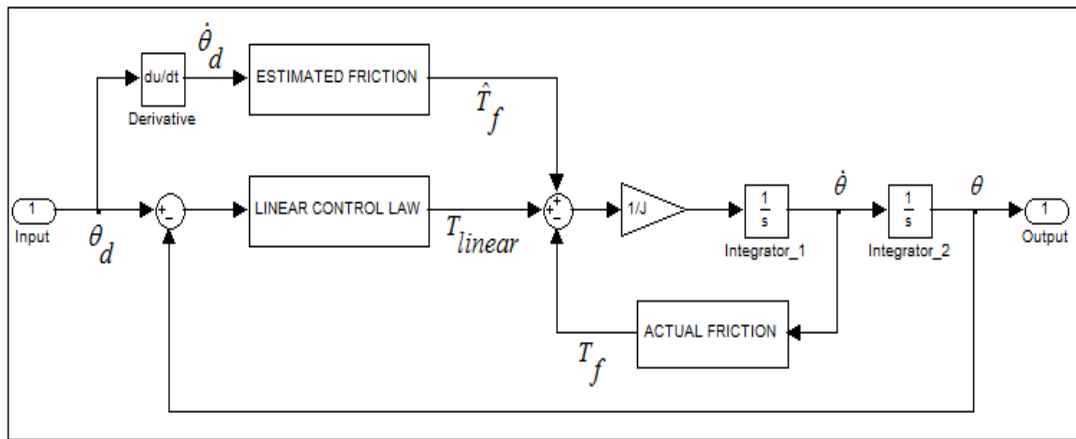
Figure 3.3. Block diagram of the closed loop system with model-based feedforward friction compensation
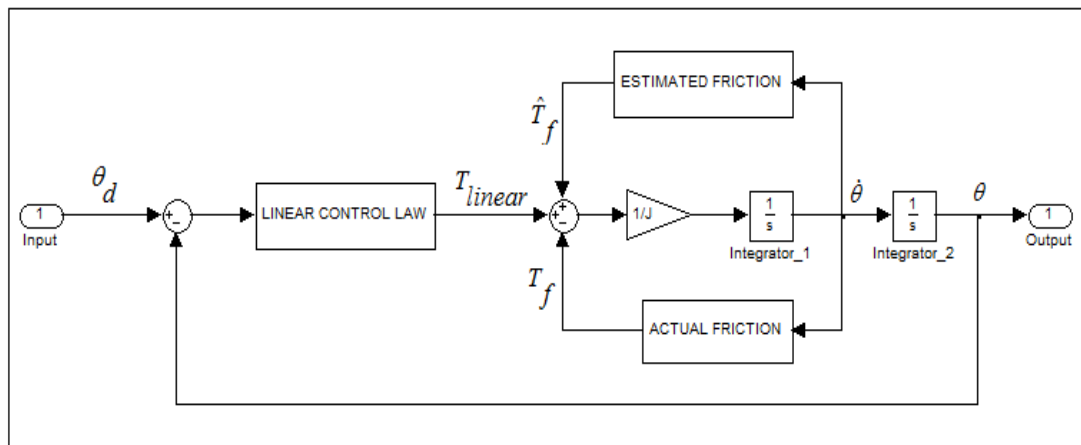
Figure 3.4. Block diagram of the closed loop system with model-based feedback friction compensation

Here, the linear part of the controller is assumed to be composed of a proportional with rate feedback (PR) control or PD feedback control actions, and a PID control action. When the nonlinear part of the control algorithm, i.e. $\hat{T}_f$, is considered, the compensation approaches are classified into two categories as model-based feedforward friction compensation and model-based feedback friction compensation schemes according to the fact that the estimated friction torque $\hat{T}_f$ is

38

whether a function of the desired velocity or measured velocity. The block diagrams of the closed loop systems with different compensation approaches are shown in Figure 3.3 and Figure 3.4. These figures demonstrate the complete version of the closed loop control system with friction and the simulations will be performed regarding these diagrams.

3.1.1 Linear part of the control law

3.1.1.1 PR and PD control actions

The linear part of the control law is necessary to diminish or eliminate the tracking errors when the friction is not present or totally compensated. The linear part of the controller can be given as in (3.4) and (3.5) according to which control action, i.e. proportional with rate feedback or proportional with derivative control actions, will be used.

$$T_{linear\_pr} = k_p \, (\theta_d - \theta) - k_d \, \dot{\theta} \qquad (3.4)$$

$$T_{linear\_pd} = k_p \, (\theta_d - \theta) + k_d \, (\dot{\theta}_d - \dot{\theta}) \qquad (3.5)$$

where k_p and k_d denote the proportional and derivative gains of the controller while θ_d and $\dot{\theta}_d$ are the desired, or reference, angular position and velocity of the closed loop system, respectively.

Using only the linear part of the controller and the transfer function of the plant without friction, the closed loop transfer function of the system without friction (or with totally compensated friction) is obtained for the two different linear control strategies, i.e. for the PR control when $T_{linear} = T_{linear\_pr}$ and for the PD-type feedback control when $T_{linear} = T_{linear\_pd}$, as in (3.6) and (3.7), respectively.

39

$$G_{CLS\_PR}(s) = \frac{\theta(s)}{\theta_d(s)} = \frac{k_P}{J s^2 + k_d s + k_P} \tag{3.6}$$

$$G_{CLS\_PD}(s) = \frac{\theta(s)}{\theta_d(s)} = \frac{k_d s + k_P}{J s^2 + k_d s + k_P} \tag{3.7}$$

In order to design a closed loop control system with satisfactory performance, the poles of the closed loop system should be in suitable locations to have fast response and good damping characteristics. One approach for providing a closed loop system with the desired bandwidth and damping characteristics is the 'pole placement' approach. Here, placing the poles to the desired locations in the left-hand s-plane, the linear control system is guaranteed to be stable, and satisfactory response characteristics can be attained.

Here, the pole placement approach is applied by treating the closed loop system as a standard 2nd order system with the characteristic equation given in (3.8) as follows [28]:

$$D(s) = s^2 + 2\zeta\omega_n s + \omega_n{}^2 \tag{3.8}$$

According to this equation, the poles of this polynomial are located on a circle of radius ω_n which corresponds to the desired bandwidth of the closed loop control system, and the damping of the system having this polynomial as a characteristic equation is represented by ζ. Then, by forcing the characteristic equations of the above derived closed loop systems, i.e. (3.6) and (3.7), to be equal to the (3.8), the bandwidth and damping characteristics of the linear closed loop system without frictional effects are adjusted to the desired values.

In this respect, the normalized characteristic eqauations of both closed loop transfer functions in (3.6) and (3.7) are given below:

$$D_{CLS}(s) = s^2 + \frac{k_d}{J}s + \frac{k_p}{J} \qquad (3.9)$$

Then, equating the polynomials in (3.8) and (3.9), the proportional and derivative gains of the linear controllers are found as in (3.10).

$$\begin{aligned} k_p &= J\,\omega_n^2 \\ k_d &= 2\,J\,\zeta\,\omega_n \end{aligned} \qquad (3.10)$$

3.1.1.2 PID control action

In the simulations, the PID control action is also used as a linear controller alone, i.e. without any nonlinear friction compensation term, for the comparison purpose. In this respect, the linear part of the controller can also be given as in (3.11).

$$T_{linear\_pid} = k_p\,(\theta_d - \theta) + k_d\,(\dot{\theta}_d - \dot{\theta}) + k_i \int (\theta_d - \theta) \qquad (3.11)$$

where the additional parameter k_i and $\int$ sign denote the integral gain of the linear controller and integral operator, respectively whereas the other parameters represent the same meaning as in (3.5).

The parameters of the PID control law can be determined by using the same procedure as in the previous section 3.1.1.1. In this respect, the closed loop transfer function of the system without friction (or with totally compensated friction) is obtained for this control strategy when $T_{linear} = T_{linear\_pid}$ and given in (3.12).

$$G_{CLS\_PID}(s) = \frac{\theta(s)}{\theta_d(s)} = \frac{k_d s^2 + k_p s + k_i}{J s^3 + k_d s^2 + k_p s + k_i} \qquad (3.12)$$

Here, the ideal characteristic equation of the closed loop system is chosen as in (3.13) for the pole placement approach in such a way that the closed loop system with the PID control action has the same bandwidth as the systems with the PD and PR control actions. On the other hand, the normalized characteristic equation of the closed loop transfer function given in (3.12) is derived in (3.14).

$$D(s) = (s^2 + 2\zeta\omega_n s + \omega_n^{\,2})(s + \omega_n) \tag{3.13}$$

$$D_{CLS}(s) = s^3 + \frac{k_d}{J}s^2 + \frac{k_p}{J}s + \frac{k_i}{J} \tag{3.14}$$

Then, equating the polynomials in (3.13) and (3.14), the proportional, derivative and integral gains of the linear PID controller are found parametrically and given in (3.15).

$$\begin{aligned} k_p &= J\,\omega_n^{\,2}(1+2\zeta) \\ k_d &= J\,\omega_n(1+2\zeta) \\ k_i &= J\,\omega_n^{\,3} \end{aligned} \tag{3.15}$$

As a final part of the modelling of dynamic system, the actual frictional behaviour in the plant, the different friction compensation models which will be used in the friction estimation term $\hat{T}_f$ in the control law in (3.3) and the tunings of their parameters will be described.

3.1.2 Actual frictional behaviour in the plant

In this study, the actual frictional behaviour is modelled by the GMS friction model since it includes most of the dynamic behaviours of friction and fits to the real friction characteristics in a better way than the other dynamic models [19], [20].

According to the relevant studies in the literature, the GMS friction model with 4 elementary blocks is sufficient to model the real frictional behaviour, and increasing the number of elements further does not affect the accuracy of the friction model in a valuable manner in approximating the real frictional behaviour when the load of the additional model parameters due to the increased number of elements is considered [4], [20], [22], [25]. Regarding these facts, the actual friction torque is assumed to be formed by the **4-element GMS model** with the sliding regime parameters taken from the [14], and the pre-sliding regime parameters taken from the [25]. According to these assumptions and the formulations given by equations (2.16) through (2.18), the nominal parameters of the actual friction are given in Table 1.

Table 1. Nominal parameters of the 4-element GMS model of actual friction

Pre-sliding region parameters			Sliding region parameters		
Parameter	Value	Unit	Parameter	Value	Unit
k_1	1.0×10^4	N·m/rad	F_S	0.335	N·m
k_2	0.7×10^4	N·m/rad	F_C	0.285	N·m
k_3	0.5×10^4	N·m/rad	v_s	0.01	rad/s
k_4	0.3×10^4	N·m/rad	δ_s	2	-
-	-	-	σ_2	0.018	N·m·s/rad
-	-	-	C	24	N·m/s
-	-	-	$\alpha_1, \alpha_2, \alpha_3, \alpha_4$	0.25	-

Here, the reason why the sliding regime parameters are selected from the [14] is that the levels of the static and Coulomb friction torques in the experimental set-up are considered to be adjusted in the order of the parameters in [14]. Since [14] is related to the LuGre friction model and does not include the parameters of the GMS friction model, the pre-sliding region parameters of the GMS model are taken from

the [25]. The pre-sliding region parameters given for a linear system in [25] are adapted to the rotary system model in this thesis.

Below, two input velocity profiles which will be applied later during the simulations are given in equations (3.16) and (3.17). According to the parameters in Table 1, the response of the GMS friction model to the velocity profile given in (3.17) is shown in Figure 3.5 as an example of the actual frictional behaviour.

$$\dot{\theta}_d(t) = 0.0251\sin(0.4x2\pi t) \qquad (rad/s) \qquad (3.16)$$

$$\dot{\theta}_d(t) = 0.3142\sin(0.1x2\pi t) \qquad (rad/s) \qquad (3.17)$$
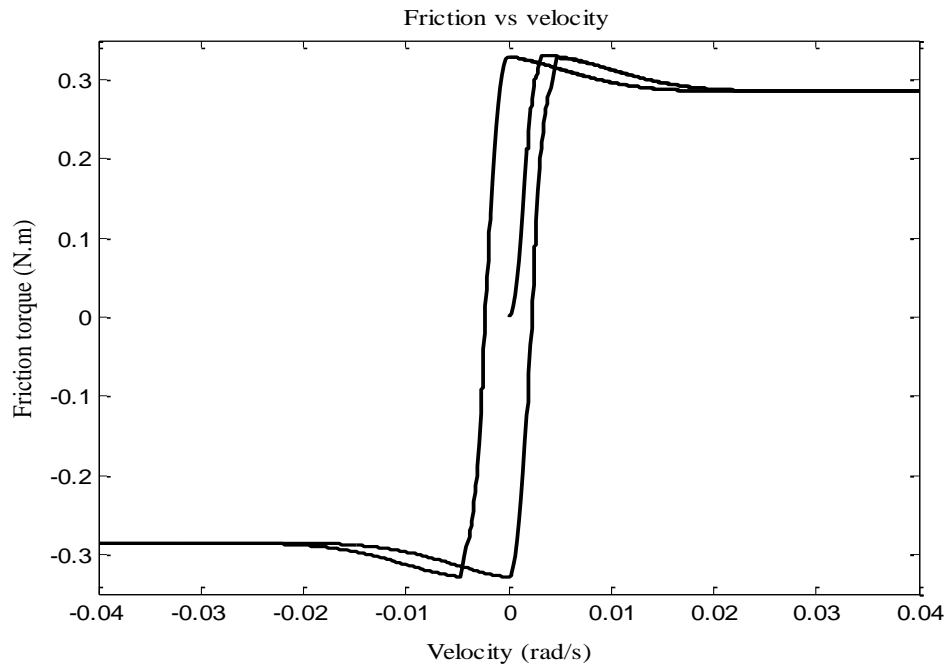
Figure 3.5. The response of the GMS model of actual friction versus velocity

As the implementation of the GMS friction model is considered, the block diagram of an element of the GMS model is demonstrated in Figure 3.6. Since the GMS model needs two different switching functions to pass through from the pre-sliding region to sliding region and vice-versa, this switching event is implemented using the state-flow blocks of the MATLAB® SIMULINK®. Also, the necessary conditions for the switching to occur is implemented with the hit-crossing block of the SIMULINK® instead of using comparison blocks to determine the crossing points. According to the Figure 3.6, there are four subsystems in the model. The subsystems called as 'sticking regime' and 'sliding regime' include the formulation of the GMS model whereas the subsystem called 'enable block' is composed of the switching conditions. The simulations always begin in sticking mode of friction. When a switching condition is satisfied, the state-flow block gives a corresponding output which enables either 'sticking regime' or 'sliding regime' subsystems to obtain the friction torque. As a result, the actual frictional behaviour is obtained by adding a term into which viscous friction is lumped to the four of these block diagrams in Figure 3.6.
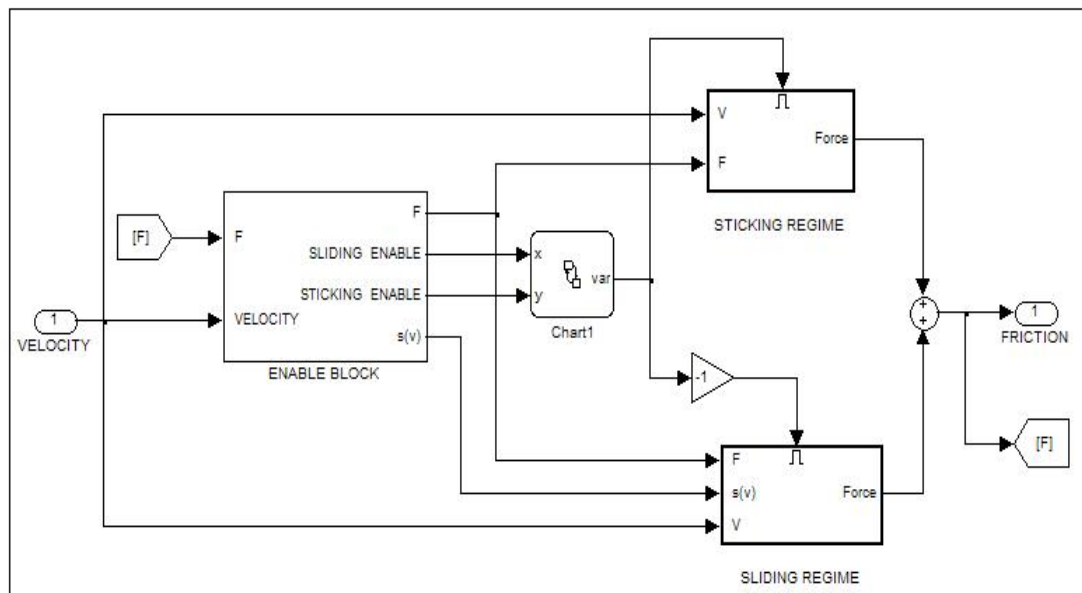
Figure 3.6. Block diagram of an element of the GMS model

3.1.3 Nonlinear part of the control law

The nonlinear part of the controller is composed of the output of the friction compensation models. Friction compensation models are the models that will give an instantaneous estimation of frictional behaviour to diminish the performance deterioration of the system due to the negative effect of the friction. To make the compensation accurately, the parameters of the friction models, whose outputs are added to the control input, should be identified and tuned well. As mentioned at the beginning, four friction models will be used in the compensation of friction, which are the Coulomb with viscous friction model, the Stribeck friction model, the LuGre friction model, and the 3-element GMS friction model. Before the friction compensation task, the parameters of these models will be identified successively.

While finding the model parameters of all four friction models, i.e. two static and two dynamic models, which will be used in the control system for friction compensation purpose, the parameters of the actual frictional behaviour given by 4-element GMS model are assumed to be unknown to the control engineer as in the real world. Thus, identification techniques will be applied to the GMS model of actual friction to find both the pre-sliding region and sliding region parameters of the four models to be used in the compensation approaches.

The identification process is repeated for both the pre-sliding and sliding regimes for the dynamic friction models whereas identification is done only in the sliding regime for static friction models as a nature. The sliding region parameters, i.e. the parameters representing the constant velocity steady-state behaviour of friction, found from the identification process are the same for all static and dynamic models used in the compensation since the sliding parameters of them represent the same meaning of frictional behaviour. The difference among the friction models occurs at the identification of the pre-sliding region parameters, since each model has its own unique coefficients to represent the same shape of pre-sliding behaviour.

In accordance with these conditions, identification of the sliding region parameters will be done at once for all models. On the other hand, the parameter identification for the pre-sliding region of friction is only conducted for the dynamic

models, i.e. the LuGre model and the 3-element GMS model, which will be used for friction compensation.

3.1.3.1 Identification of the sliding region parameters of the friction compensation models

To identify the sliding region parameters, the closed loop control system which is composed of a linear controller (without friction compensation) and plant with friction is forced to track the constant velocities. The reason for this can be seen from (3.1). Theoretically, when the velocity is constant, the acceleration becomes zero and the motor torque (control input) will be equal to the friction torque in the system. Thus, the friction identification is done based on the motor torque produced, which in turn depends on the motor torque constant and the current output of the motor. However, the identification can be theoretically done independent of the closed loop system, since the actual friction model is assumed to be available for computer simulations.

To find the parameters of the sliding region, some constant velocity values are applied to the GMS model of actual friction as an input to the model and the output friction values are recorded as if one made an experiment on the closed loop system by applying some constant velocities. In equation (3.18), the applied constant velocities are given, and the friction-velocity map of the GMS model of actual friction is shown in Figure 3.7. As can be seen from this map, the frictional behaviour is not linear, thereby requiring nonlinear identification techniques. By applying a nonlinear least square curve fitting algorithm in MATLAB$^{®}$, all parameters of the sliding regime represented by the steady-state curve of friction in (2.6) are found to be the same as the parameters of the GMS model of actual friction as given in Table 1. Again in Figure 3.7, the curve fitted to the friction data to be used in all four friction compensation models is shown.

$$\dot{\theta} = (0.001; \, 0.025; \, 0.03; 0.04; 0.05; 0.1; 0.2; 0.3; 0.4; 0.5; 0.7; 1.0) \, (rad/s) \quad (3.18)$$
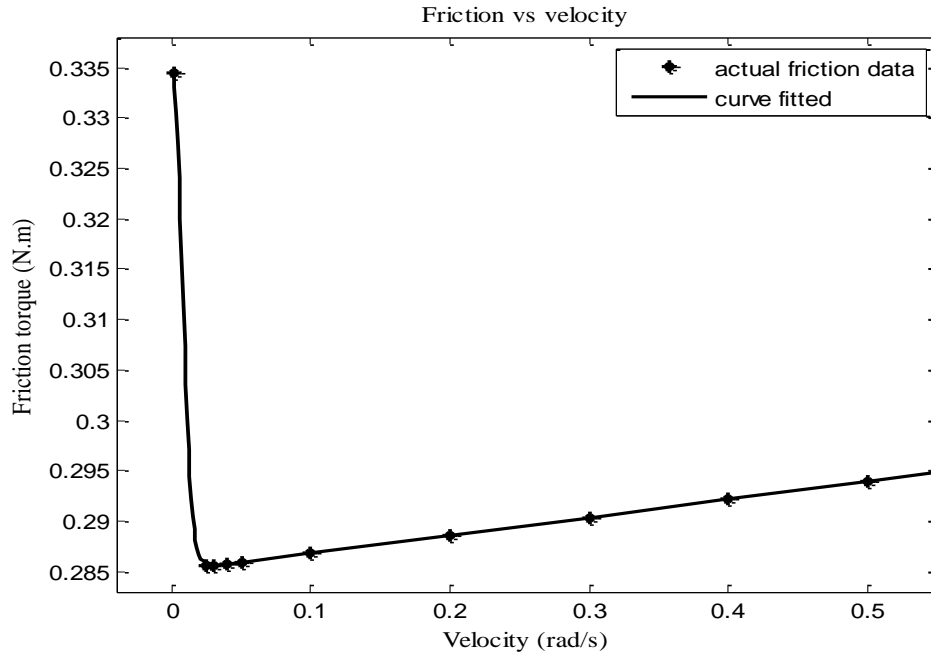
Figure 3.7. Friction data of the GMS model of actual friction and curve fitted to the data versus input velocities

However, there is an important point here, avoidance of which can cause parameter deflections and errors in friction estimation. The friction in the sliding region at the low velocities has a downward bend as mentioned before. This downward bend is function of the four parameters of the Stribeck curve of friction, which are static (break-away) torque F_S, Stribeck velocity v_s, Stribeck shape factor δ_s, and Coulomb torque F_C. Moreover, the first three parameters change depending on each other in the identification process. Thus, it is seen in the identification process that the first aforementioned three parameters may deviate from the actual ones for different initial guesses given to the curve fitting algorithm, since more than one curve can be fitted at the low-velocity regime if insufficient data points are collected in this regime. To solve this problem and find the sliding region parameters accurately, one should catch at least one friction data point from the part of the downward bend, how far away from the break-away force region. Then, even there is

one of the friction data available towards the end of the downward bend, the sliding region parameters can be obtained in an accurate manner.

In this study, the identification process includes one friction torque - velocity point near to the end of the downward bend of the Stribeck curve and accurate results are obtained with different initial conditions given to the three parameters, F_S, v_s, and δ_s. To show the deviation of these parameters with different initial conditions, the 2nd data point is removed from the data collected by identification work. The identified inaccurate curves with different initial guesses are demonstrated in Figure 3.8.
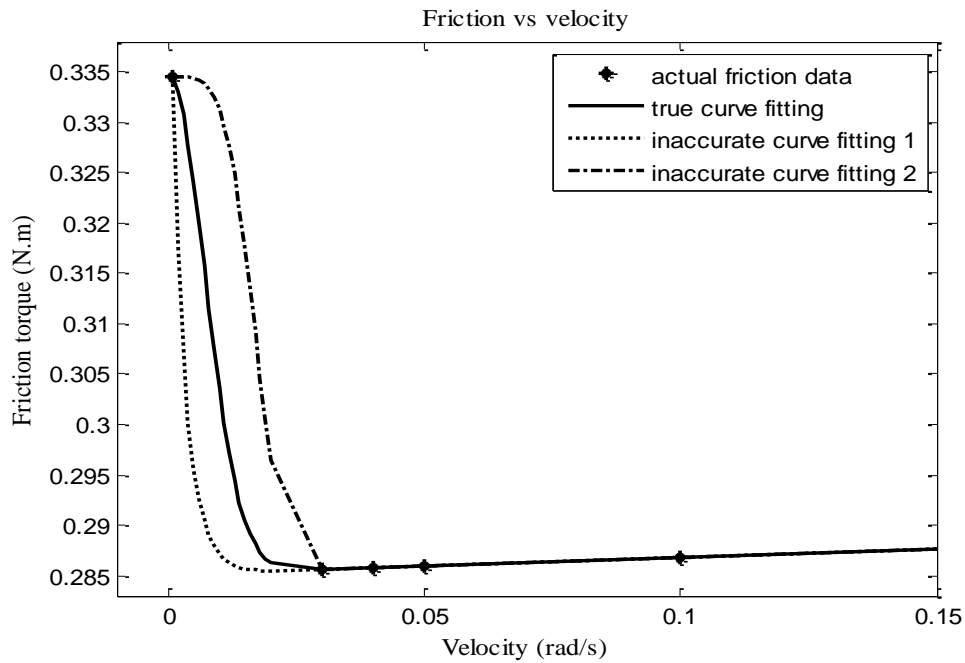
Figure 3.8. Inaccurate results of curve fitting to the friction data

3.1.3.2 Friction compensation models

3.1.3.2.1 *Classical Coulomb with viscous friction compensation model*

One of the static models selected for the friction compensation purpose is the model reflecting the classical Coulomb with viscous friction. This is the simplest

compensation model used among the others and it includes only some frictional behaviours in the sliding region while not containing any term related to the pre-sliding region. In this respect, the formulation is given as in (3.19).

$$\hat{T}_f = F_C \, sign(\dot{\theta}) + \sigma_2 \, \dot{\theta} \qquad (3.19)$$

where F_C and σ_2 represent the Coulomb friction torque and linear viscous friction coefficient whereas $\dot{\theta}$ and $sign(.)$ stand for the angular velocity variable and signum function defined in equation (2.2), respectively.

As one can see from this formulation, the model has a discontinuity at zero velocity due to the signum function. According to the identified parameters of the sliding region before, the parameters of the Coulomb with viscous friction compensation model are given in Table 2 as follows:

Table 2. Parameters of the Coulomb with viscous friction compensation model

Pre-sliding region parameters			Sliding region parameters		
Parameter	Value	Unit	Parameter	Value	Unit
-	-	-	F_C	0.285	N·m
-	-	-	σ_2	0.018	N·m·s/rad

As far as the simulations are considered, this model is implemented by using the build-in block of the SIMULINK®, as shown in Figure 3.9. Then, according to the knowledge of the parameters as in Table 2, the responses of the GMS model of actual friction and the Coulomb with viscous friction model to the velocity profile given in (3.17) are shown in Figure 3.10 as a function of velocity to show the accuracy of friction estimation. Note that only the parts of the responses upto ±0.04 rad/s are shown in Figure 3.10 in order to see the difference clearly.
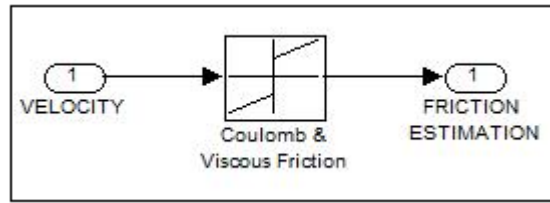
Figure 3.9. SIMULINK® block diagram of classical Coulomb with viscous friction compensation model
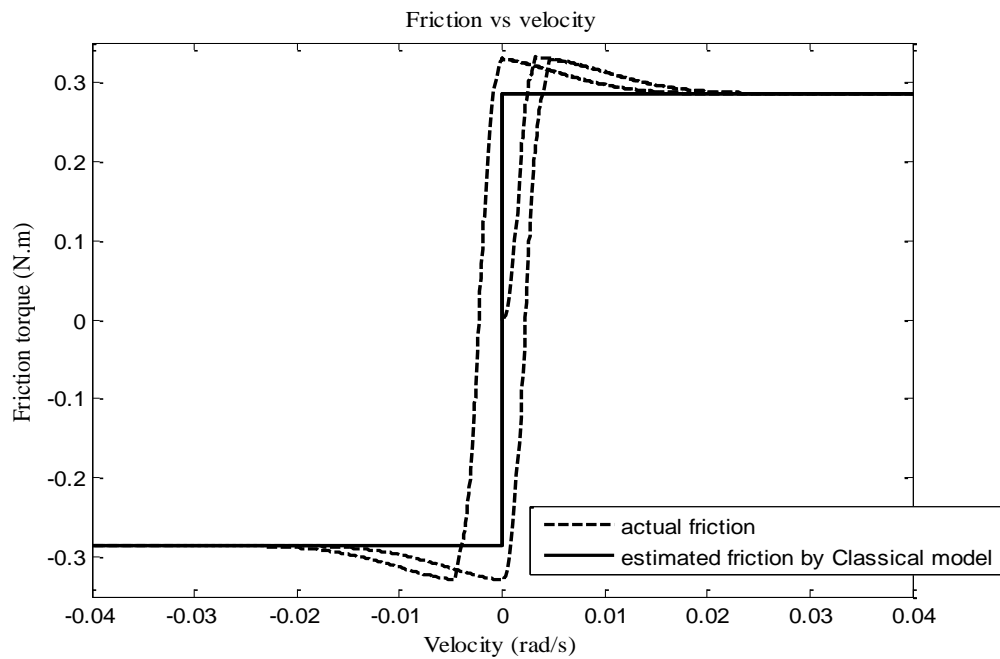
Figure 3.10. Comparison of the plant friction and the estimated friction by the classical Coulomb with viscous friction model

3.1.3.2.2 *Stribeck friction compensation model*

Stribeck friction compensation model is also a static friction model that only describes the sliding region of friction. It accurately describes most of the properties of the sliding region of the actual friction given by the 4-element GMS model while not including the pre-sliding region behaviour. The formulation of the Stribeck friction model is given in (2.6). However, in order to avoid the discontinuity of this

model in the simulations, a stiff slope is provided to the model at the jump discontinuity and this slope is hand-tuned by examining the response of the plant friction model to the velocity input profiles given in (3.16) and (3.17). Because of this slope, the Stribeck friction compensation model can be seen as if it represented the pre-sliding region with a single-stiff spring without hysteresis. According to these assumptions, for the implementation of the Stribeck friction compensation model, the formulation is changed as seen in (3.20).

$$\hat{T}_f = \begin{cases} k\dot{\theta} & if \; \left| k\dot{\theta} \right| \le \left| s(\dot{\theta}) \right| \\ \\ s(\dot{\theta}) & otherwise \end{cases} \qquad (3.20)$$

$$where \quad s(\dot{\theta}) = sign(\dot{\theta})(F_C + (F_S - F_C)e^{-\left|\frac{\dot{\theta}}{v_s}\right|^{\delta_s}}) + \sigma_2 \dot{\theta}$$

In equation (3.20), the additional k parameter represents the stiff slope for the implementation of the Stribeck friction model whereas the other parameters have the same meaning as the ones in equation (2.6), which represents the Stribeck friction model. According to this formulation, the identified parameters of this model are given in Table 3 as follows:

Table 3. Parameters of the Stribeck friction compensation model

Pre-sliding region parameters			Sliding region parameters		
Parameter	**Value**	**Unit**	**Parameter**	**Value**	**Unit**
k	3.5×10^4	N·m·s/rad	F_S	0.335	N·m
-	-	-	F_C	0.285	N·m
-	-	-	v_s	0.01	rad/s
-	-	-	δ_s	2	-
-	-	-	σ_2	0.018	N·m·s/rad

At the implementation of this structure, the switching conditions are determined with the help of comparison blocks in SIMULINK®. According to the parameters and formulation given above, the responses of the Stribeck friction compensation model and the GMS model of actual friction to the velocity profile in (3.17) are shown in Figure 3.11 as a function of velocity to show the estimation accuracy. Note that only the parts of the responses upto ±0.04 rad/s are shown in Figure 3.11 in order to see the difference clearly.
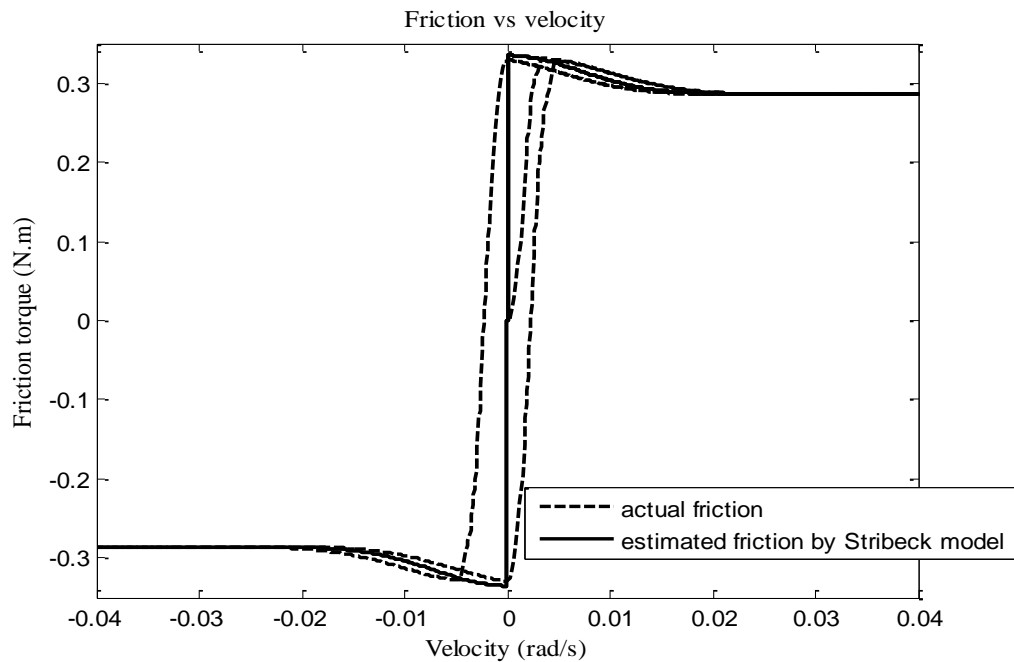
Figure 3.11. Comparison of the plant friction and the estimated friction by the Stribeck friction model

3.1.3.2.3 *LuGre friction compensation model*

LuGre friction compensation model is one of the dynamic models considered for the compensation purpose here. The model shows both the pre-sliding and sliding region characteristics of friction. It accurately describes all of the properties of the sliding region of the actual friction given by the 4-element GMS model whereas not describing the pre-sliding region behaviour as good as it does in sliding region. The

sliding region parameters of the LuGre model come from the identification of the sliding region parameters and are given in Table 4 with the same values as in Table 1. However, another identification technique should be applied in order to find the dynamic (pre-sliding region) parameters of the LuGre friction compensation model. This procedure is described below.

The formulation of the LuGre friction compensation model is the same as given in equations (2.8) through (2.10) and is implemented as it is. The advantage of this formulation is that there is no need for a switching function; thus, it makes the LuGre dynamic model implementation easier.

3.1.3.2.3.1 Identification of the dynamic parameters of the LuGre model

The dynamic (pre-sliding region) parameters of the LuGre model can be found by some identification techniques in the literature: By minimizing the peak tracking error of the response [18], [21], or by applying an open loop experiment [14]. Actually, the latter one will be applied here since the former one provides an input signal specific identification [18].

For the identification purpose, an input torque which can cause a stick-slip motion and velocity reversals in the system is given to the open loop system with friction and the actual position is measured. Recall that the actual friction is given by means of the 4-element GMS friction model in simulations. On the other hand, the fictitious open loop system where the LuGre friction model is considered to give the actual friction is simulated with the same torque input and the position response is recorded again. Then, the dynamic parameters of the LuGre model, i.e. σ_0 and σ_1, are identified by minimizing the tracking error between the actual and fictitious responses of the open loop system with friction.

For this purpose, a sinusoidal torque input whose amplitude is higher than the breakaway torque of the system is given here. The sinusoidal torque whose amplitude is 0.35 N.m and whose frequency is 1 Hz is chosen as an input to the open loop system. After the application of the input, the MATLAB$^{\circledR}$ SIMULINK$^{\circledR}$ Response Optimization tool is used for the comparison of the responses. In this respect, the identified dynamic parameters of the LuGre model are given in Table 4,

and the comparison of the actual and fictitious position responses of the open loop system is given in Figure 3.12.

Table 4. Parameters of the LuGre friction compensation model

Pre-sliding region parameters			Sliding region parameters		
Parameter	**Value**	**Unit**	**Parameter**	**Value**	**Unit**
σ_0	3.5×10^4	N·m/rad	F_S	0.335	N·m
σ_1	0.1	N·m·s/rad	F_C	0.285	N·m
-	-	-	v_s	0.01	rad/s
-	-	-	δ_s	2	-
-	-	-	σ_2	0.018	N·m·s/rad
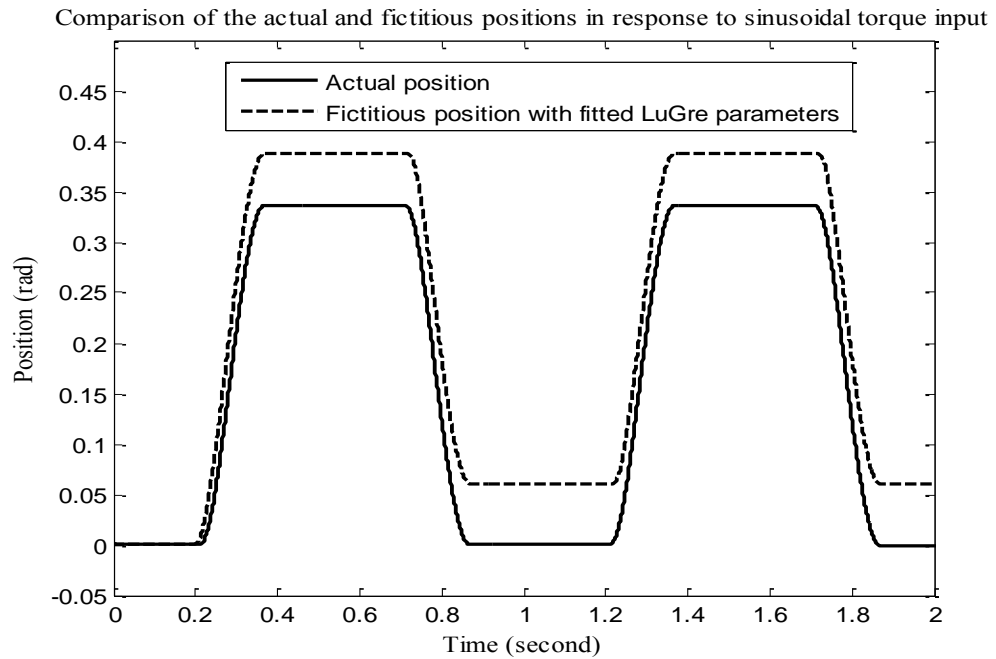
Figure 3.12. Comparison of the actual and fictitious positions of the open loop system with friction

55

Using all the identified parameters of the LuGre model in Table 4, the response of the LuGre friction compensation model to the velocity profile in (3.17) is obtained and compared with the response of the GMS model of actual friction in Figure 3.13 to show the estimation accuracy. Note that only the parts of the responses upto ±0.04 rad/s are shown in Figure 3.13 in order to see the difference clearly.
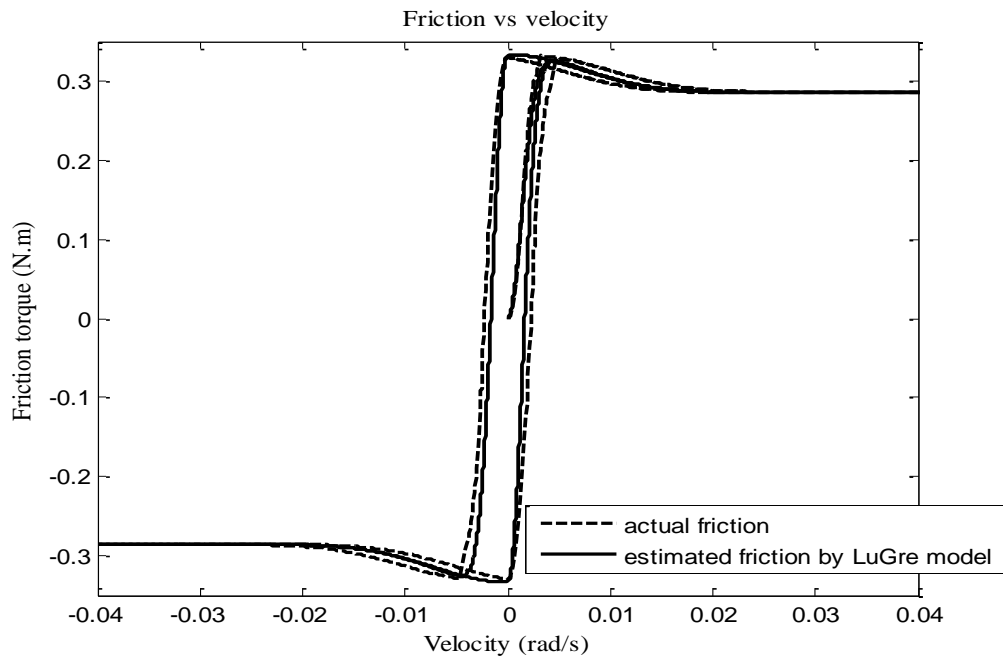

Figure 3.13. Comparison of the plant friction and the estimated friction by the LuGre friction model

3.1.3.2.4 GMS friction compensation model

As mentioned before, the actual friction is given by the 4-element GMS model. Then, if one considers again a 4-element GMS friction compensation model for compensating the effects of the actual frictional behaviour in the system, the performance of the system will be extremely satisfactory and there will be no need for simulations because a perfect match will occur between the parameters of the actual friction (plant friction) and the parameters of friction estimated by the GMS

model in the identification process. Thus, the number of elements in the GMS friction compensation model is selected to be 3 for this case because the aim is to show the modelling capacity of the GMS friction model in approximating the plant friction. Moreover, the α_{ic} ($i=1,2,3$) parameters, which represent the constant fractional parameter of each element in the 3-element GMS friction compensation model, will be selected equal as in the case of the 4-element GMS model.

The formulations of the GMS friction compensation model are the same as in equations (2.16) through (2.18). The sliding region parameters of the GMS compensation model come from the identification process of the sliding region and are given in Table 5 with the same values as in Table 1. However, the pre-sliding region parameters and the attraction parameter (C_C) of the GMS compensation model should be identified separately as described below.

3.1.3.2.4.1 Identification of the pre-sliding region parameters of the GMS model

As mentioned before, the control system with friction exhibits very small displacements, i.e. pre-sliding displacements, in the sticking regime. To identify the parameters of the GMS model which determine the model behaviour in the pre-sliding region of friction, the system should be forced to move in this region without exceeding the range of the pre-sliding displacement. In this respect, a sinusoidal torque input, or ramp input, whose maximum value is below the break-away torque is applied to the plant, and the resultant displacements are measured. Then, the pre-sliding region parameters are found by making a curve fit between the outputs of the GMS model and the obtained torque-displacement hysteresis curve.

Since the actual frictional behaviour in the system is assumed to be known here, the actual hysteresis curve can be obtained by applying a very small sinusoidal displacement profile whose maximum value is within the bounds of the pre-sliding displacement to the actual friction model and recording the friction output of the model. The subsequent identification process of the parameters requires a nonlinear curve fitting technique. Then, the parameters of the 3-element GMS model are found using a nonlinear least square curve fitting algorithm in MATLAB[®]. In this respect, the position profile given in equation (3.21) is applied to the actual friction model.

Using the obtained friction-displacement curve, the pre-sliding region parameters of the 3-element GMS friction compensation model are found as given in Table 5.

$$\theta = 2.75 x 10^{-5} \sin(0.2x2\pi t) \quad (rad) \quad (3.21)$$

3.1.3.2.4.2 Identification of the attraction parameter of the GMS model

The attraction parameter is mainly related to the frictional lag at the downward bend of the Stribeck curve, i.e. at the low-velocity portion of sliding region. To find this parameter, a uni-directional non-steady-state [19], [26] sinusoidal velocity profile whose range does not exceed the end of the downward bend of the Stribeck curve of friction can be applied to the closed loop system. Then, regarding the obtained friction-velocity hysteresis curve, the attraction parameter C_C of the GMS friction compensation model is identified in a suitable manner. Again, this identification can be theoretically done by applying an aforementioned-type velocity profile to the actual friction model represented by the 4-element GMS model.

To obtain the attraction parameter of the 3-element GMS compensation model, the velocity profile given in equation (3.22) is applied to the GMS model of actual friction. Using the obtained response, the value of the attraction parameter is found as given in Table 5.

$$\dot{\theta} = 0.011\cos(0.2x2\pi t) + 0.012 \quad (rad/s) \quad (3.22)$$

Considering the parameter values in Table 5, the responses of the GMS friction compensation model and the actual friction model to the velocity profile given in equation (3.17) are obtained and compared in Figure 3.14 to show the estimation accuracy. Note that only the parts of the responses upto ±0.04 rad/s are shown in Figure 3.14 in order to see the difference clearly. As one can see from this figure, friction estimation is highly accurate such that the difference between the friction estimation and the actual friction is not distinguishable.

Table 5. Parameters of the 3-element GMS friction compensation model

Pre-sliding region parameters			Sliding region parameters		
Parameter	**Value**	**Unit**	**Parameter**	**Value**	**Unit**
k_{1c}	1.2896×10^4	N·m/rad	F_S	0.335	N·m
k_{2c}	0.8141×10^4	N·m/rad	F_C	0.285	N·m
k_{3c}	0.4273×10^4	N·m/rad	v_s	0.01	rad/s
-	-	-	δ_s	2	-
-	-	-	σ_2	0.018	N·m·s/rad
-	-	-	C_C	23.8782	N·m/s
-	-	-	$\alpha_{1c}, \alpha_{2c}, \alpha_{3c}$	1/3	-
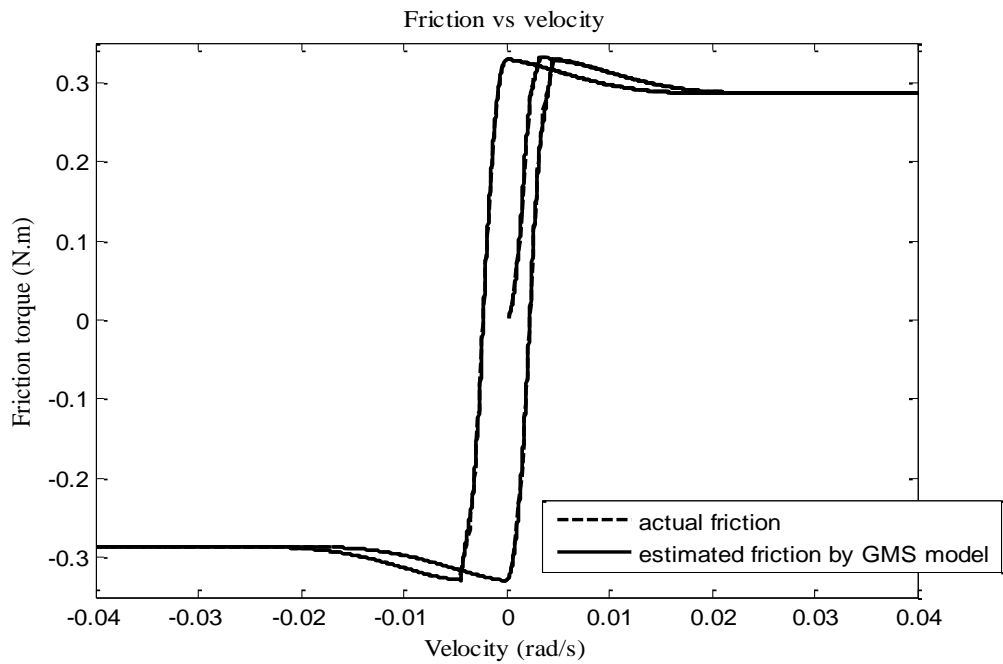
Figure 3.14. Comparison of the plant friction and the estimated friction by the 3-element GMS friction model

In the computer simulations, the α_i ($i = 1,\ldots,4$) parameters of the 4-element GMS model of plant friction and the α_{ic} ($i = 1,2,3$) parameters of the 3-element GMS compensation model are selected equal in themselves. Also, the number of elements in the GMS model of actual friction is selected as 4 in order to reflect the friction in the plant according to the general tendency mentioned in the literature [4], [20], [22], [25]. However, the other options, such as α_i parameters different from each other and number of elements greater than 4, will be studied in the experimental identification of friction which will be done in Chapter 4 to see the accuracy of the results taken from the literature.

3.2 Simulation studies of the closed loop system with friction

3.2.1 Determination of the integration time step and solver

For the comparison of the GMS model of actual friction with the other models to be used in compensation in terms of the friction estimation capability and for the simulation purposes, a solver and a time step of integration should be determined to be used in all simulations to have a coherence between them. As alternatives of the sampling time, 10^{-3}, 10^{-4} and 10^{-5} seconds have been selected, and as an alternative to the solvers, ODE1 fixed step solver, ODE5 fixed step solver, and ODE15s variable step solvers have been selected. In order to reach a suitable solution, the different combination of the solvers and integration time steps have been tried on the 4-element GMS friction model in SIMULINK$^{\circledR}$ by applying different input velocity profiles. On the other hand, an m-file code, the programming file format of MATLAB$^{\circledR}$, which is the text version of the 4-element GMS model has been run with sampling time of 10^{-5} seconds. The comparison of the results of the MATLAB$^{\circledR}$ SIMULINK$^{\circledR}$ model with the m-file code has given the followings:

- 10^{-5} seconds in SIMULINK$^{\circledR}$ gives accurate results. However, the running time of simulation is much higher than the others.
- ODE1 and ODE5 fixed step solvers with time steps of 10^{-3} seconds give lower accuracy according to the m-file code.

According to these facts, three alternatives, ODE1 with 10^{-4} seconds, ODE5 with 10^{-4} seconds, and ODE15s with maximum time step of 10^{-3} seconds have arisen among others. The comparisons among them show that the accuracy of the models are close to each other. On the other hand, the run time of the ODE15s solver with maximum time step of 10^{-3} seconds is less than one third of the minimum run time of the others in response to different velocity profiles. Thus, **the ODE15s variable step solver with maximum step size of 10^{-3} seconds** is chosen for all the simulations conducted thereafter.

3.2.2 Simulation parameters and cases

As mentioned before, the aim of the present thesis is the position control of a control system under the effect of friction. Thus, to see the behaviour of the closed loop system with controller consisting of a linear feedback part and a nonlinear friction estimation part, different types of simulations have been done. In these simulations, the performance characteristics of the closed loop system with PD control action alone, PID control action alone, and PD control action with different friction compensation models added have been compared in the sense of the accuracy of the position tracking. In this respect, both the model-based feedforward friction compensation technique based on the desired velocity profile, and the model-based feedback friction compensation technique based on the velocity measurement (velocity output of the system) have been applied to the closed loop system. Moreover, using both of these techniques, the performance of the friction compensation models are examined under the different friction regions emphasizing different dominant friction characteristics of the system by applying suitable position and velocity input profiles to the closed loop system.

3.2.2.1 Inputs for simulations

Considering the above conditions, the reference position and velocity profiles for the simulations are selected as in equations (3.23) and (3.24), and graphically shown in Figure 3.15, Figure 3.16 and Figure 3.17. Note that the reference velocity signals below are the same as in equations (3.16) and (3.17), and the step position input is represented only in graphical form.

The reference position signal and the velocity signal, which is the derivative of given position signal, for the simulations where the behaviour of the pre-sliding region of friction dominates are chosen to be:

$$
\begin{aligned}
\theta_d(t) &= 0.01(1 - \cos(0.4x2\pi t)) \quad (rad) \\
\dot{\theta}_d(t) &= 0.0251\sin(0.4x2\pi t) \quad\quad (rad/s)
\end{aligned}
\tag{3.23}
$$

and the reference position and velocity signals for the simulations where the behaviour of the sliding region of friction dominates are chosen to be:

$$\theta_d(t) = 0.5(1 - \cos(0.1 x 2\pi t)) \quad (rad)$$
$$\dot{\theta}_d(t) = 0.3142 \sin(0.1 x 2\pi t) \quad (rad/s)$$

$$(3.24)$$

These profiles have been selected such that the system will move more in pre-sliding region of friction for the dominant pre-sliding region simulations, and more in sliding region of friction for the dominant sliding region simulations. Similar to these cases, the step input simulations emphasize the pre-sliding region of friction at steady-state.
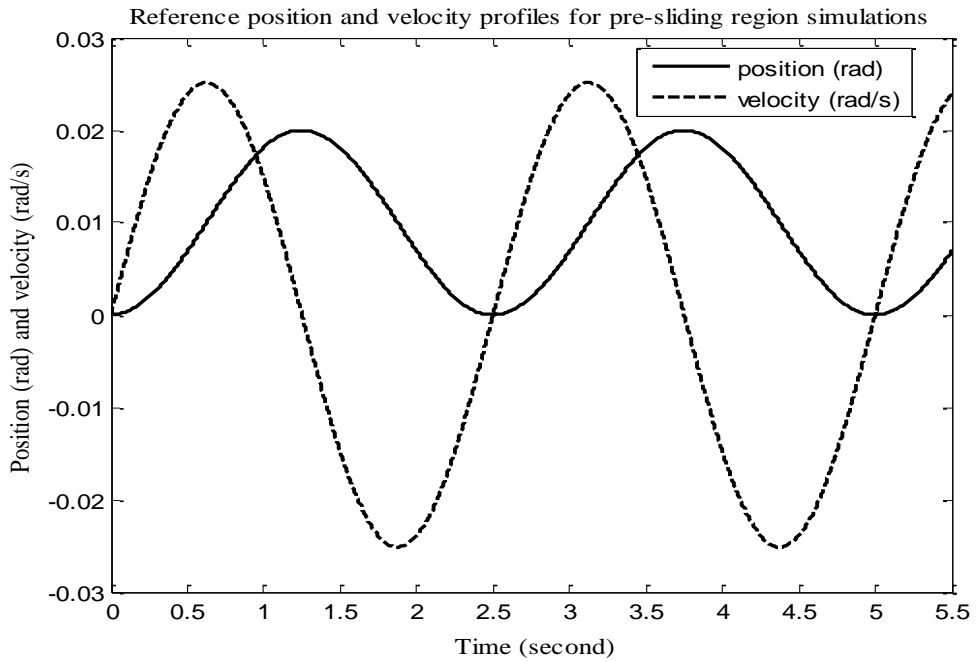
Figure 3.15. Reference position and velocity signals for the low-velocity sinusoidal position input simulations
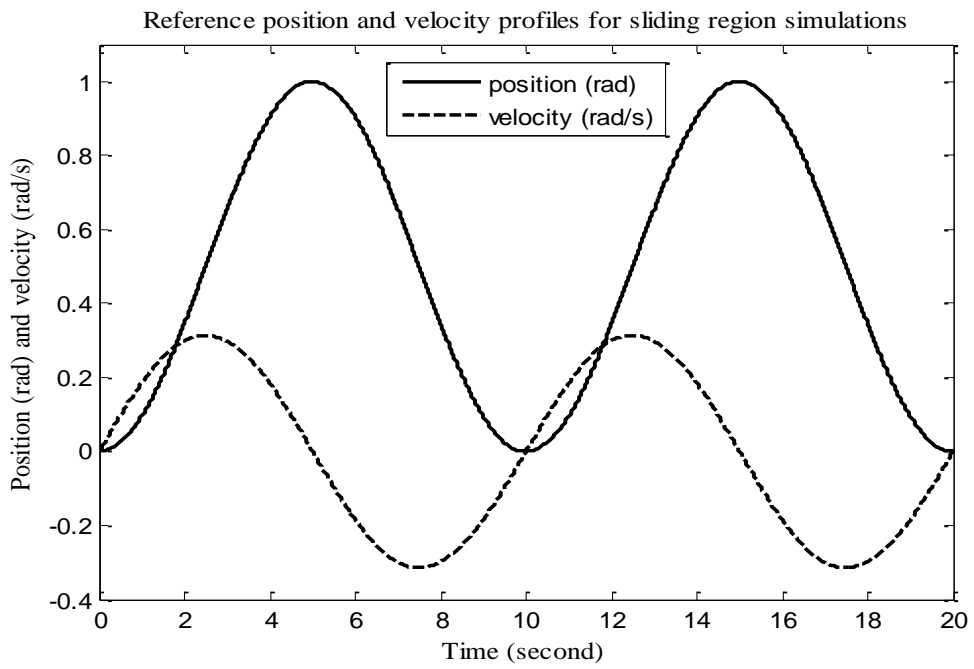
Figure 3.16. Reference position and velocity signals for the high-velocity sinusoidal position input simulations
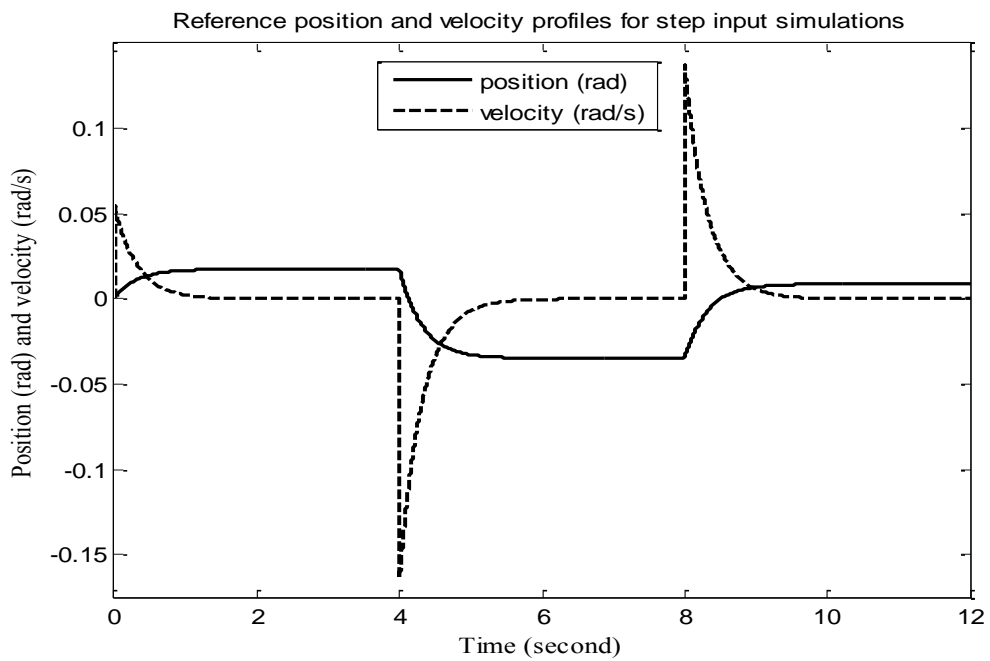
Figure 3.17. Reference position and velocity signals for the step position input simulations

3.2.2.2 Selection of the linear controllers and its parameters

For the three different input cases mentioned in 3.2.2.1, the controller parameters have been selected separately. Since the closed loop system should be more damped and faster in the pre-sliding region to track the small position and velocity input signals without exhibiting stick-slip phenomenon, the bandwidth and damping quantities of the linear controller have been adjusted to higher values. According to this fact, the damping and bandwidth values of the linear feedback controllers (PD and PID) for the sinusoidal and step input simulations are given in Table 6 and Table 7, respectively. The controller parameters k_p, k_d, k_i, which are calculated according to the equations (3.10) and (3.15), are also given in Table 6 and Table 7. Note that the selected, relatively higher bandwidth value in the dominant pre-sliding region simulations (simulations with low-velocity sinusoidal and step position inputs) cannot be feasible in reality since it can cause oscillations due to the system nonlinearity and higher noise sensitivity, and require high sampling frequency that cannot be provided due to the implementation limitations. However, this can be applied in simulation environment without requiring higher sampling frequency and help us examine the results more comfartably.

Recall that to find the linear controller parameters, one needs the total inertia value of the plant referring to the equations (3.10) and (3.15). The total inertia value is calculated as explained in section 3.1 by using the inertia values of the parts used in the experimental set-up from the catalogue pages and it is approximately found as $J = 3.8623\,x10^{-4}\,kg.m^2$.

Table 6. Linear controller parameters for the sinusoidal input simulations

Parameters for the low-velocity sinusoidal input			Parameters for the high-velocity sinusoidal input		
Parameter	Value	Unit	Parameter	Value	Unit
ζ	1.0	-	ζ	0.85	-
ω_n	36	Hz	ω_n	10	Hz
PD controller			PD controller		
k_p	19.7612	N·m/rad	k_p	1.5248	N·m/rad
k_d	0.1747	N·m·s/rad	k_d	0.0413	N·m·s/rad
PID controller			PID controller		
k_p	59.2836	N·m/rad	k_p	4.1169	N·m/rad
k_d	0.2621	N·m·s/rad	k_d	0.0655	N·m·s/rad
k_i	4469.9	N·m/(s·rad)	k_i	95.8049	N·m/(s·rad)

Table 7. Linear controller parameters for the step input simulations

Parameters for the step input		
Parameter	Value	Unit
ζ	0.9	-
ω_n	35	Hz
PD controller		
k_p	18.6786	N·m/rad
k_d	0.1529	N·m·s/rad
PID controller		
k_p	52.3001	N·m/rad
k_d	0.2378	N·m·s/rad
k_i	4107.6	N·m/(s·rad)

As stated in section 3.1.1, the linear part of the control law might be composed of a PR or PD control action. The aim is here to compare the performance of the friction compensation techniques regarding a fixed linear controller. Therefore, the responses of the closed loop system with and without friction (or totally compensated friction) are compared in the cases of using PR and PD control actions in order to eliminate one of these two controllers. For this purpose, the reference position and velocity signals given in (3.24) are applied to the closed loop system with and without friction with the controller parameters selected as in Table 6 (parameters for the high-velocity sinusoidal input). According to the comparison of the tracking errors of the closed loop control system with these linear controllers, the system with the PD control action is observed to track the desired position and velocity signals in a slightly more accurate manner in both of the cases with and without friction as can be seen from the tracking errors in Figure 3.18 and Figure 3.19. Note that the tracking errors for the position and velocity signals are shown for one cycle of inputs in Figure 3.18 whereas they are given for a half cycle of inputs in Figure 3.19 in order to see the difference between the controllers clearly in the system with friction. As a result, all the forthcoming simulations will be performed with the control law whose linear part includes the **PD control action**.
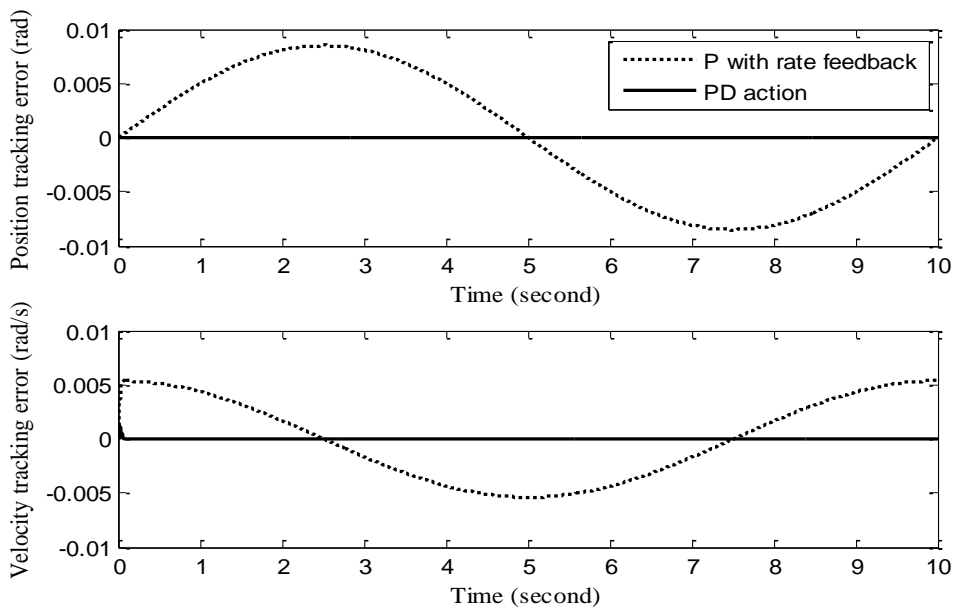
Figure 3.18. The comparison of the position and velocity tracking errors of the proportional with rate feedback control action and proportional with derivative control action in the system without friction
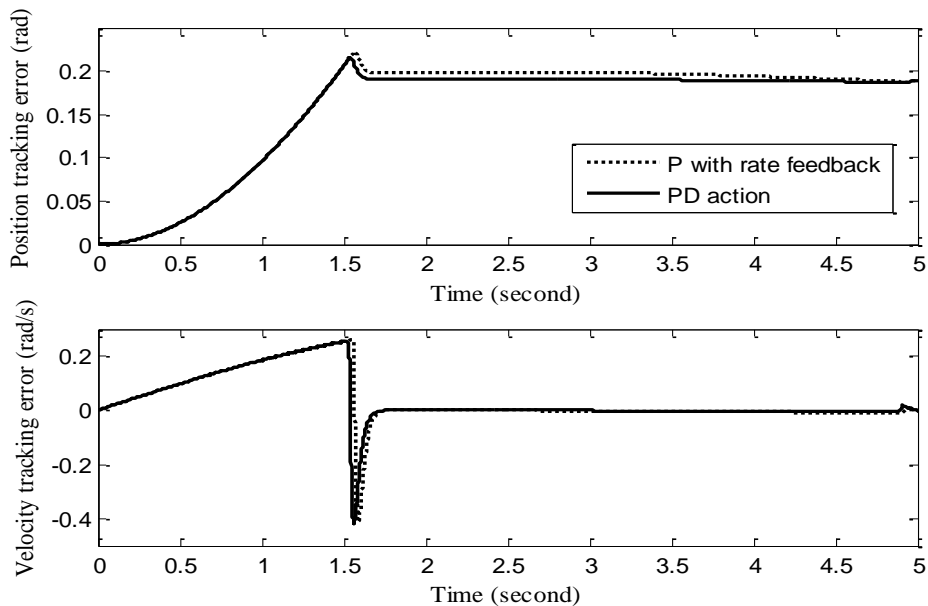
Figure 3.19. The comparison of the position and velocity tracking errors of the proportional with rate feedback control action and proportional with derivative control action in the system with friction

68

3.2.2.3 Nominal and perturbed actual friction models

In the physical world, the friction can exhibit different characteristics time to time due to the change in the normal force acting on the considered system, texture of the rubbing surfaces, contamination, decrease in lubricant etc. Thus, the identified friction models found in anytime might not reflect the friction characteristic in another time when the friction in the system changes due to the above reasons.

Considering the above explanation, the friction compensation performance of the four friction models will be compared for three different cases of actual friction. First of all, the nominal actual friction model whose parameters are given in Table 1 will be used as if it reflected the real frictional behaviour in the plant. Then, the two perturbed friction models, which are the models involving the parameters perturbed in both positive and negative directions, will be used as an actual friction in the system and compensation results will be presented. While simulating the closed loop system under these three cases of actual friction, the parameters of the control law will be held fixed for the sake of being faithful and consistent, i.e. the same linear control law parameters in Table 6 and Table 7, and the same previously identified, nominal friction compensation model parameters in Table 2, Table 3, Table 4, and Table 5 will be used to compare the results.

To see the performance deterioration of the system with the fixed friction compensation models whose parameters have been identified theoretically according to the nominal actual friction, the actual friction will be perturbed from its nominal state. The mentioned perturbation task will be performed assuming that only the normal force on the system changes and this affects only the static force F_S and Coulomb force F_C, and that the other static and dynamic parameters will remain constant.

According to the data taken from the experimental set-up designed, the static force during one revolution of the shaft deviates from the mean value for about 20% and when the standard deviation of these data is compared with the mean of the data, 10% perturbation is seen to be suitable for our case. Then, to obtain the perturbed actual frictional behaviour and simulate this condition on the closed loop system, the

F_S and F_C parameters of nominal actual friction, which are given in Table 1, will be deviated in the positive sense at an amount of 10% to obtain positively-perturbed actual friction model, and in the negative sense at 10% to obtain negatively-perturbed actual friction model. As a demonstration, the responses of the nominal and two perturbed actual friction models to the input velocity profile given in (3.17) are shown in Figure 3.20.
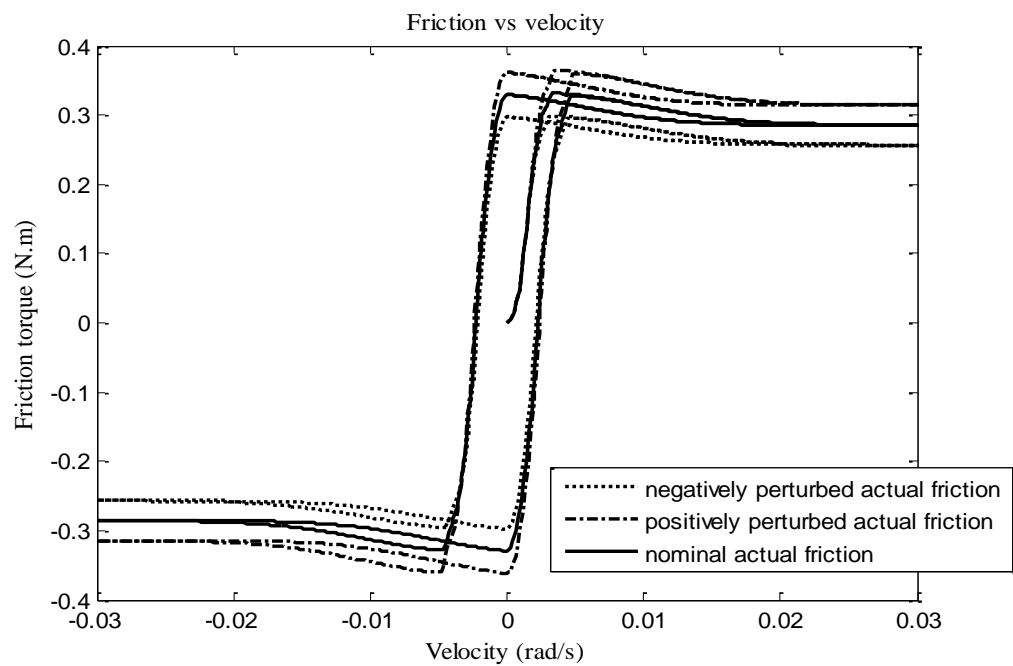
Figure 3.20. Responses of the nominal and perturbed actual friction models as a function of velocity

3.2.3 Simulation results

3.2.3.1 Nominal actual friction case

3.2.3.1.1 Simulations for the low-velocity sinusoidal position input

In Figure 3.21 and Figure 3.22, model-based feedforward and feedback friction compensation results are given for the dominant pre-sliding region simulations, respectively. When both figures are examined, one can find that the system can not follow the position trajectory without the friction compensation term in the control law. Thus, addition of friction compensation term of any friction model improves the tracking accuracy in both feedforward and feedback cases.

In the feedforward compensation given in Figure 3.21, the Stribeck, LuGre and GMS models produce responses close to each other which are much better than the classical Coulomb with viscous model. When these three models are examined in detail, actually the GMS model gives slightly better response than the LuGre and Stribeck friction models. However, even at GMS model, the stick-slip occurs at the peak of the trajectory which is near to the zero velocities because of the inexact estimation of the actual friction torque in the system.

On the other hand, for the feedback compensation case in Figure 3.22, the order of the accuracy of the responses are again the same as in the feedforward compensation, i.e. the GMS model gives the best, even perfectly matched response, and the LuGre, Stribeck and Coulomb with viscous follow it respectively. However, the responses become more oscillatory because of the extreme velocity fluctuations which can be resulted from the stability problems of the feedback compensation.

In these figures, the compensation result of using only the PID controller whose bandwidth is the same as the PD control action is also given. It is seen that the system with PID control action exhibits a stick-slip behaviour through the trajectory. Furthermore, the PD control action with added feedforward friction compensation terms usually gives smoother response than the PID control action in non-zero velocity regions. Moreover, specifically in the feedback compensation, the PD with GMS compensation model has better stick-slip property than the PID action near zero velocity regions.

71
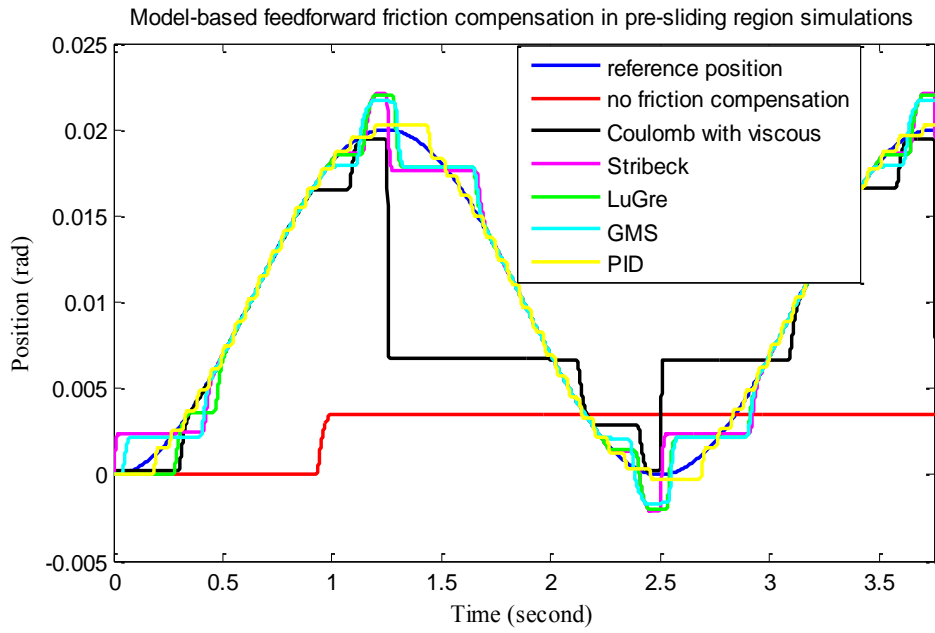
Figure 3.21. Simulated model-based feedforward friction compensation of system with nominal actual friction in response to the low-velocity sinusoidal position input
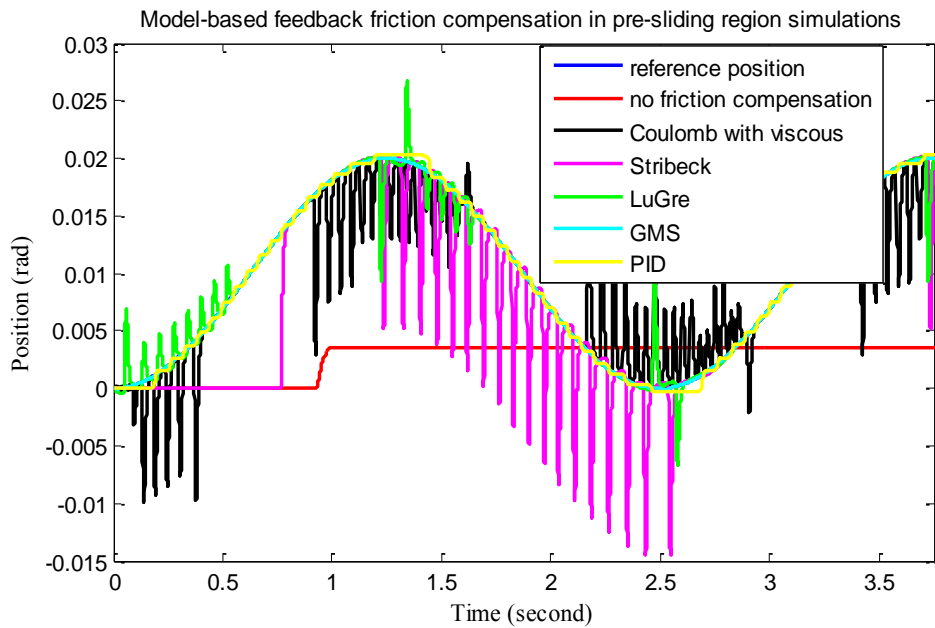
Figure 3.22. Simulated model-based feedback friction compensation of system with nominal actual friction in response to the low-velocity sinusoidal position input

3.2.3.1.2 Simulations for the high-velocity sinusoidal position input

As seen from Figure 3.23 and Figure 3.24, the tracking capability of the closed loop system becomes higher when the friction compensation term of any model is added to the linear control law by using both the feedforward and feedback friction compensation.

For the feedforward simulations in Figure 3.23, the responses of both the static and dynamic models are close to each other and follow the desired position trajectory with approximately the same accuracy. This result is expected because the system moves more in the viscous part of the sliding regime and all friction compensation models include this term in their formulations.

As far as the feedback compensation is considered, whose results are shown in Figure 3.24, the actual position response of the system with the GMS compensation model follows the desired position perfectly without any oscillation. In this case, the response of the classical Coulomb with viscous friction model is slightly better than the LuGre model because of the oscillatory behaviour of the LuGre model here. Also, the Stribeck friction compensation gives worse result than the others in this simulation. This may be caused by the velocity oscillations based on the stability problems of feedback compensation.

In this sliding region dominant trajectory, the system with PID control action having the same bandwidth as the PD control action gives similar responses as the system with PD with friction compensation terms. Both have smooth in non-zero velocity regions and show stick-slip near zero velocity regions for feedforward compensation case. This is expected because the system moves in viscous region mostly. In the feedback compensation case, the PD with GMS friction model compensation gives better and much smoother result than the PID control action at the peaks of the trajectory.
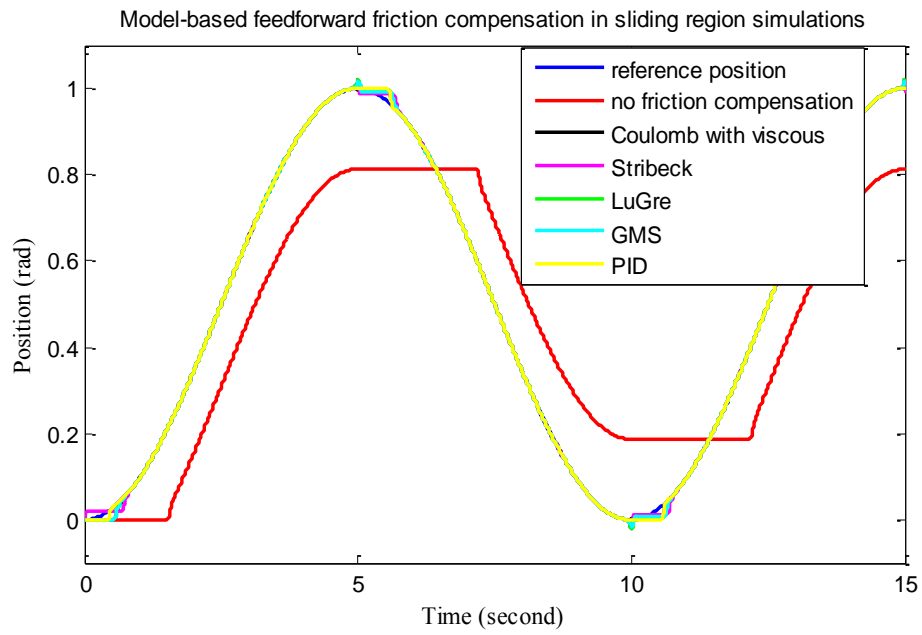
Figure 3.23. Simulated model-based feedforward friction compensation of system with nominal actual friction in response to the high-velocity sinusoidal position input
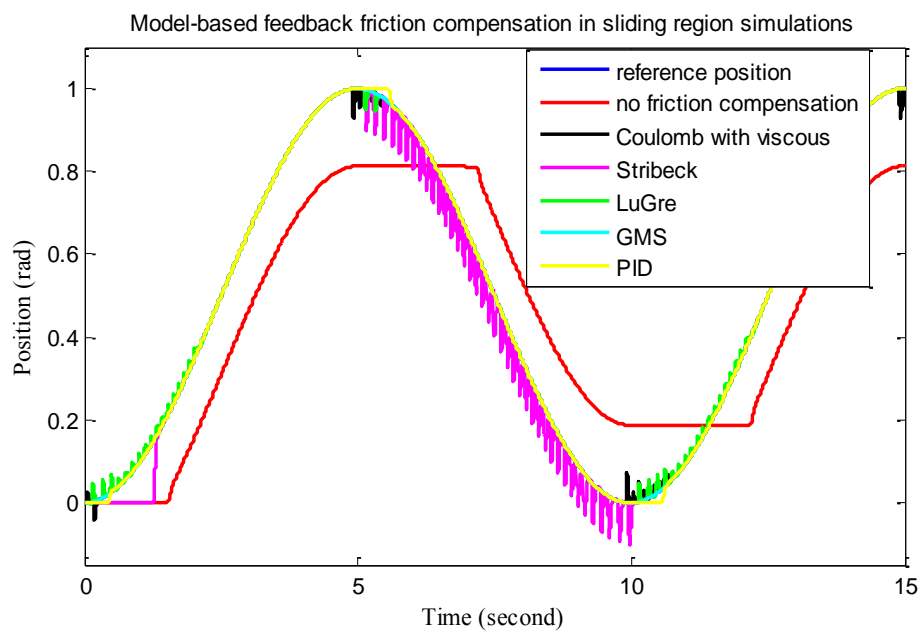
Figure 3.24. Simulated model-based feedback friction compensation of system with nominal actual friction in response to the high-velocity sinusoidal position input

3.2.3.1.3 Simulations for the step position input

In Figure 3.25 and Figure 3.26 respectively, the step responses of the system with the applied model-based feedforward and feedback friction compensation methods are given. One can see from both of these figures that the PD control action alone are not adequate to make the system follow the given trajectory.

According to the feedforward compensation in Figure 3.25, the addition of any friction compensation term improves the tracking ability. In this case, the Coulomb with viscous friction model gives actually the best response with least steady-state error. The other three friction models including dynamic models have similar responses and approximately the same steady-state errors greater than the Coulomb with viscous friction model.

On the other hand, in Figure 3.26 where the results of the feedback friction compensations are given, the responses of the static models become oscillatory. There is a small amplitude, high frequency chattering in Coulomb with viscous friction model whereas a larger amplitude but lower frequency oscillations exist in the response of the Stribeck model. In this approach, the dynamic models overperform the static models even with a non-oscillatory and smooth responses. Between the dynamic models, the GMS model gives nearly perfectly-matched response without jumps in position as compared to the LuGre model.

In response to the step input, the PID control action with the same bandwidth as the PD control action shows a stick-slip behaviour at steady-state (it is called 'hunting') in contrast to the response of the PD control action with feedforward friction compensation terms which is smooth, but with steady-state error. In the feedback compensation case, the PD control action with dynamic friction compensation models, especially with the GMS model, gives much better and smoother responses without steady-state errors than the pure PID action.
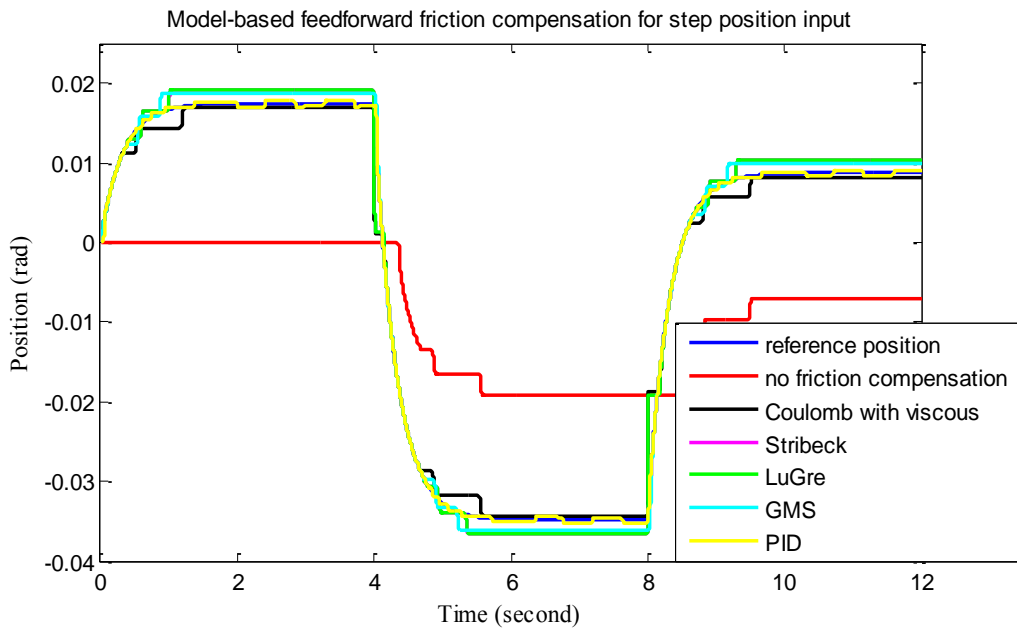
Figure 3.25. Simulated model-based feedforward friction compensation of system with nominal actual friction in response to the step position input
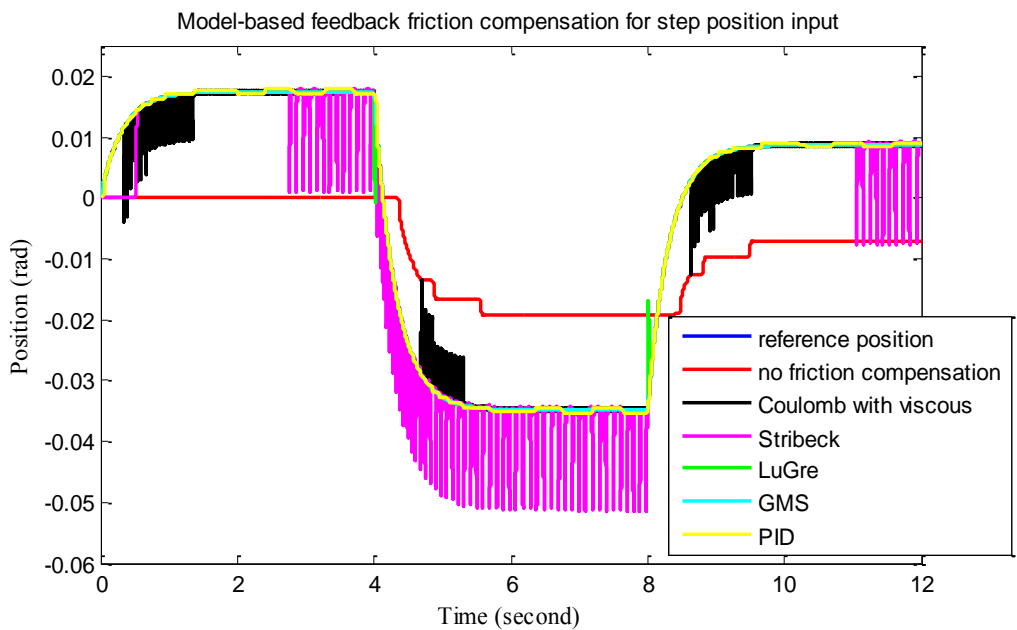
Figure 3.26. Simulated model-based feedback friction compensation of system with nominal actual friction in response to the step position input

3.2.3.2 Positively-perturbed actual friction case

3.2.3.2.1 Simulations for the low-velocity sinusoidal position input

In Figure 3.27 and Figure 3.28, the responses of the closed loop system to the pre-sliding trajectory when the actual friction is changed by perturbing its parameters in positive direction is presented. Here, this is the case of undercompensation, since the parameters of the compensation models remain the same, and they are smaller than the parameters of the positively-perturbed actual friction model.

As can be seen in Figure 3.27, the responses seem fairly well although the actual friction changes and the compensation model parameters still remain the same. The responses of the system with the GMS, LuGre and Stribeck friction compensations are nearly the same and better than the classical Coulomb with viscous model compensation. However, any compensation model added to the control law increases the accuracy of the system according to the system with no friction compensation.

Considering the feedback compensation only, the Coulomb with viscous model gives the best results and LuGre, GMS and Stribeck compensation models follow it respectively. However, the velocity oscillations and frequency of oscillations of the Coulomb and LuGre models are too large to be acceptable in a control system. Thus, the responses of them cause chatterring as can be seen in Figure 3.28. Furthermore, there occurs a lag in the response of both feedforward and feedback compensations due to the perturbed actual friction model.

As in the nominal actual friction case, the system with PID action shows a stick-slip behaviour throughout this sticking region dominant trajectory. In the feedforward friction compensation here, the PD with compensation models exhibits smoother, but delayed response (due to the undercompensation of friction and lack of the integral gain) than the PID control action in non-zero velocity regions while all have the similar stick-slip behaviour near zero velocity regions. For the feedback compensation case, the PD action with Coulomb with viscous model and LuGre model exhibits better tracking than the PD control action with GMS model and PID even if they both have chattering effects in their responses.
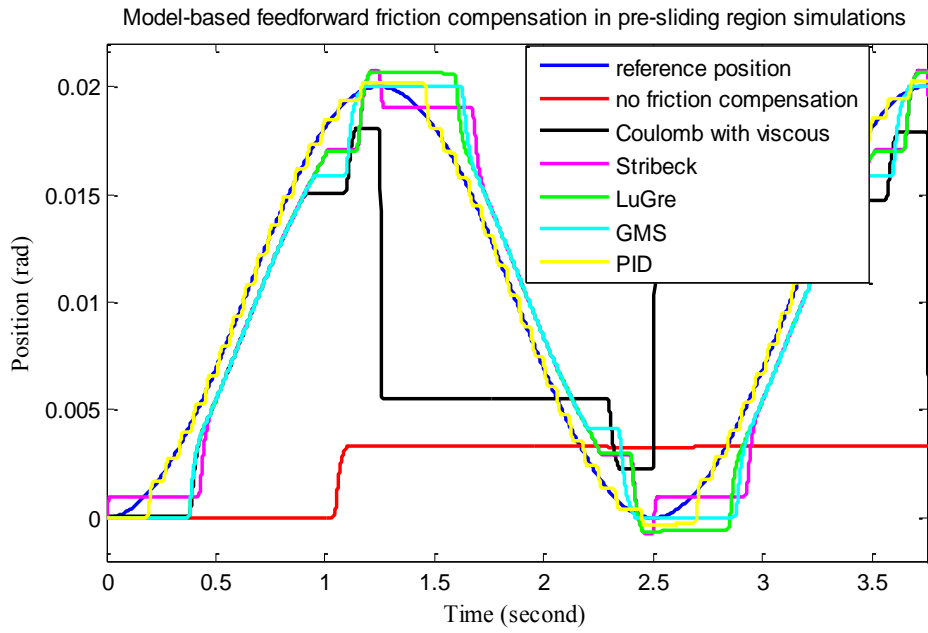
Figure 3.27. Simulated model-based feedforward friction compensation of system with positively-perturbed actual friction in response to the low-velocity sinusoidal position input
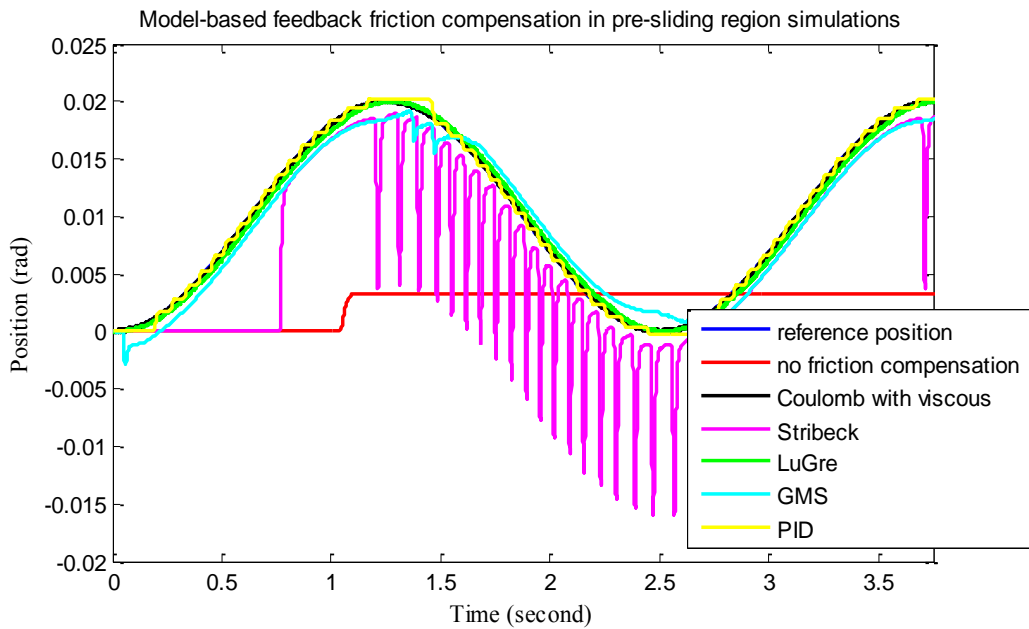

Figure 3.28. Simulated model-based feedback friction compensation of system with positively-perturbed actual friction in response to the low-velocity sinusoidal position input

78

3.2.3.2.2 *Simulations for the high-velocity sinusoidal position input*

The sliding region simulation results of the system with positively-perturbed actual friction are given in Figure 3.29 and Figure 3.30. From both figures, the improvement of the response curves can be seen according to the case of no compensation of friction.

For the feedforward compensation used, the responses have nearly the same accuracy, i.e. which one is better is not distinguishable actually. However, all of them enter stick-slip region at very low velocities as can be observed from Figure 3.29 near the peak of the position profile.

On the other hand, in the feedback compensation, the GMS model gives the best response. The LuGre and Coulomb with viscous friction model compensations follow it; however, the tracking accuracy of these two model are close to each other. The Stribeck model yields again the worse result as in pre-sliding simulation owing to the velocity oscillation which can be due to stability problems arising from feedback compensation.

For the feedforward compensation case, PD controller with friction compensation models and PID control action have similar and smooth responses as expected except that the responses of the PD with compensation models are delayed due to the undercompensation of actual friction. On the other hand, the PD control action with GMS model gives much closer response to the PID control in the feedback compensation case as the smoothness of the responses is considered.
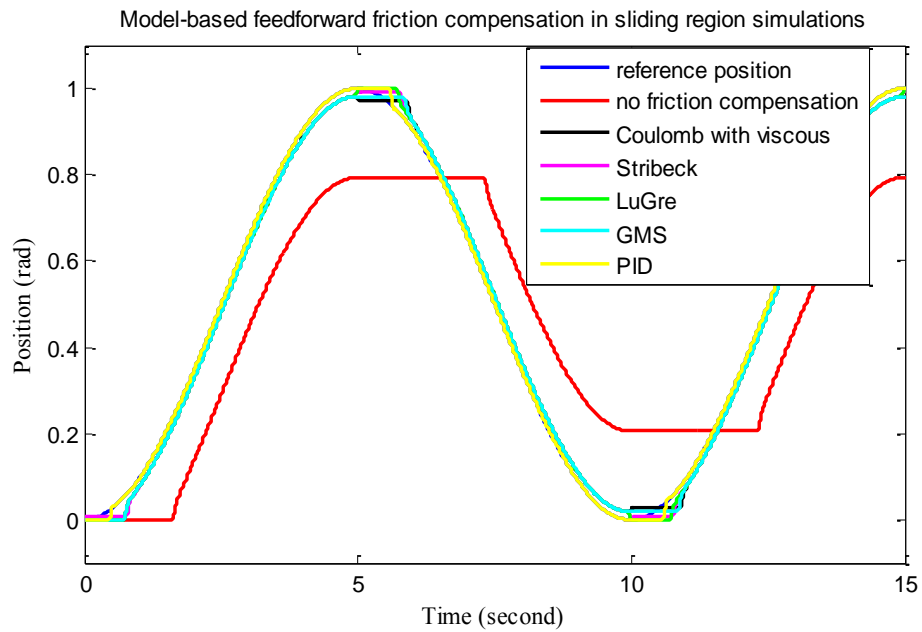
Figure 3.29. Simulated model-based feedforward friction compensation of system with positively-perturbed actual friction in response to the high-velocity sinusoidal position input
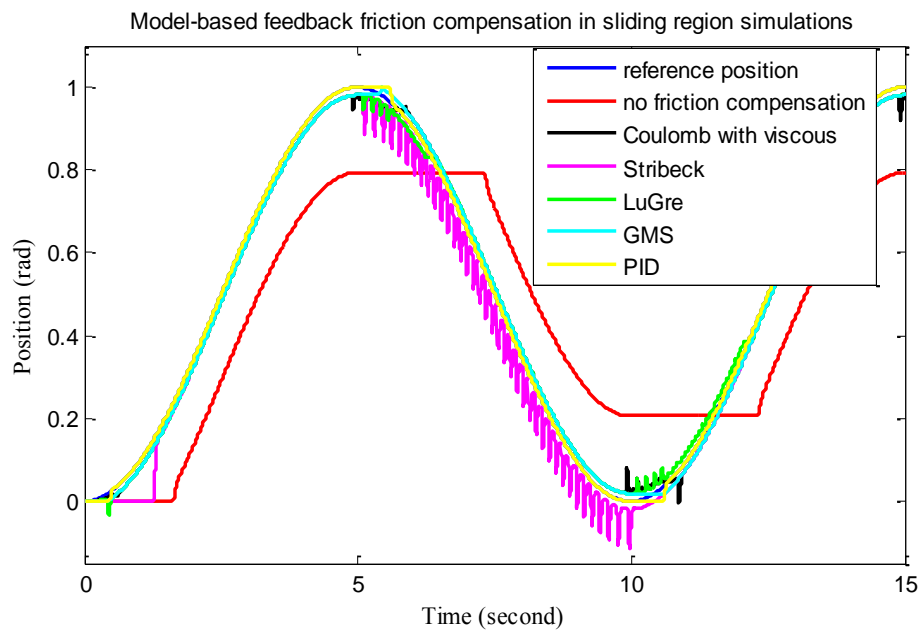
Figure 3.30. Simulated model-based feedback friction compensation of system with positively-perturbed actual friction in response to the high-velocity sinusoidal position input

3.2.3.2.3 *Simulations for the step position input*

For the case of increased actual friction, the step responses of the system with model-based feedforward and feedback compensation techniques applied are given in Figure 3.31 and Figure 3.32, respectively. As in the nominal friction case, the PD controller without any friction compensation term cannot follow the trajectory well enough.

As the friction compensation terms are added by feedforward friction compensation approach as in Figure 3.31, the response is highly improved and has the lowest steady-state error in the use of the GMS model. In this simulation, the static Stribeck model and dynamic LuGre model give nearly the same shape of the response and steady-state errors, which are slightly larger than the GMS model response. In contrast to the Stribeck model, the static Coulomb with viscous friction model gives the worst response with the largest steady-state error, but with an improved response in comparison to the pure PD control action used.

In Figure 3.32, where the feedback friction compensation techniques are applied, the Coulomb with viscous friction model seems to have the best response in terms of the steady-state error requirement. However, it represents a high frequency chattering undesirable for any control system. Similar to the Coulomb with viscous friction model, the static Stribeck friction model exhibits also chattering as in the nominal actual friction case, but with a higher amplitude and lower frequency than the Coulomb with viscous model. In contrast to the static models, both dynamic models give non-oscillatory and smooth responses with some steady-state errors which are not present in the Coulomb with viscous model. Also, the GMS model gives the best response between dynamic models.
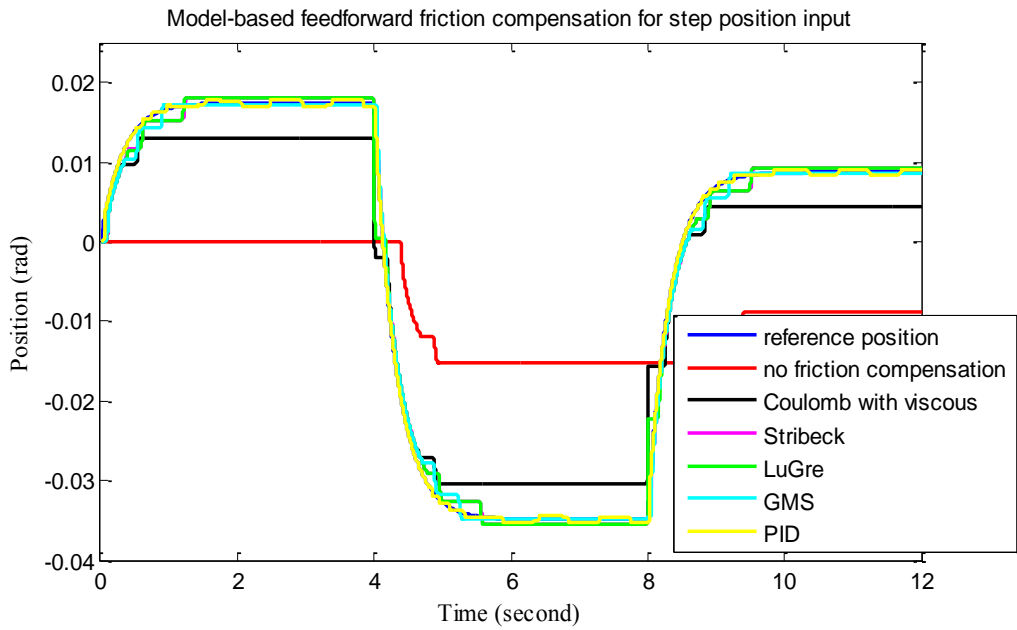
Figure 3.31. Simulated model-based feedforward friction compensation of system with positively-perturbed actual friction in response to the step position input
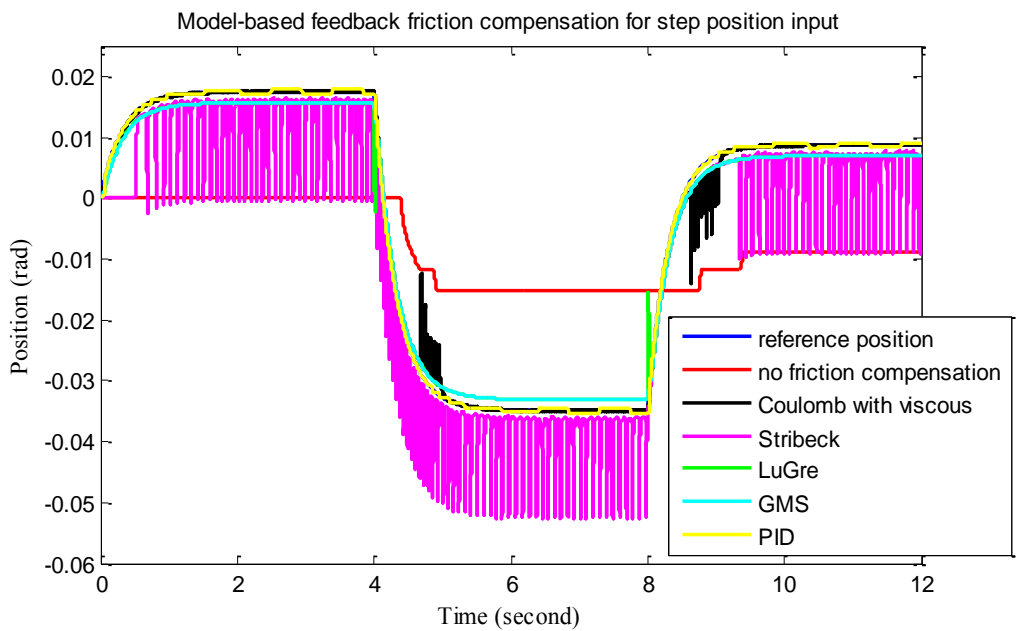


Figure 3.32. Simulated model-based feedback friction compensation of system with positively-perturbed actual friction in response to the step position input

At this step input trajectory emphasizing the dominant pre-sliding region friction at steady-state, the PD action with all compensation models gives smooth and non-oscillatory response with some steady-state errors as compared to the stick-slip limit cycling of the PID controller in the feedforward compensation case. Moreover, the PD with GMS model follows the input trajectory better than the PID control action since its steady-state error remains inside the stick-slip limit cycle of the PID control action. In the feedback compensation case; however, the steady-state errors of the dynamic models are outside the PID limit cycle although their responses are much smoother than the PID control action. Here, the PD with Coulomb with viscous model gives best response without steady-state errors, but with a high frequency chattering whose magnitude is within the PID limit cycle.

3.2.3.3 Negatively-perturbed actual friction case

3.2.3.3.1 *Simulations for the low-velocity sinusoidal position input*

This case can be seen as the overcompensation of friction since the friction estimation is larger than the negatively-perturbed actual friction torque which is obtained by perturbing the F_S and F_C parameters of the nominal actual friction model in the negative direction.

The compensation results for the pre-sliding trajectory are shown in Figure 3.33 and Figure 3.34. For the feedforward compensation, the GMS and LuGre compensation approaches give relatively close responses which are better than the Coulomb with viscous model and Stribeck model. On the other hand, the Coulomb model response is better than the Stribeck model although the latter one models the sliding region more accurately. Moreover, as expected, adding of friction compensation model to the control law improves the response very much. However, the undesired stick-slip phenomenon is present in all responses.

In the feedback compensation case whose results are shown in Figure 3.34, the GMS model gives the most accurate and smooth results without oscillations in contrast to other compensation models. The LuGre compensation, Coulomb with viscous and Stribeck models follow the GMS model in terms of accuracy. However, undesired oscillations begin in these three compensation at very low velocities.
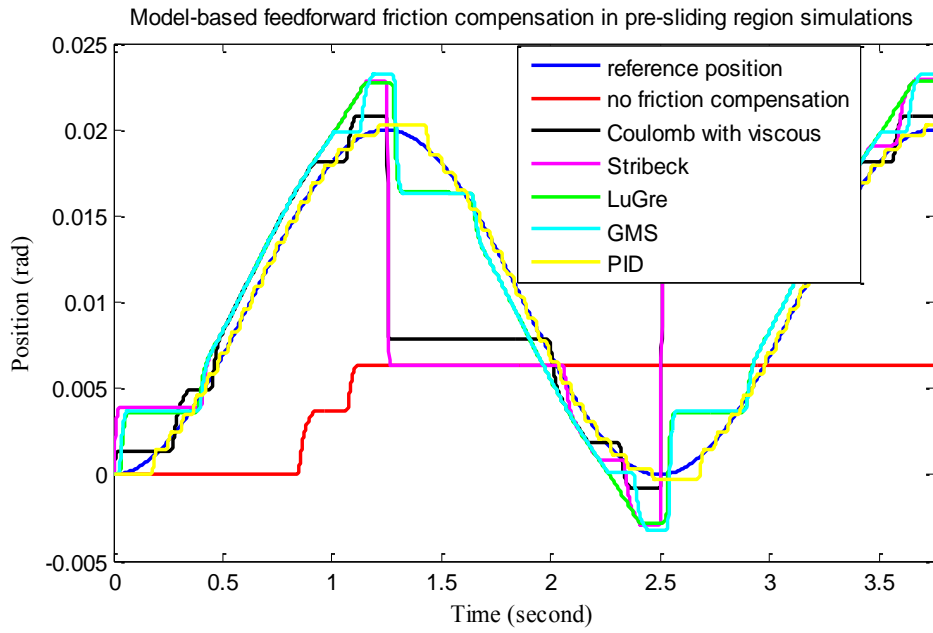
Figure 3.33. Simulated model-based feedforward friction compensation of system with negatively-perturbed actual friction in response to the low-velocity sinusoidal position input
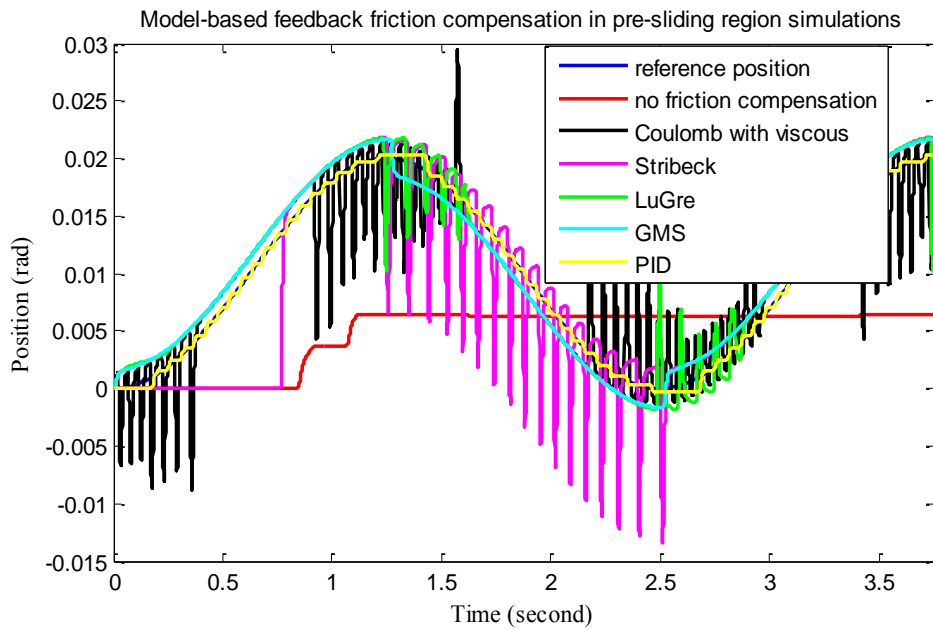

Figure 3.34. Simulated model-based feedback friction compensation of system with negatively-perturbed actual friction in response to the low-velocity sinusoidal position input

In comparison to the PID controller, the system with the PD control action with dynamic friction model-based feedforward compensations gives smoother results in non-zero velocity regions with some tracking errors due to the overcompensation of actual friction. The feedforward friction compensations with all models exhibit stick-slip behaviour near zero velocity regions more than the PID controller does. In the feedback compensation case, only the PD with GMS model gives response which is non-oscillatory and without stick-slip near zero velocities. This response is better than the response of the PID controller, but with some tracking errors which do not exist in the PID control action.

3.2.3.3.2 *Simulations for the high-velocity sinusoidal position input*

In the sliding region simulations, all four compensation models exhibit good tracking and nearly the same responses in the feedforward compensation case as in Figure 3.35. As this figure is examined in detail, actually the Coulomb with viscous friction compensation method has slightly lower peak to peak error in comparison to other models because of the jump in responses of the other compensation models at the peak of the trajectory. Again, the improvement at the response of the system without friction compensation can be observed in Figure 3.35.

For the feedback compensation case whose responses are given in Figure 3.36, the GMS compensation model again shows smooth tracking without oscillations and has the best response. Then, LuGre, Coulomb with viscous, and Stribeck friction models follow it in terms of tracking. However, oscillations begin with the LuGre model as in the model-based feedback friction compensation of all three cases of actual friction.
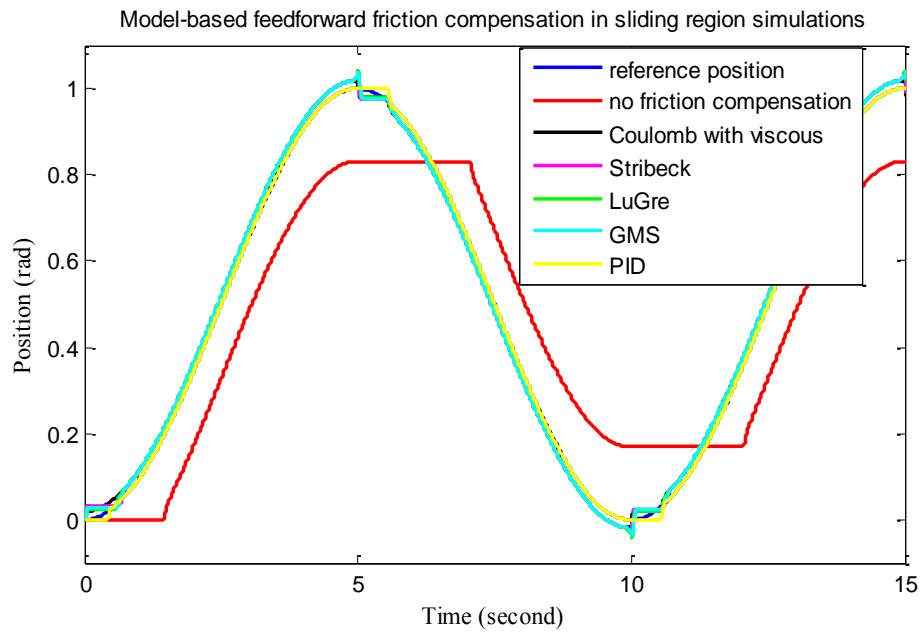
Figure 3.35. Simulated model-based feedforward friction compensation of system with negatively-perturbed actual friction in response to the high-velocity sinusoidal position input
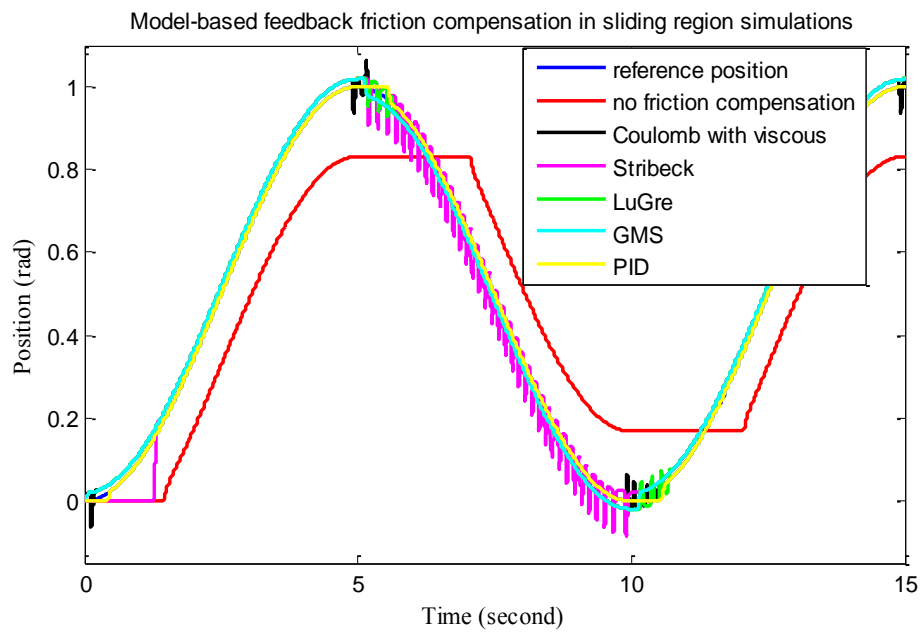
Figure 3.36. Simulated model-based feedback friction compensation of system with negatively-perturbed actual friction in response to the high-velocity sinusoidal position input

Here, the system with only PID control action and the system with PD action with feedforward friction compensation terms have similar, smooth responses including stick-slip near zero velocities. The only difference between them is that the system with friction compensation models has some tracking errors due to the overcompensation of actual friction. In the feedback compensation case, again only the PD control with GMS model gives a smooth and much closer response to the PID action. This response does not include stick-slip near zero velocities as in the PID action whereas it has some tracking errors in non-zero velocity regions, which do not exist in the PID control action.

3.2.3.3.3 Simulations for the step position input

The results of the model-based feedforward and feedback friction compensation of friction in the case of decreased actual friction are given in Figure 3.37 and Figure 3.38, respectively. Similar to the previous cases of actual friction, the PD action alone cannot compensate the actual friction adequately, and the step response is not satisfactory.

As far as the feedforward friction compensation in Figure 3.37 is considered, the responses follow the same accuracy as in the nominal friction case in section 3.2.3.1.3. That is, the static Coulomb with viscous friction model gives the best response with least steady-state error among others which are higher steady-state errors. However, it can be concluded that the addition of any friction compensation term improves the response to the way of perfect tracking.

In the feedback friction compensation simulations in Figure 3.38, the static friction models make the system oscillatory in contrast to the feedforward compensation. While the response of the system with Coulomb with viscous friction model shows high frequency oscillation about the trajectory, the Stribeck model gives oscillations having higher amplitude and less frequent than the Coulomb with viscous model with steady-state error in tracking. Both dynamic models give highly smooth responses with steady-state errors as compared to the static models. The GMS model again presents better response than the LuGre model.
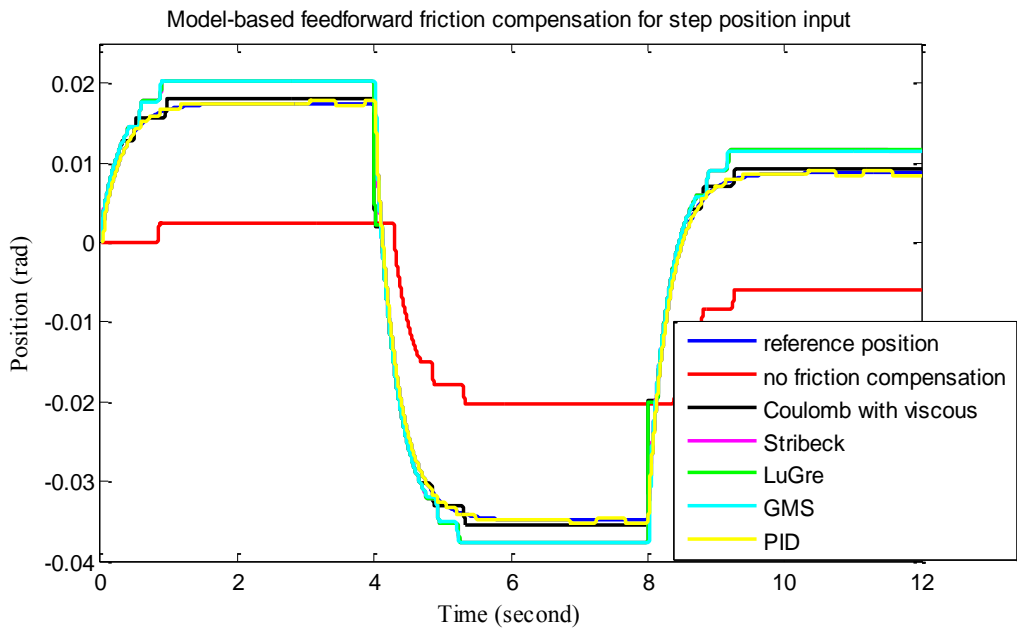
Figure 3.37. Simulated model-based feedforward friction compensation of system with negatively-perturbed actual friction in response to the step position input
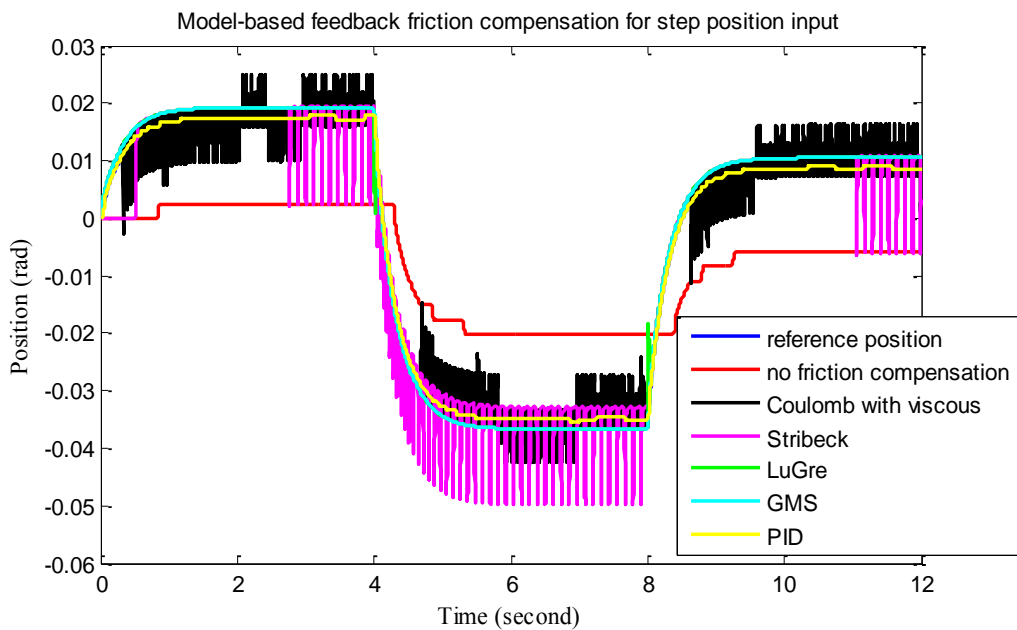


Figure 3.38. Simulated model-based feedback friction compensation of system with negatively-perturbed actual friction in response to the step position input

As in the previous case, the responses of the PD with feedforward friction compensation terms are all smooth and without stick-slip cycle at steady-state, but with some steady-state errors in contrast to the PID action with stick-slip effect. On the other hand, the PD with dynamic friction models gives smoother response than the PID action throughout the trajectory in the feedback compensation approach although they have some steady-state errors beyond the stick-slip limit cycle of pure PID control action. In this case; however, the steady-state errors of the system with dynamic friction compensation models are smaller than the feedforward compensation case.

3.2.4   Comments on the simulation results

According to the computer simulations conducted on the closed loop system with different levels of actual friction, generally the system with the GMS friction compensation model has given least oscillatory, smooth responses and the best results overall in terms of both the feedforward and feedback friction compensation. In most of the cases above, the system with the LuGre friction model-based compensation follows the one with the GMS friction model. As expected, both of these dynamic models usually give better results than the static models.

As the static models are considered, the Coulomb with viscous compensation model has generally given less oscillatory and better results than the Stribeck friction compensation model although the latter one represents the sliding region of friction more accurately as compared to the GMS model of actual friction.

Finally, the accuracy of these simulation results will be seen by experimental studies on the control system which will be described in the next chapter. Afterward, the more realistic comments can be made on the accuracy of the friction models ranging from static to complex dynamic models in approximating, modelling, and compensating the real frictional behaviour.

CHAPTER 4

EXPERIMENTAL STUDIES

In this study, an experimental set-up has been established to validate and compare the different model-based fixed parameter friction compensation techniques mentioned in Chapter 3 on a plant with friction. Moreover, this set-up is aimed to be used for looking at the accuracy of the results of the different friction compensation approaches in simulation environments. In this respect, the experimental set-up designed will be explained firstly. Then, the parameter identification of the plant will be performed to reach the value of the system inertia. After that, the two case studies with different friction characteristics will be applied to the experimental set-up and the obtained results will be presented. In each of the case study, the friction structure in the system will be examined and the parameter identification methods for four friction compensation models, which are the Coulomb with viscous friction model, Stribeck model, LuGre model, and GMS model, will be described. Substituting the identified parameters of the system and friction compensation models, position tracking experiments will be conducted to reach the performance indices of the compensation approaches. While doing this, both model-based feedforward and feedback fixed parameter friction compensation methods will be applied. Futhermore, the system will be run for three different position and velocity inputs which emphasize the pre-sliding and sliding region behaviours of friction. By means of these experiments, the effectiveness of the models will be also seen in different friction regions. By comparing the experimental results in themselves and with the simulation results, the two case studies will be completed. At the end of the chapter, a repeatability analysis for the responses will be done for a sample case chosen in order to verify the accuracy of some experimental results, and the flexibility effects in the system will be examined approximately.

4.1 Design of the test set-up

The 3D drawing of the test set-up can be seen in Figure 4.1. Note that there is an auxiliary part in the experimental set-up different from the one given for simulation studies in Chapter 3. According to the mentioned drawing, the set-up is established as a direct-drive system without any reduction element to eliminate the backlash problem. Here, the working principle of the system can be described as follows.
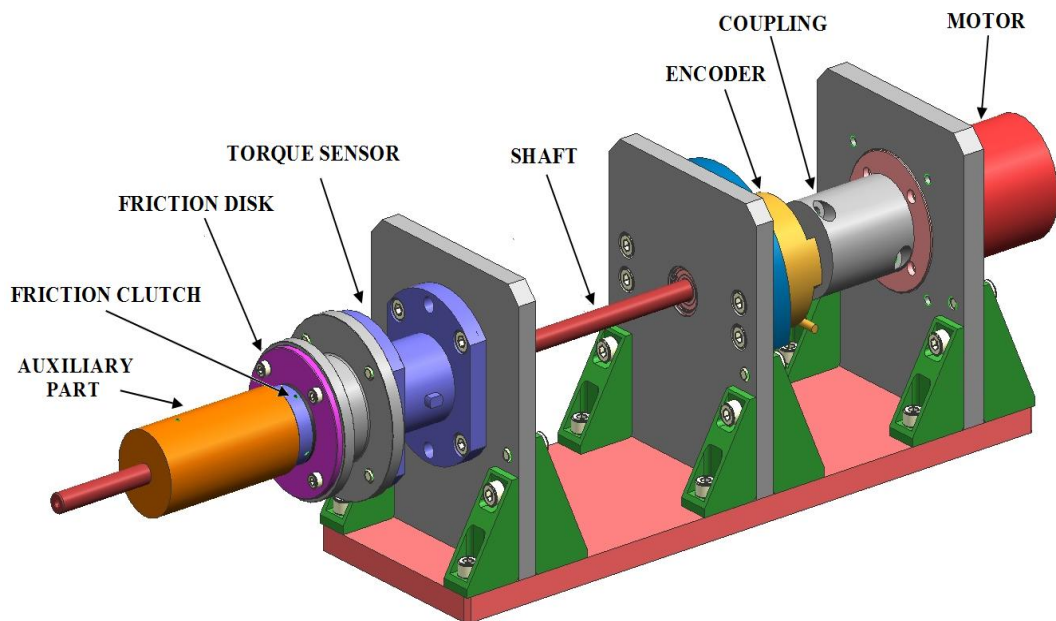
Figure 4.1. 3D drawing of the experimental set-up

The motor which is directly connected to a shaft by means of a torsionally-stiff coupling drives the system under frictional effects. Friction is intentionally applied to the system near the free end of the shaft by using a friction clutch which has an interface both with the shaft and a torque sensor. The friction produced by the friction clutch only during the rotation of the system is measured by the torque sensor. While the system rotates, the position and velocity measurements required for the control of the system are feedback to the controller by means of an incremental

encoder directly coupled to the shaft near motor rotor. Note that the system is considered to be a 1-DOF system due to the torsionally-stiff coupling used between the motor and the shaft; thus, the position measurement data required for the position control of the system are taken from the shaft side, not from the motor rotor side, of the coupling. The effects of this situation will be discussed at the end of the chapter.

As can be understood from the above paragraph, there are six main mechanical parts to be described in this test set-up, which are the motor, coupling, shaft, encoder, friction clutch, and the torque sensor.

As an actuator in the system, a housed, brushless, and permanent magnet direct current (PMDC) servo motor is selected to drive the system. Considering mainly that the friction torque level in the system does not exceed approximately 0.35 N.m and the acceleration levels will be relatively low, the motor with a torque constant of 0.22 N.m/A has been used in the system. Note that the noise from the motor affects the measurement from the encoder and torque sensor although the voltage level of the motor driver is low. Thus, the motor house and rotor are seperated from the remaining parts of the system using a non-conductive-material adapter parts between the motor and the system to further decrease the noise problem.

A torsionally-stiff coupling is used between the motor rotor and shaft in the system to transmit the rotation of the rotor part of the motor to the shaft. The coupling can compensate for misalignments between the motor rotor and shaft due to the mechanical assembly of the system to some extent in the axial and radial directions. However, it is torsionally-stiff to make a torque transmission without a loss as much as possible. In this respect, the coupling with a torsional stiffness of 17800 N·m/rad has been selected.

A shaft with a diameter of 12 mm is used in the system in order to intentionally apply an additional friction torque on the system. It is a stainless steel precision shaft with high surface quality.

In the system, an incremental, hollow-shaft, rotary quadrature encoder with a maximum resolution of 1.000.000 (20 bit) pulse per revolution (PPR) is used to measure the position and velocity of the shaft (assuming rigid). The resolution of the

encoder has been selected as high as possible since the identification of the pre-sliding region of friction requires the measurement of very small angular positions in the level of about 10^{-6} radians and there is not a reduction part in the system to be used to increase the resolution of the position measurement.

A hollow-shaft mechanical clutch is used in this test set-up to apply a friction torque on the system. This clutch can give a friction torque until the level of 10 N.m. The produced friction torque is manually adjusted by tightening a nut which changes the normal force on the friction disk of the clutch by means of two spring. Note that this clutch originally has a backlash in it due to its mechanical assembly. In order to eliminate the backlash as much as possible, an adapter similar to the original part of the clutch, but without a backlash, has been produced and used in the clutch instead of its original part.

As an another transducer in the system, a reaction-type, hollow-shaft torque sensor is used to measure the friction torque coming from only the friction clutch. This sensor measures the torque based on the strain gages in it and reads the torque values lower than 12 N.m. It is a reaction-type sensor since one end is fixed to the system while the other end rotates according to the friction applied by the clutch during the system run.

In addition to these parts, there are two ball bearings and retaining rings in the system to support the shaft. Thus, the total friction in the system actually comes from mainly the friction clutch, ball bearings, motor bearings, and encoder bearings. Furthermore, there is an auxiliary part made from aluminium and centered from the free end of the shaft in front of the friction clutch in order to press the friction clutch onto the surface of the friction disk more uniformly.

According to the selections mentioned above, the assembly of the experimental set-up is demonstrated in Figure 4.2, and the technical drawing which shows some critical dimensions is given in Figure 7.1 in Appendix.

Except from the mechanical parts, the electronic parts of the system are composed of a motor driver, signal conditioner circuits for the torque sensor, counter/timer card for encoder, an analog input/output card for data acquisition, and a PC (controller).

The servo motor is driven by a digital amplifier operating on the current mode. The amplifier can be operated in the supply voltage range between 20 and 60 VDC and controls the current to the motor by means of Pulse Width Modulation (PWM) signal. The voltage range of amplifier is selected relatively small to decrease the noise in the current output of the motor and vibration in the rotor part of the motor. Moreover, the continuous current output of the amplifier, which is 6 Amperes, are sufficient for the friction level in the system.
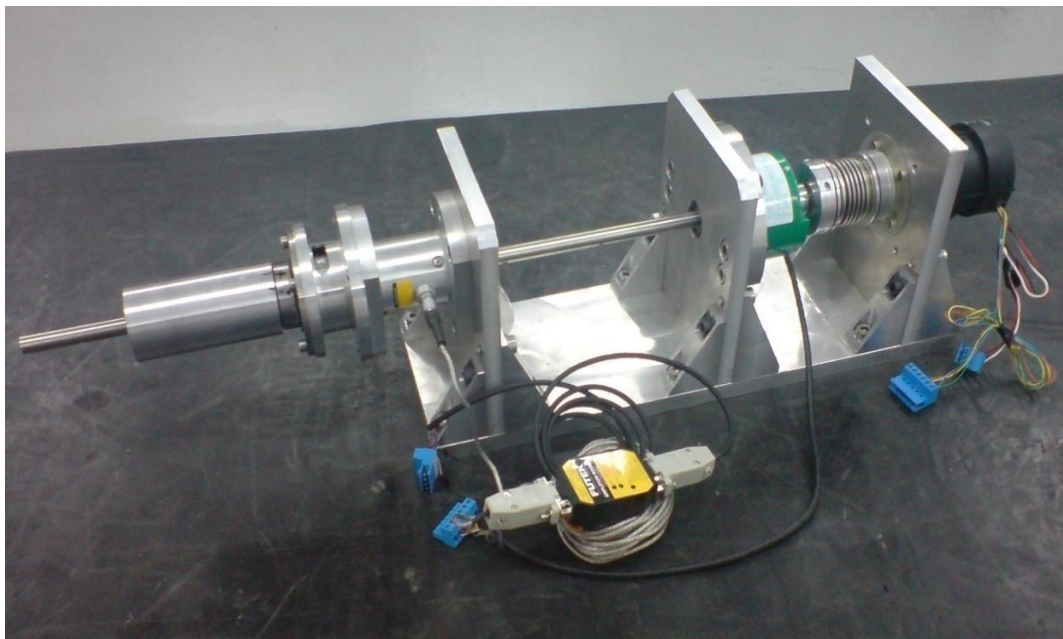
Figure 4.2. Experimental set-up

The signal conditioner unit for the torque sensor is used to regulate and increase the voltage level from the sensor in order to be read by xPC target.

The counter/timer card (data acquisiton card) for the encoder is used to count the encoder pulses, and then, send the encoder readings to the PC (controller). This card can make a quadrature reading and give an output with 32 bit resolutions, which are suitable for the encoder used in the test set-up.

In the system, an analog input/output card (data acquisition card) is used to convert the digital data from the PC to the analog data and vice versa. Also, it

processes the signals in a suitable manner for rejecting noise and other disturbances on signals. Here, this card has 8 analog input channels, 2 analog output channels, and 8 digital I/O channels for data transmission.

Finally, a PC is utilized for the implementation of control algorithms and off-line data processing. Here, the PC produces a control signal (current signal for the motor) according to the measured data from the encoder and torque sensor, and sends this signal to the motor amplifier, which in turn produces current for the motor. While doing this real time applications, the data transmission and timing between the PC, sensors, and amplifier are managed by the xPC target computer by using the xPC target module of MATLAB® SIMULINK® installed in that PC.

As a whole, both the mechanical and electronic components used in the experimental set-up and their properties are summarized in Table 8.

Table 8. Components used in the experimental set-up

Components	Properties	
Servo motor (RBEH-01516-A00)	Torque constant	: 0.22 N·m/A
	Continuous stall torque	: 1.085 N·m
Torsionally-stiff coupling (TOOLFLEX 30S)	Torsional stiffness	: 17800 N·m/rad
	Torque capacity	: 35 N·m
Shaft (SKF precision shaft)	Material	: Stainless steel
	Diameter	: 12 mm
	Length	: 600 mm
Encoder (GPI, R176H-05000Q-5L50-BN18SP-24MN)	Resolution	: 10^6 counts/rev
	Maximum speed	: 360 rpm
		(after quad decode)
Friction clutch (MAYR, 0-106.110)	Torque	: Upto 10 N·m
Torque sensor (FUTEK, TFF425)	Torque capacity	: ±12 N·m
Ball bearings (6001-2Z/C3) and internal rings	-	
Amplifier (AMC, B12A6)	Supply voltage	: 20 - 60Volts
	Continuous current	: 6 Amperes
Counter/Timers card (NI PCI-6602)	Resolution	: 32 bits
	Measurement type	: Quadrature
	Max. count frequency	: 80MHz
Multifunction DAQ (NI PCI-6030E)	# of channels	: 8 AI, 8 DIO, 2 AO
	Resolution	: 16 bits
	Update rate (maximum)	: 100 kS/sec

4.2 Identification of the system inertia

Recall that the inertia of the system has been found in section 3.2.2.2 by using the catalogue values, and then, used in linear controller design. In practice; however, the inertia value of the real system can deviate from the theoretical one. Thus, it should be identified experimentally to have a more accurate description of the system together with a more precise control of the system required for both the identification and compensation of friction.

In order to identify the system inertia, open loop experiments on the system are evaluated such that the open loop system is assumed to be composed of an inertia and effective linear viscous friction only. During the open loop experiments, an input current signal is applied to the system and the position response of the system is measured. According to the input-output relationship obtained, the frequency response function (FRF) of the plant is formed.
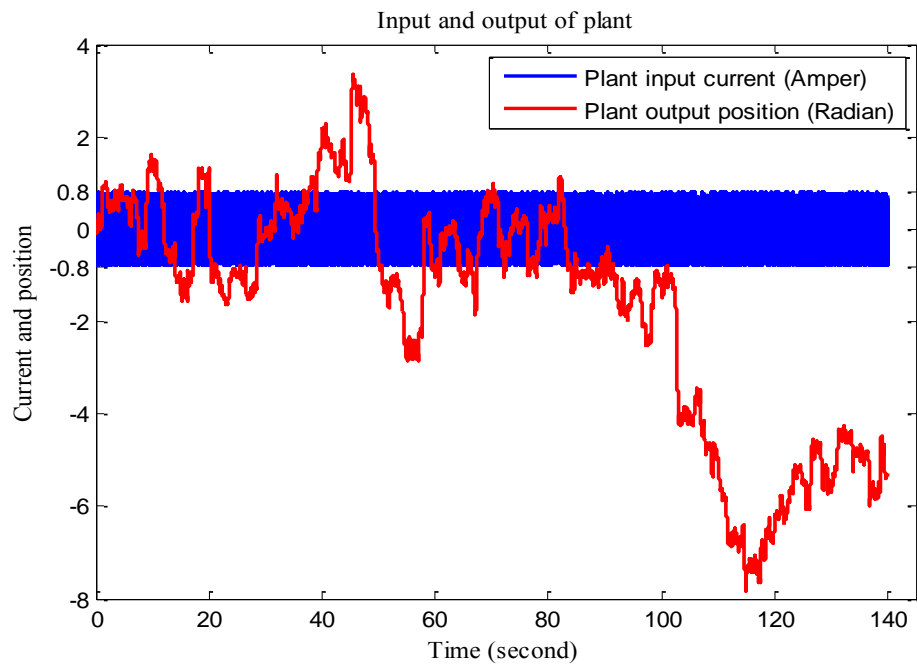
Figure 4.3. Input and output of the open loop experiment

In order to do this, open loop experiments are repeated with different input amplitudes. Both 0.8 A and 1.6 A random input currents are applied to the open loop

system. As an example, 0.8 A random input and the corresponding output of the system are shown in Figure 4.3. While obtaining the FRFs of the system, the measured data are windowed with an hanning window and the corresponding FRFs of the open loop system are formed in the frequency range of 0.2-100 Hz. In this respect, the FRFs of the open loop system are given in Figure 4.4. One can see from this figure that the open loop system has an elastic mode near 85 Hz. This unexpected mode is considered to arise from the encoder assembly instead of the structure of the system whose analysis is simply given in section 4.5. Then, the successive inertia identification is done on the 0.4-25 Hz frequency range of Figure 4.4, which is a suitable interval for the experiments in this thesis, using the system identification tool of the MATLAB$^\circledR$ SIMULINK$^\circledR$. According to the identification, the FRF of the resulting identified plant is also shown in Figure 4.4.
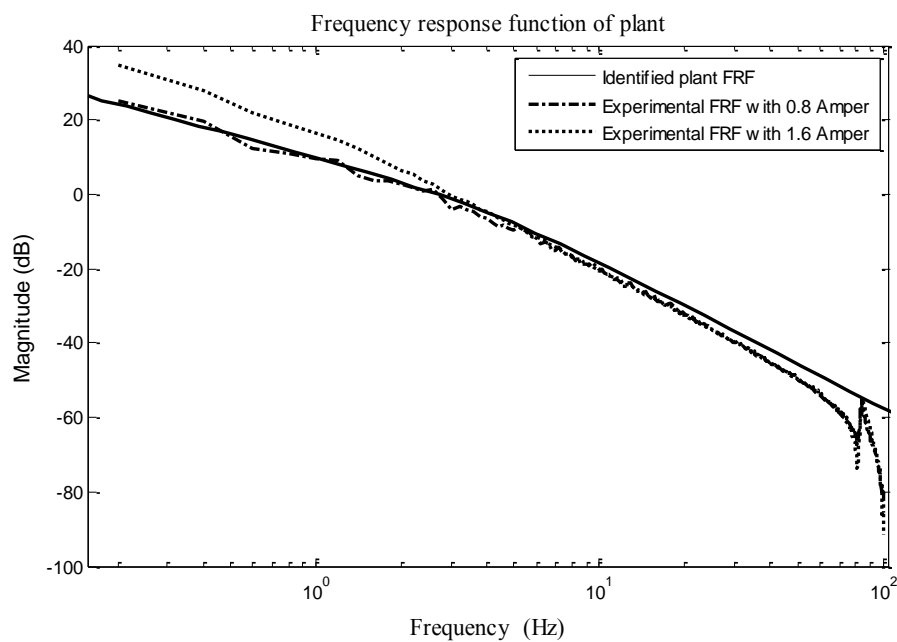
Figure 4.4. FRFs of open loop experiments and identified system

As you can see from the FRFs, the system responses are different from each other in the range of low frequencies due to the nonlinear frictional effects whereas they are closer to each other in the range of relatively high frequencies, indicating

98

approximately the same inertia value. According to the results, the identified inertia is given as $J = 4.2757x10^{-4} \, kg.m^2$. This value is %10 greater than the theoretical value found.

4.3 Case studies

4.3.1 Dry friction case

In this case study, the friction clutch applies completely dry friction to the friction disk. That is, there is no lubricant or grease between the friction clutch and the friction disk. The lubricants come from the shaft supporting bearings, motor bearings and encoder bearings. According to this condition, the friction characteristic of the system will be examined both in the pre-sliding and sliding regions, and the parameters of the different friction models will be identified experimentally. Then, the identified friction models will be used in friction compensation of the system with dry friction.

4.3.1.1 Identification of the parameters of the friction compensation models for dry friction case

4.3.1.1.1 Break-away torque experiments

To find the break-away torque of the system, open loop experiments are done. During these experiments, the current into the motor is gradually ramped up to find the break point. When the velocity of the system is greater than a defined velocity level, i.e. when a considerable motion is seen, it is considered that the transition from stick to slip occur and the torque input at this time is treated as a break-away torque of the system.

As will be mentioned in the next section, the position dependency of the friction torque during the rotation of the system is considerable. Because of this reason, the break-away torque also changes with position. Thus, to reach the break-away characteristic of the system and find the average value of it, the aforementioned break-away experiments are done with an angle interval of 10˚ through 360˚ rotation of the shaft. In this respect, the results of these experiments and the average of the

break-away torque for positive velocity direction can be seen in Figure 4.5. In this figure, measurement data from both the motor current and torque sensor are shown. It can be extracted that the trend of the break-away friction torques follow approximately the same shape for both the motor and torque sensor measurements.

Since the aim is here to model the total break-away torque, the measurement from the motor side will be taken as the break-away torque of the system and its average value will be used as the friction torque at zero velocity in the identification of the sliding region parameters. In this respect, the average value of the break-away torque measured from the motor current is 0.2951 N·m and given in Table 9 as F_S parameter.
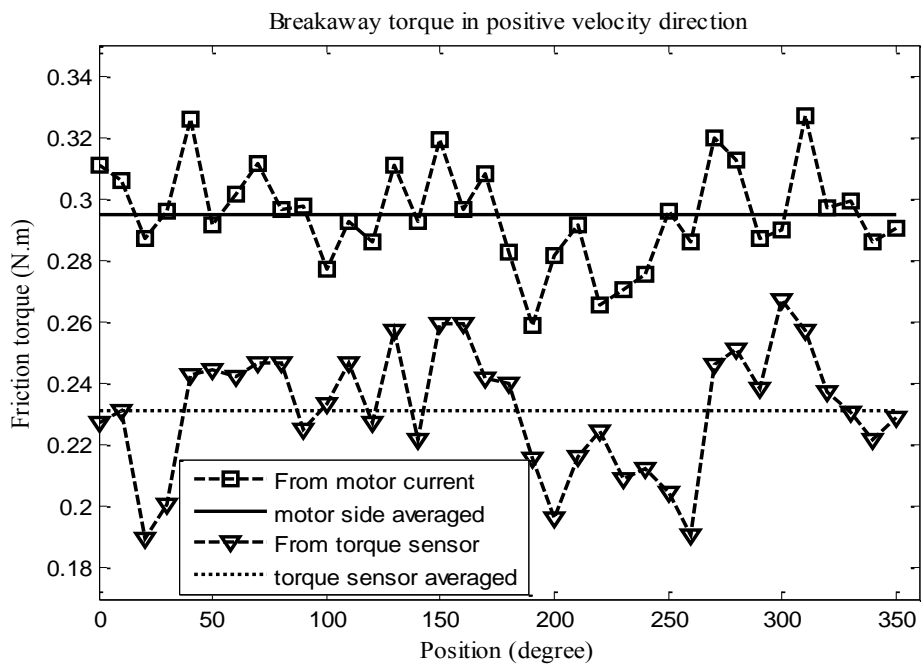
Figure 4.5. Break-away torque measurements both from the motor and torque sensor in positive velocity direction for dry friction case

4.3.1.1.2 Sliding region experiments

As mentioned before, the friction torque in sliding region is found by constant velocity (or ramp position input) experiments. By forcing the system to move with constant velocity, the inertial effects are decreased to zero as much as possible, thereby making the friction torque equal to the motor torque, which in turn equals the motor current multiplied by motor torque constant. Here, a robust H_∞ controller whose input and output are position error and motor current respectively, is applied to the open loop system to track the ramp position input with different velocities. In this respect, the velocities applied to the system both in the negative and positive directions are given in (4.1). Through the experiments, these velocities are applied to the system in positive and negative directions starting from the greatest one.

$$\dot{\theta} = (1.4; 1.2; 1.0; 0.8; 0.6; 0.5; 0.4; 0.3; 0.2; 0.1; 0.08; 0.06; 0.04; 0.02) \quad (rad/s) \text{ (4.1)}$$

During the experiments, it is seen that the friction torque on the contact surface of the clutch-disk system is dominantly position dependent. This condition requires the averaging of the friction torque data for all constant velocities for the identification of sliding region curve. Therefore, all constant velocity experiments are done for one full revolution of the shaft to obtain an accurate averaged friction torque measurement. Moreover, the shaft is turned 380° during the experiments to avoid from the transients in the first 20°-angle span. According to the experiments, the position dependency of friction torque for different positive and negative constant velocities are shown in Figure 4.6 and Figure 4.7, respectively. Note that these measured data are from the torque sensor and filtered to show the position dependency clearly. If one examines both of the figures, the maximum peak to peak deviation in friction torque can be seen to be 0.05 N.m.
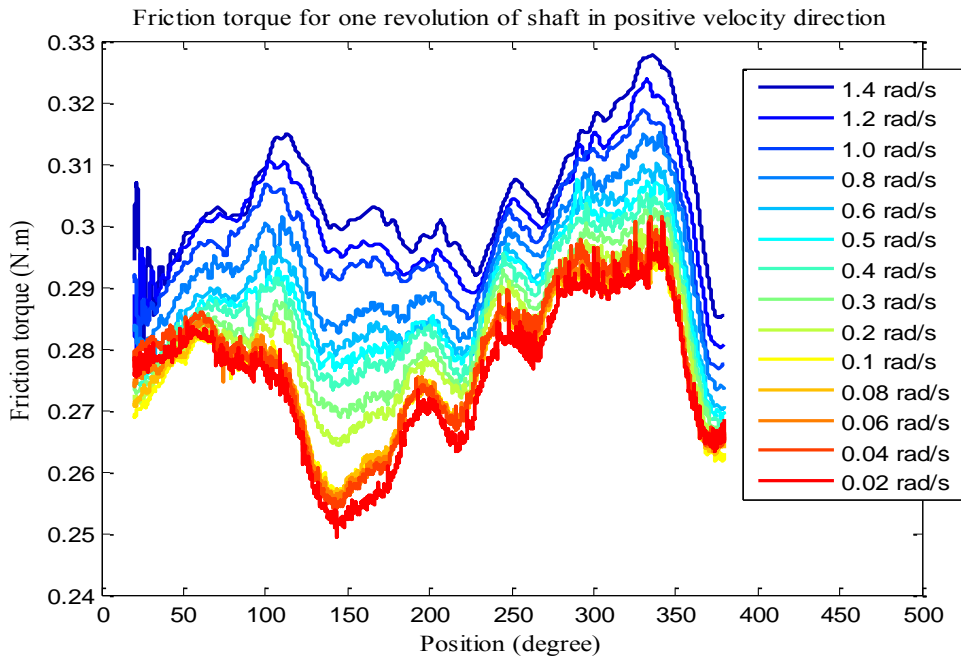
Figure 4.6. Position dependent friction torque for positive velocities for dry friction case
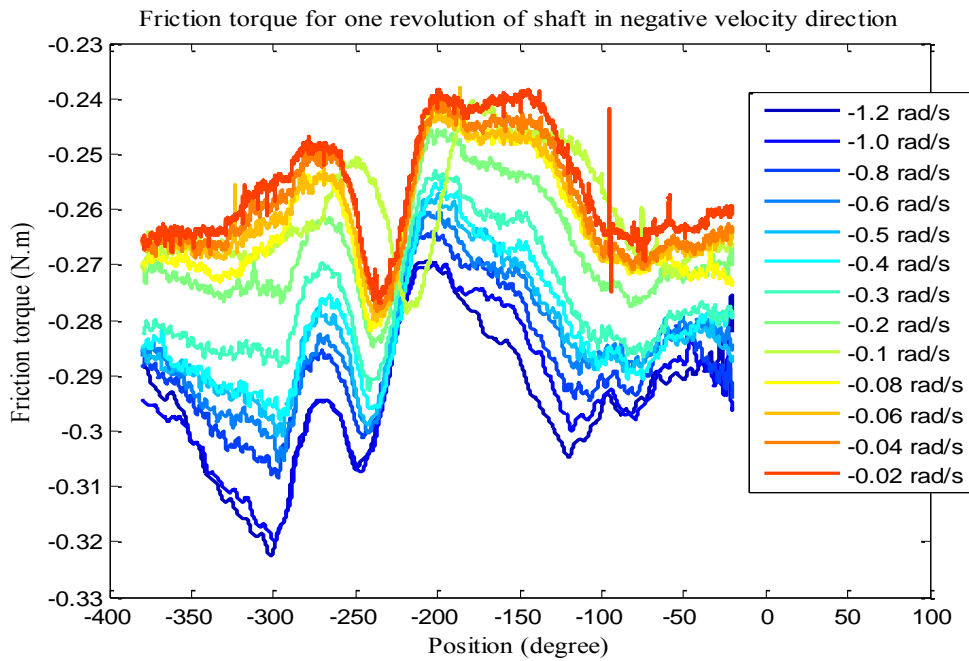
Figure 4.7. Position dependent friction torque for negative velocities for dry friction case
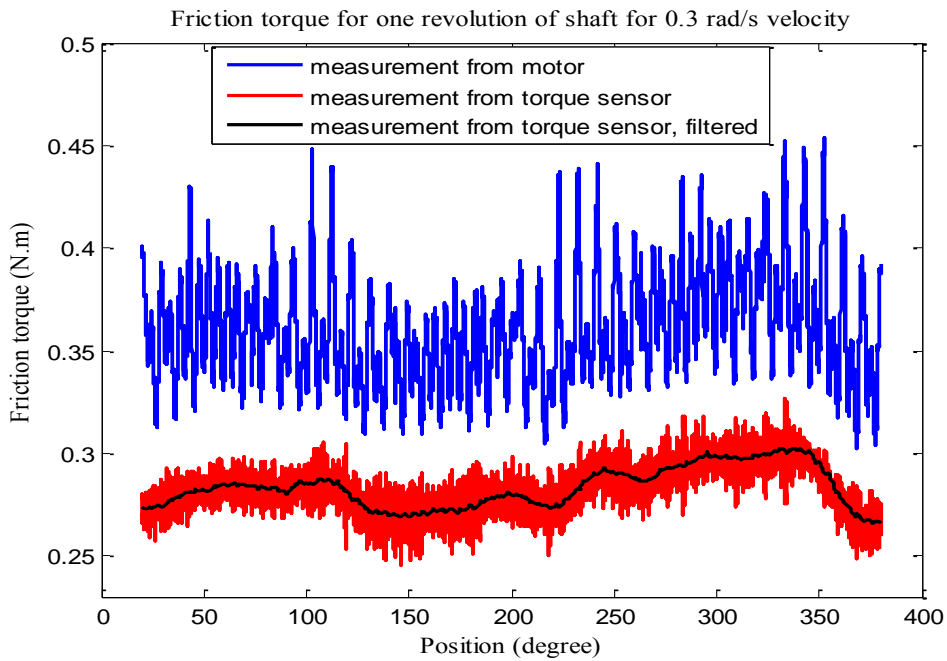
Figure 4.8. Friction torque from motor current and torque sensor for dry friction case

Recall that the friction torque not only comes from the friction clutch, but also from the bearings in the system. Hence, the total friction torque should be identified for the accurate friction compensation task. This can be obtained from the motor torque, i.e. motor current or control input. As a result, to find the friction torque for any constant velocity given in (4.1), the motor torque (current, control input) will be averaged for one revolution of the shaft in that velocity. As a demonstration, the motor torque measurement, the torque sensor measurements with and without filter are shown in Figure 4.8 for 0.3 rad/s constant velocity experiment. Note that the aim of using the torque sensor measurements in figures here is to see the correspondence of the shape of the data obtained from the motor current to the friction torque data from the sensor.

Now, identification of the friction in sliding region is done by using the average break-away torque from 4.3.1.1.1 for zero velocity together with the average friction torque values obtained here for different velocities. The identified steady-state curve of friction in sliding region as defined in equation (2.6) is shown only for positive velocities in Figure 4.9.
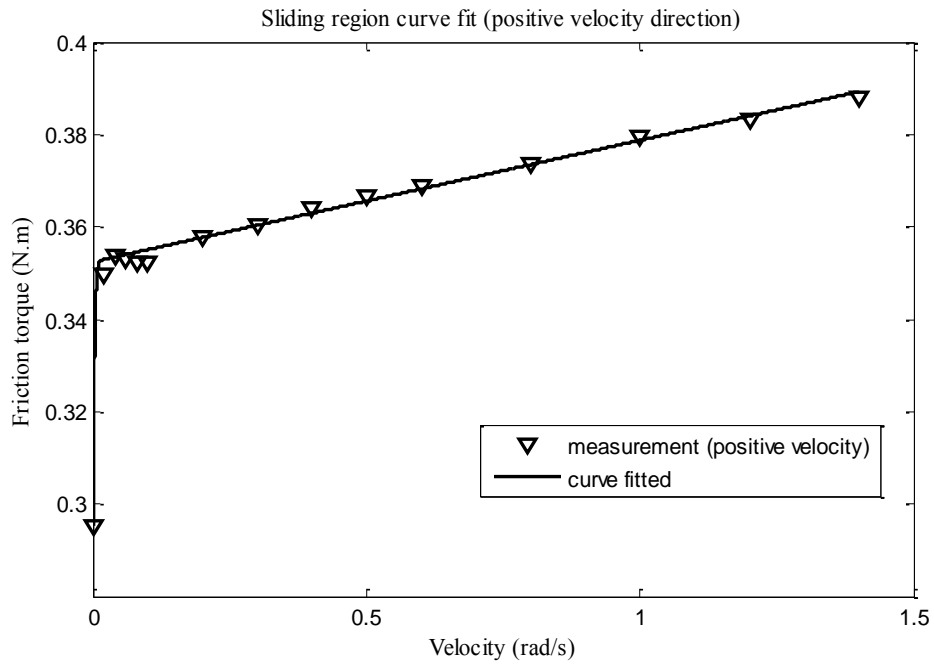
Figure 4.9. Sliding region curve fit to the measurements in positive velocity direction
for dry friction case
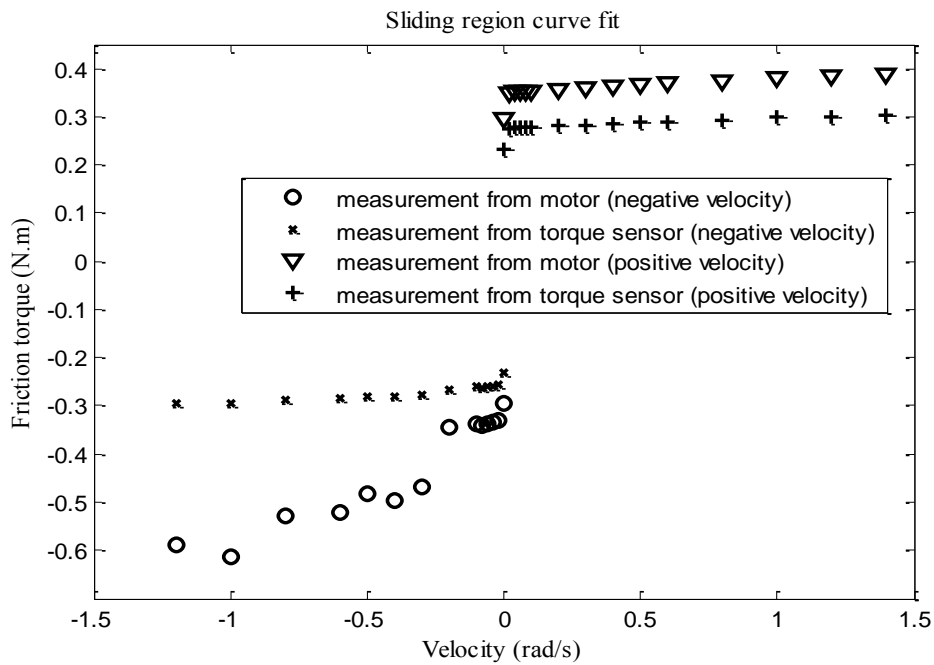
Figure 4.10. Sliding region measurements from motor current and torque sensor in
positive and negative directions for dry friction case

In Figure 4.10, friction torque measurements both from motor current and torque sensor are shown for negative and positive velocities. It is seen that the trend of the friction curve for positive velocities is the same for motor and torque sensor measurements. However, this condition is not kept for negative velocity direction. The trends of the friction torques for the motor and torque sensor data in negative velocity direction follow the same path only in low velocities up to 0.2 rad/s. Additionally, the trend and amplitude of the friction data from torque sensor are the same for both the negative and positive velocity directions. Due to these findings, the curve fit for positive velocity direction will be used bidirectionally in the model-based friction compensation experiments.

It is useful here to state that there is an approximately constant difference between the friction torque of the torque sensor and motor torque (current) measurements as seen in Figure 4.10. This behaviour is similar to the Coulomb with viscous friction level. Since the difference is resulting from the bearings in the system, it can be concluded that the friction in bearings can be treated as it is composed of Coulomb and viscous friction levels.

Note that all static and dynamic friction models uses the same curve fit above to describe the sliding region of friction. Thus, all have the same sliding region parameters and these parameters are given in Table 9.

4.3.1.1.3 Pre-sliding region experiments

The pre-sliding region experiments are conducted to obtain the hysteresis curve between the friction torque and position in pre-sliding region. Although the hysteresis curve is regarded by the dynamic LuGre and GMS friction models, the identification process here is only valuable for the GMS friction model because of the direct usage of the identified hysteresis curve parameters.

To obtain the hysteresis curve, open loop experiments are performed on the system. By applying a sinusoidal torque input whose maximum value is lower than the average break-away torque obtained from the motor current (0.295 N.m) in section 4.3.1.1.1 and measuring the corresponding position output of the system, the desired hysteresis curve is obtained. In this respect, the three cycle of the input in

equation (4.2) is applied to the open loop system and the resultant measured hysteresis curve is demonstrated in Figure 4.12.

$$\dot{\theta} = 0.18\sin(0.1x2\pi t) \qquad (rad/s) \tag{4.2}$$

For the identification of the hysteresis curve parameters of the GMS model, 3 and 4-element GMS models are selected for comparison. Since the hysteresis curve fit of the GMS model originally includes a transient at the start of the curve, the identification process is only performed on the 2nd cycle of the measured data. According to the description, the measured and identified hysteresis curves for the 2nd cycle are given in Figure 4.11. As can be seen from Figure 4.11, there is not much difference in identified hysteresis curves of 3 and 4-element GMS models in comparison to the measured one. Hence, the 3-element GMS model is adequate for the modelling of hysteresis in pre-sliding and is used for compensation.
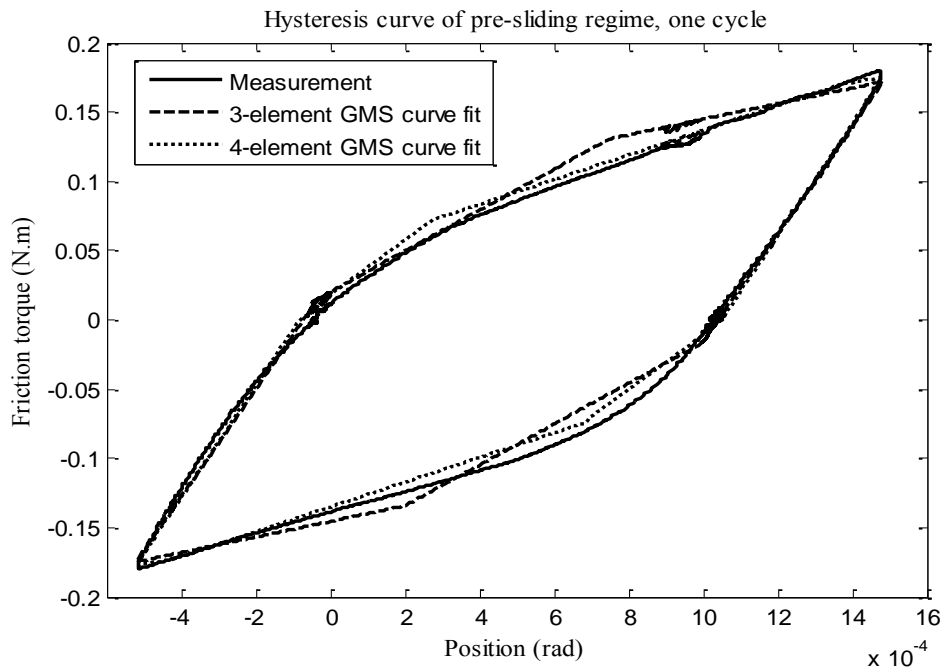
Figure 4.11. Measured and identified hysteresis curves for the 2nd cycle of input for dry friction case
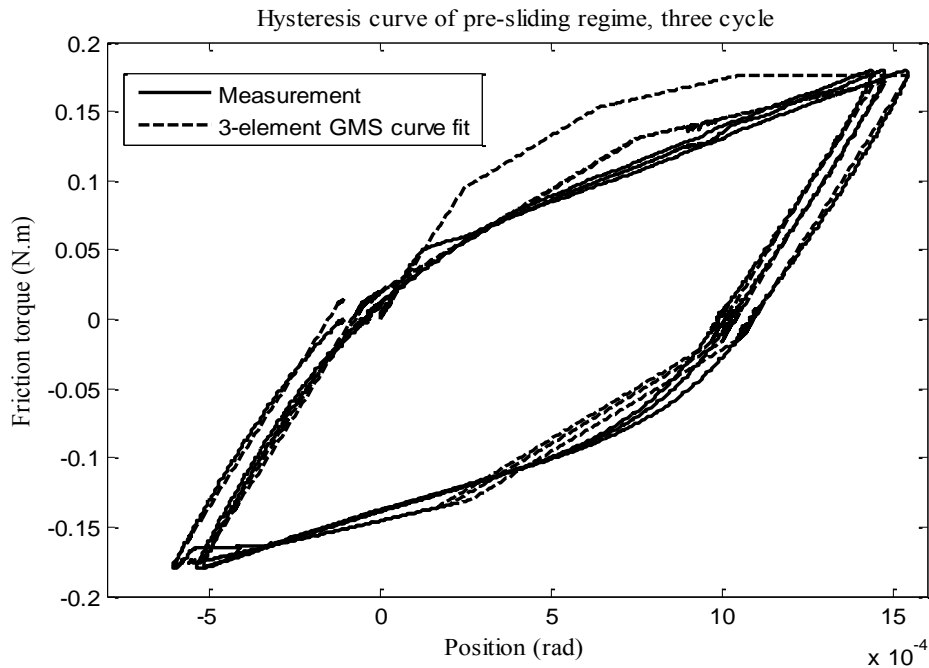
Figure 4.12. Measured and identified hysteresis curves for dry friction case

In this respect, the identified hysteresis curve for the 3-element GMS model and measured hysteresis curve can be seen in Figure 4.12 for the whole cycle of the input. According to the identification, the corresponding parameters of the GMS model are given in Table 9.

4.3.1.1.4 *Identification of the dynamic parameters of the LuGre model*

The dynamic parameters of the LuGre model are important for the characteristic of the stick-slip motion and transition from stick (slip) to slip (stick) motion of the LuGre model. The two dynamic parameters of the LuGre model, i.e. σ_0 and σ_1, are obtained by open loop experiment. To do this, an input torque including stick-slip motion (causing velocity reversals) is given to the open loop system and the output position is measured [14]. On the other hand, the open loop system with the measured inertia and with the LuGre model as the actual friction in the system is run in simulation environment with the same torque input. Then, the dynamic parameters are found by comparing the measured position of the real system with the position response of the simulated system.

Comparison of the measured and simulated positions in response to sinusoidal torque input
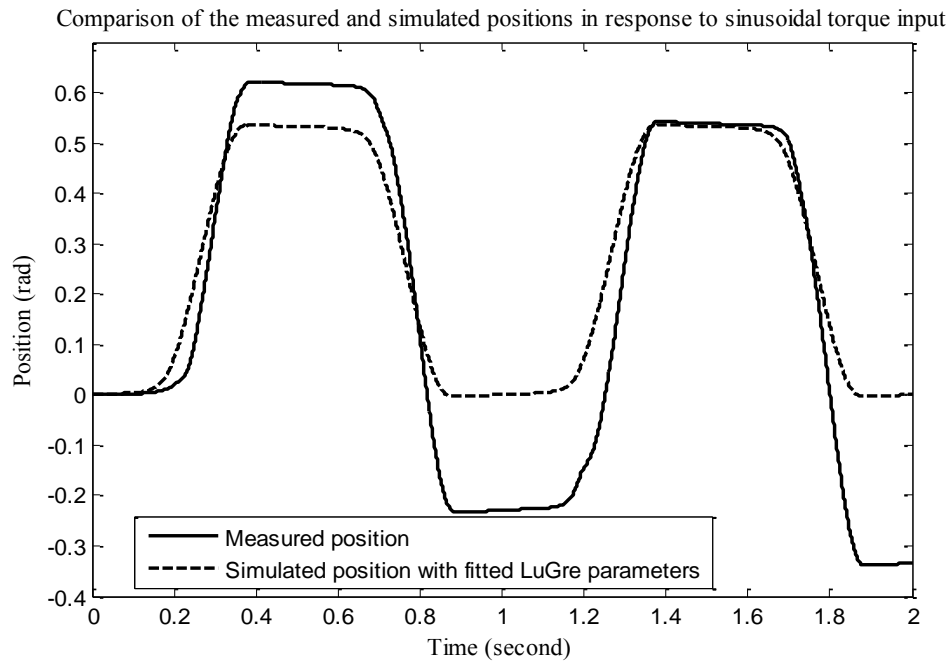
Figure 4.13. Comparison of the measured and simulated positions of the open loop system for dry friction case

Here, a sinusoidal torque input whose amplitude is 0.45 N.m and whose frequency is 1 Hz is given to the open loop system. Since the friction in the system is highly position dependent, the measured position response is not much repeatable. Hence, the best choice of the responses and identifications is tried to be done among different responses by using the MATLAB® SIMULINK® Response Optimization tool. According to the identified parameters, the measured and simulated responses of the system are figured out in Figure 4.13, and the values of the dynamic parameters of the LuGre model are given in Table 9.

4.3.1.1.5 *Identification of the attraction parameter of the GMS model*

The attraction parameter of the GMS model is related to the hysteresis between the velocity and friction torque in sliding region, and directly determines the rate at which the GMS model follows the steady-state friction curve in sliding region.

The identification of the attraction parameter C is normally done according to the hysteresis behaviour in sliding by forcing the open loop system to follow a sinusoidal velocity profile in the range of Stribeck effect, and then measuring the

friction torque. However, we know from section 4.3.1.1.1 that the break-away torque is lower than the Coulomb friction torque, and thus, Stribeck effect and hysteresis behaviour in sliding region are not possible to mention. Moreover, the highly position dependent structure of the friction does not permit us to see a usable hysteresis curve measurements. Therefore, the attraction parameter will be tuned manually.

To determine the attraction parameter here, a 5 rad/s constant velocity signal is applied to the GMS friction model with the identified pre-sliding and sliding region parameters and responses are examined in simulation environment. The *C* parameter of the model exhibiting first response without overshoot is chosen as the identified attraction parameter. For comparison purpose, the plots showing the responses of the GMS models with different attraction parameter values are given in Figure 4.14. According to this selection method, the identified attraction parameter value is given in Table 9.

Friction torques of GMS model for different C values for 5 rad/s constant velocity input
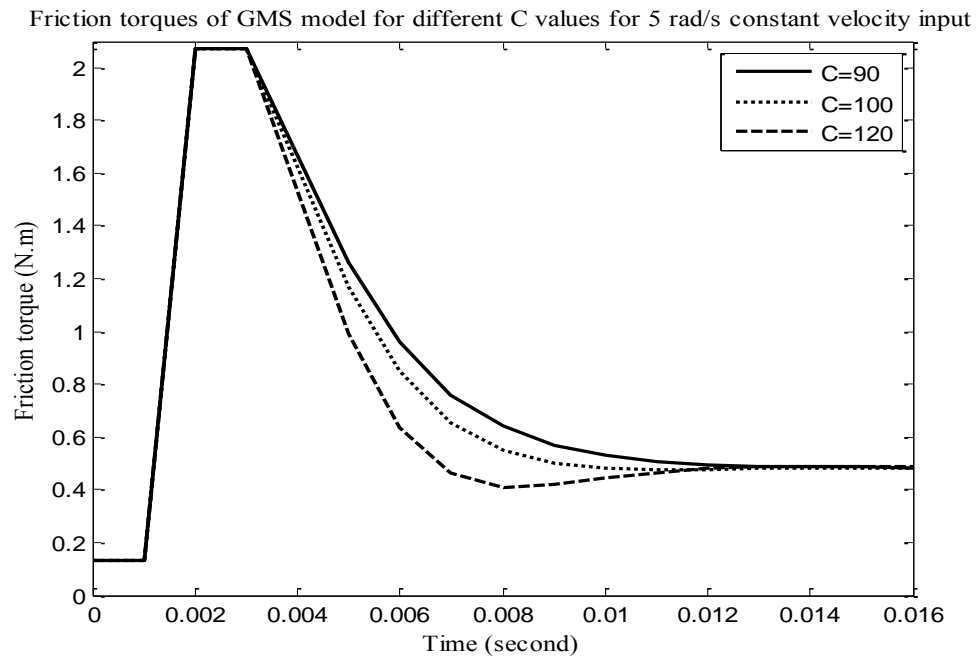
Figure 4.14. Comparison of GMS friction model responses to the 5 rad/s constant velocity for different C values for dry friction case

Table 9. Identified parameters of the friction compensation models for the case of dry friction

Pre-sliding region parameters			Sliding region parameters		
Parameter	**Value**	**Unit**	**Parameter**	**Value**	**Unit**
Stribeck friction model			F_S	0.2951	N·m
k	3.5×10^4	N·m·s/rad	F_C	0.3524	N·m
LuGre friction model			v_s	0.003	rad/s
σ_0	120	N·m/rad	δ_s	1.1	-
σ_1	0.01	N·m·s/rad	σ_2	0.0263	N·m·s/rad
GMS friction model					
k_1	240.6583	N·m/rad	α_1	0.1983	-
k_2	91.2208	N·m/rad	α_2	0.4008	-
k_3	56.2779	N·m/rad	α_3	0.4008	-
-	-	-	C	90	N·m/s

4.3.1.2 Experimental results of the friction compensation of the closed loop system with dry friction

In this section, the experimental results of the model-based friction compensation approaches will be given. The responses are examined and compared among each other. Although the friction characteristic in sliding region does not correspond to the one used in simulations in terms of the friction curve shape and amplitude, the comparisons between the experimental results and simulated responses will be made at least in terms of the trend of the response. In all of the experiments, the PD and PID control actions with the same parameters as in the simulation studies in Chapter 3 will be used as linear control terms in the closed loop system. In order to see the effectiveness of the model-based friction compensation techniques more clearly, a PID control strategy with friction compensation terms

added will be applied to the experimental set-up different from the simulation studies. Furthermore, an integration time step of 10^{-3} seconds will be used in all experiments for the dry friction case.

4.3.1.2.1 *Response to the low-velocity sinusoidal position input*

For this low-velocity input which emphasizes dominantly the pre-sliding region behaviour of friction, the experimental model-based feedforward and feedback friction compensation results are given in Figure 4.15 and Figure 4.16, respectively. As can be seen from these figures, the system without any friction compensation term catches the trend of the position trajectory in a deformed way and with a smaller amplitude.

In the feedforward compensation in Figure 4.15, all the responses with and without compensation terms exhibit chatterring although they all use a smooth desired velocity profile. This is due to the high bandwidth of the PD controller. As can be seen, LuGre and GMS friction model compensation follow a similar path for the responses in comparison to the Coulomb with viscous and Stribeck friction models, which in turn give similar responses. The advantage of the use of dynamic models can be seen from the continuous response characteristic at the peak of the trajectory where the Coulomb with viscous and Stribeck friction models show a discontinuous-like behaviour because of being near to the zero velocity region. As a whole, the responses are not satisfactory; however, it can be concluded that the dynamic models give much smoother and closer responses to the input trajectory than the static models. As far as the simulation results of the low-velocity sinusoidal input in Figure 3.21, Figure 3.27, and Figure 3.33 are examined, the experimental results are seen to be close to the negatively-perturbed actual friction case in Figure 3.33. This corresponds to the overcompensation of friction and it can be expected due to the highly position dependent structure of friction in the experimental set-up.

On the other hand, the feedback compensation results in Figure 4.16 show exteremely high oscillations in the response. Here, the Coulomb with viscous and Stribeck friction models give closer response to each other. This is expected because there is no Stribeck effect in this dry friction case as found in previously. The

dynamic LuGre model gives less oscillatory response than the static models. The GMS model in this case makes the system unstable. Because of this, the position measurement is filtered with a 10 Hz low-pass butterworth filter before the velocity is calculated and this velocity enters to the GMS model. According to the results, the GMS model shows a small amplitude chattering; however, the tracking and shape of the trajectory become worse. Thus, the LuGre model is said to exhibit a better response than the others. In comparison to the simulation results in Figure 3.22, Figure 3.28, and Figure 3.34, the real system shows expected oscillations but with higher amplitude. Also, the GMS model which gives the best results in simulations can not give a smooth and non-oscillatory response here. Again this is due to the friction structure of the system as well as the high gain of the PD control action.

As can be seen from Figure 4.15 and Figure 4.16, the response of the system with the PID control having the same bandwidth as the PD control action are extremely oscillatory beyond the responses of the compensation models. Although this is an unexpected condition as compared to the simulations where PID action exhibits stick-slip cycles, the system follows the input trajectory trend. Thus, to have a more smooth responses, the gains (bandwidth) of the PID action should be decreased, which will be done in the grease-added friction case.
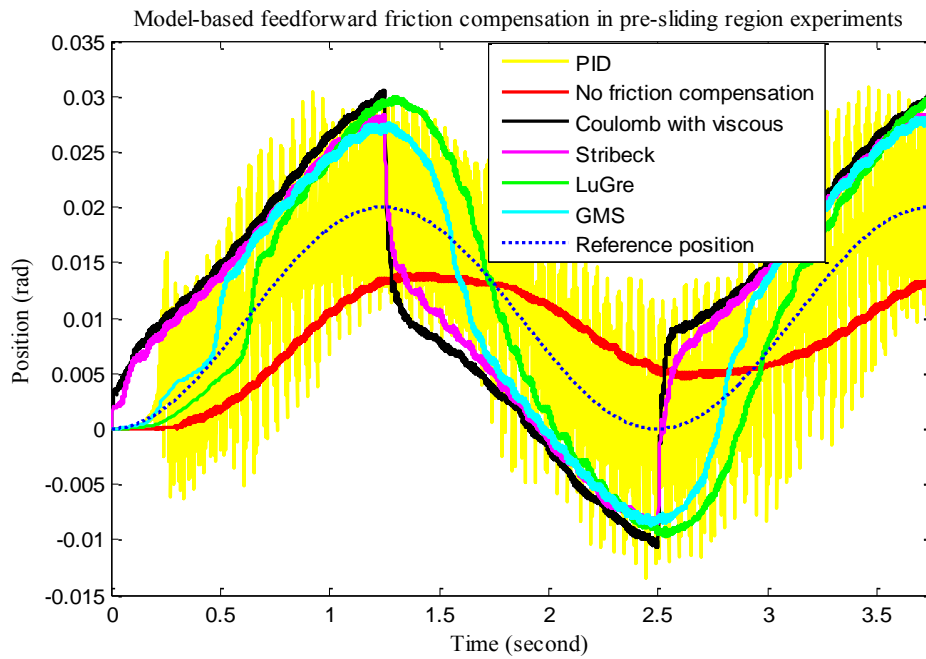
Figure 4.15. Experimental model-based feedforward friction compensation of system with dry friction in response to the low-velocity sinusoidal position input
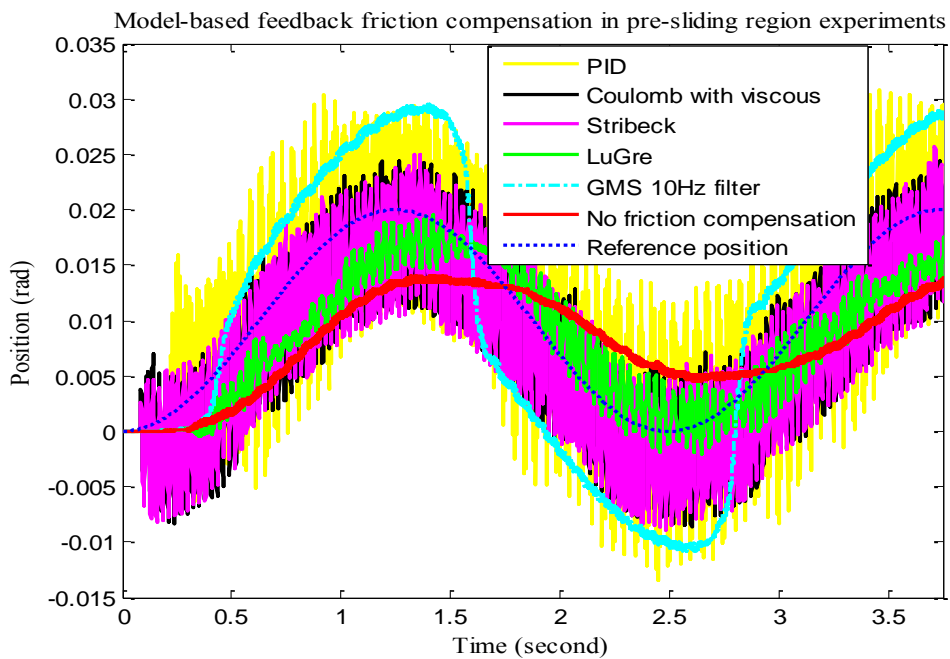
Figure 4.16. Experimental model-based feedback friction compensation of system with dry friction in response to the low-velocity sinusoidal position input

4.3.1.2.2 *Response to the high-velocity sinusoidal position input*

This profile is applied to examine the system response under the dominant sliding region behaviour of friction. In this respect, the experimental results of the model-based feedforward and feedback friction compensations are given in Figure 4.17 and Figure 4.18, respectively. In all of these experiments, the PD control without any compensation term exhibits the same stick-slip behaviour as in the simulations, and the addition of any compensation term increases the tracking accuracy.

For the feedforward compensation shown in Figure 4.17, all of the compensation models show closer responses to each other. This is expected because the system runs dominantly in the viscous region of friction, and all friction compensation models represent the sliding region of friction with the same parameters. However, it can be seen from Figure 4.17 that the responses of the dynamic models are smoother near zero velocity regions than the static models which exhibit stick-slip phenomenon more clearly in these regions. As compared to the simulation results in Figure 3.23, Figure 3.29, and Figure 3.35, there is not much difference in responses except for the exhibited stick-slip like behaviour in non-zero velocity regions of the position trajectory in experiments. This is again unfortunately due to the position-dependent structure of the friction.

In the feedback compensation case given in Figure 4.18, it is seen that the dynamic friction models give non-oscillatory and smoother responses as compared to the static models when the measured velocity is used as an input to the friction models. These oscillations are resulting from the stick-slip behaviour and measured velocity of the system, and are solved to some extent by the dynamic models which include modelling of stick in their formulations. Again, the experimental results demonstrate stick-slip like behaviour in non-zero velocity regions of the input trajectory due to the highly position-dependent characteristic of the friction in the system while not seen in simulations in Figure 3.24, Figure 3.30, and Figure 3.36. Moreover, the oscillatory behaviour of the responses is approximately guessed for static models, especially for the Stribeck friction model at the negative velocity region.
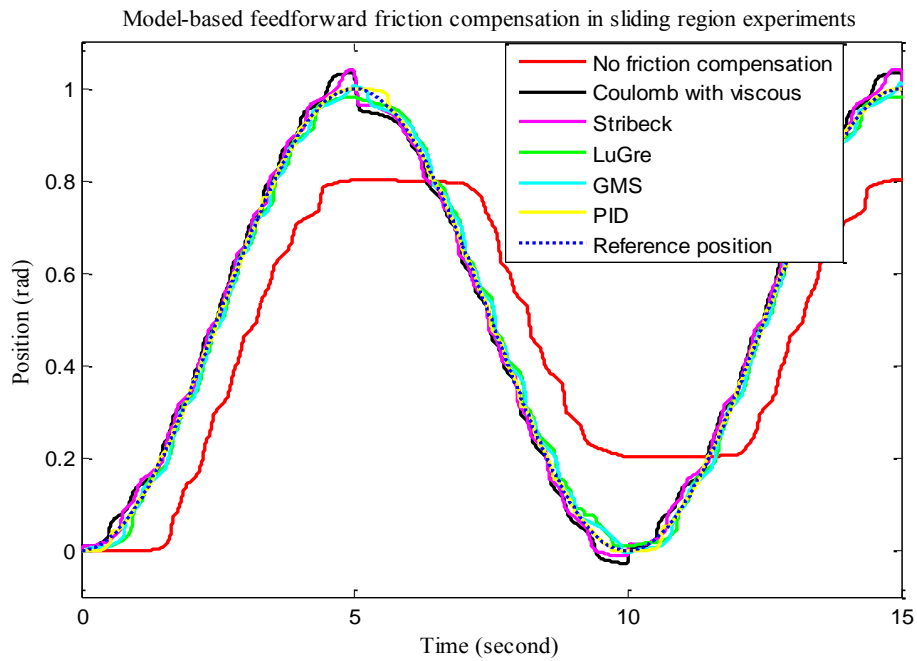
Figure 4.17. Experimental model-based feedforward friction compensation of system
with dry friction in response to the high-velocity sinusoidal position input
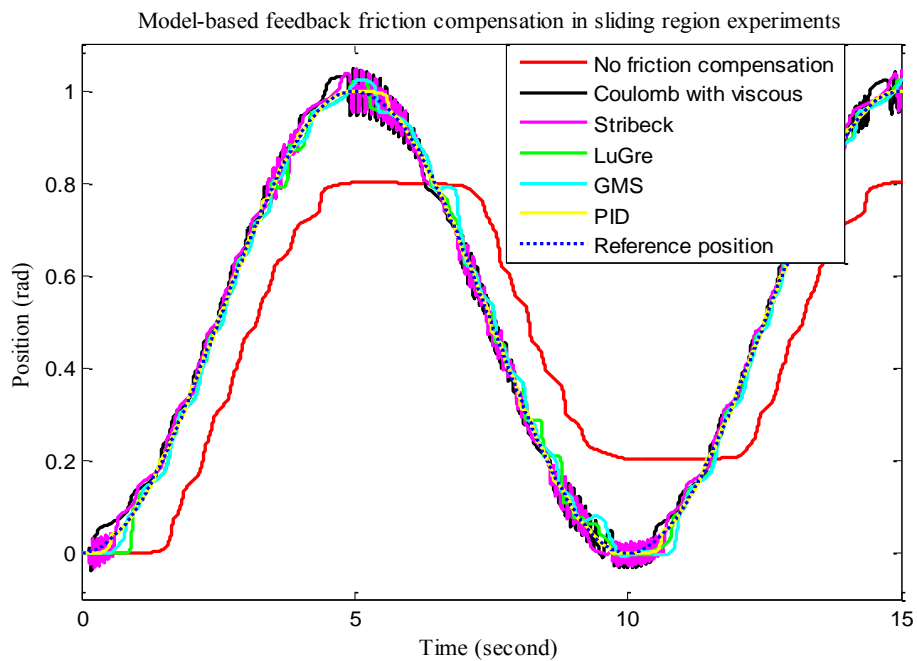
Figure 4.18. Experimental model-based feedback friction compensation of system
with dry friction in response to the high-velocity sinusoidal position input

According to the Figure 4.17 or Figure 4.18, the response of the PID control action is similar to the PD with compensation models as expected. PID action also exhibits stick-slip like behaviour in non-zero velocity regions due to the position dependency of friction and stick-slip behaviour near zero velocity regions clearly. If the position-dependency are modelled and included in the friction models, the PD action with friction compensation models can give similar or much smoother responses than the pure PID action throughout the trajectory.

Here, a case different from the simulations is studied additionally. The PID control action with 10 Hz bandwidth is also used with the friction compensation models to see the advantages of the addition of the friction compensation models. The results are shown for the feedforward and feedback compensation cases in Figure 4.19 and Figure 4.21, respectively. As the feedforward compensations are examined, it is seen that the usage of the dynamic friction models smoothens the PID response with stick-slip near zero velocities. This situation is clearly shown in Figure 4.20, which magnifies the response near a zero velocity region. In the feedback compensations, only the addition of the dynamic LuGre model can be said to make the tracking near zero velocities better while keeping the non-oscillatory, but stick-slip characteristic of the pure PID response in some degree. As in the feedforward case, this situation is clearly demonstrated in Figure 4.22 only for the LuGre friction model together with the velocity output of the system in the case of using the LuGre model-based feedback friction compensation approach. Here, the static models also improve the tracking near zero velocities, but with an additional chattering throughout the trajectory, and the GMS model with filtered input gives the highest oscillations while the GMS model makes the system unstable in the feedback compensation case although it is not shown.
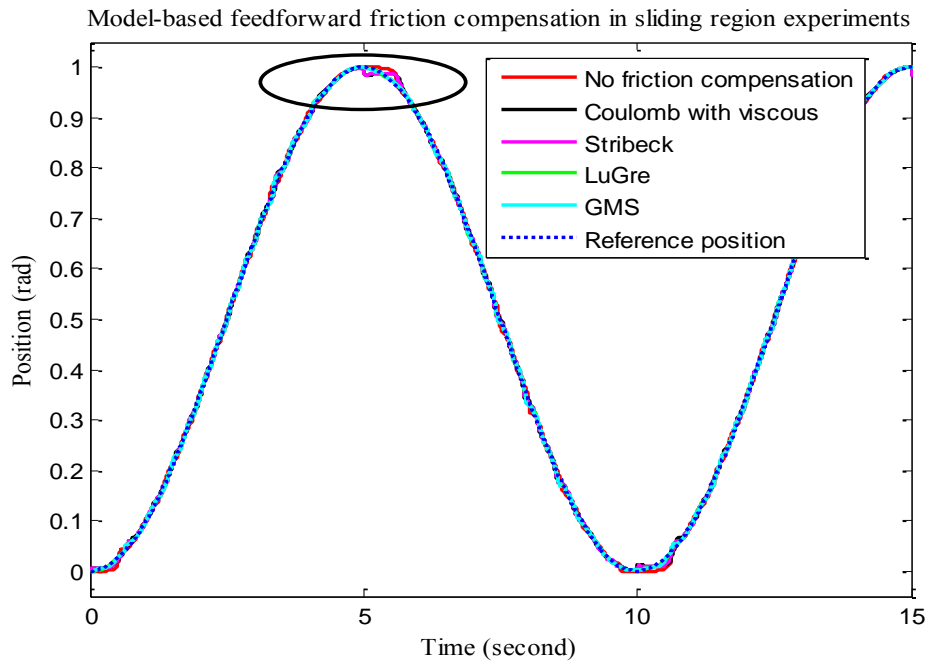
Figure 4.19. Experimental model-based feedforward friction compensation of system with dry friction in response to the high-velocity sinusoidal position input (PID with 10 Hz bandwidth)
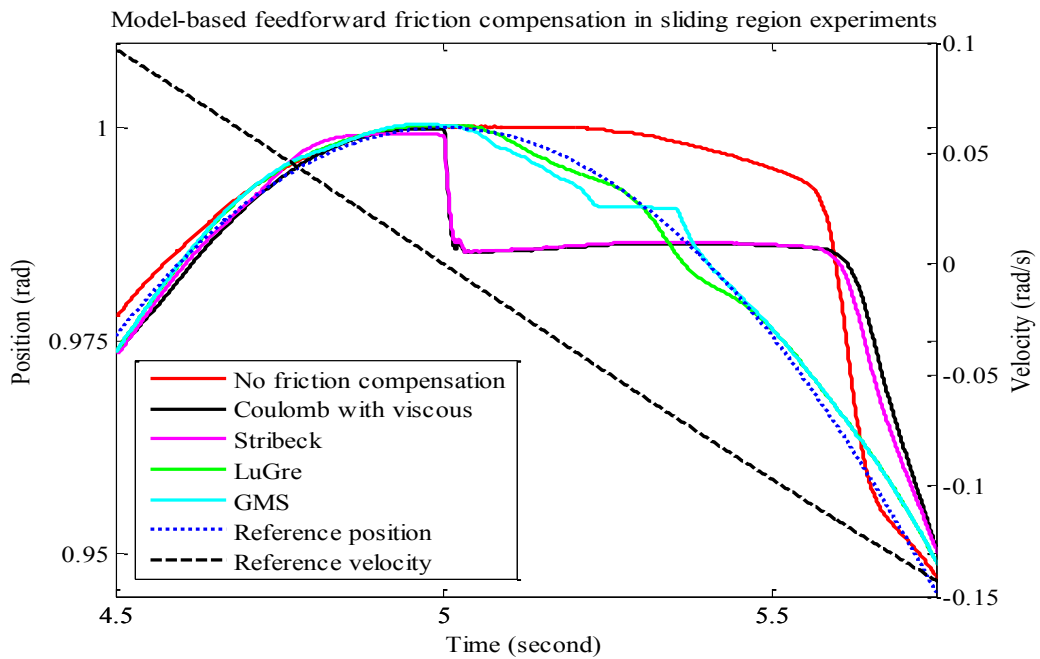
Figure 4.20. Enlarged graph of the marked region of Figure 4.19
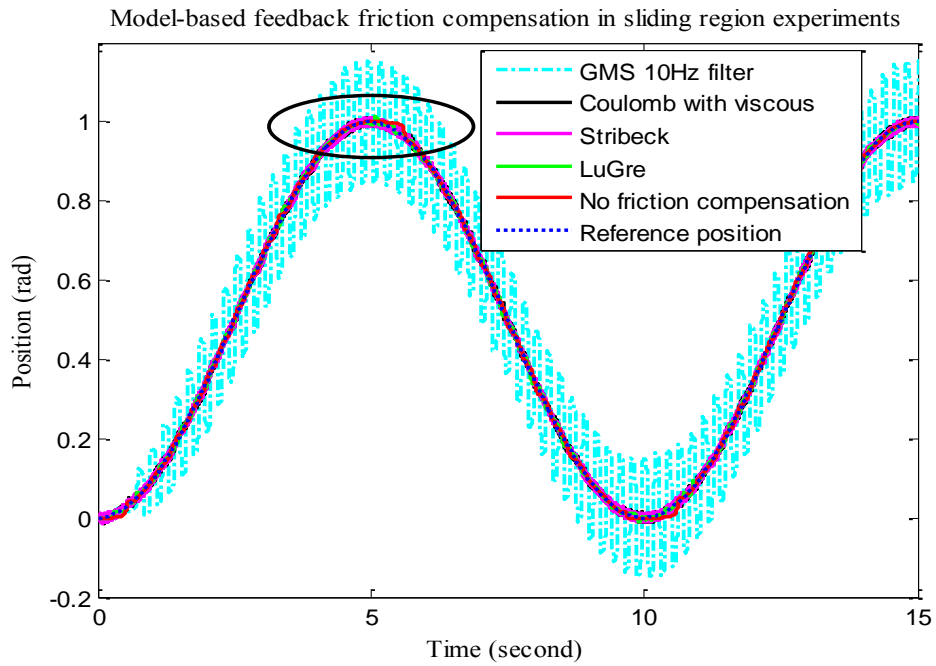
Figure 4.21. Experimental model-based feedback friction compensation of system with dry friction in response to the high-velocity sinusoidal position input (PID with 10 Hz bandwidth)
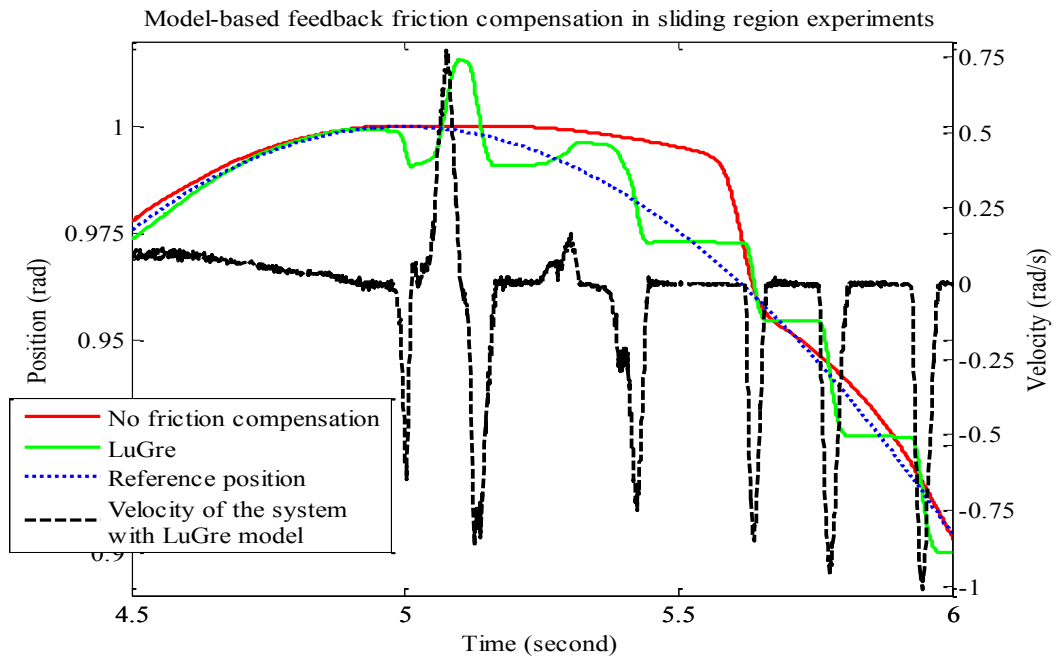
Figure 4.22. Enlarged graph of the marked region of Figure 4.21

4.3.1.2.3   *Response to the step position input*

In order to examine the stick-slip behaviour of the system, another type of input, i.e. step input, has been applied to the system. For this small amplitude step position input, the results of the feedforward and feedback compensations are illustrated in Figure 4.23 and Figure 4.24, respectively. As can be seen from figures, the PD action without any friction compensation term follows the input trajectory with steady-state error and by making small amplitude chattering.

According to the feedforward compensation results given in Figure 4.23, all compensation models keep the same tracking behaviour of the PD action with additional steady-state errors. Although the steady-state errors and responses of the system with different compensation models are not satisfactory, the Stribeck model gives the best response, and the GMS model, LuGre model and Coulomb with viscous model follow it successively. When these responses are compared with the simulated ones in Figure 3.25, Figure 3.31, and Figure 3.37, the difference in responses can be seen. Firstly, there is no chattering in simulations while it exists in experimental results. Moreover, the Coulomb with viscous model generally gives the best response and the others give closer responses in simulations whereas this result is not kept in experiments.

On the other hand, the feedback compensation results in Figure 4.24 exhibit oscillations about trajectory. Here, the static models give oscillatory and closer response to each other. Although the amplitude of the oscillations of the LuGre model is smaller than the static models, its addition to the PD control action does not change the response in a satisfactory manner. In this compensation approach, the GMS model again makes the system unstable. Even if the filtered measurement is used, the GMS model can not give a satisfactory result having undesired oscillation characteristic. In comparison to the simulations in Figure 3.26, Figure 3.32, and Figure 3.38, the experimental results do not correspond to the simulations actually. The oscillations in the feedforward compensation case in experiments do not exist in simulations. Additionally, the oscillations guessed for the static models in the feedback compensation approaches in simulations are seen experimentally; however, the smoothness of the responses of the dynamic models obtained in the simulations is

not similar to the experimental studies. This can be due to the position-dependent behaviour of the friction and the usage of the measured velocity.

Except from these results, the response when the purely PID action with the same bandwidth as the PD action is used in the system is given. The response with PID action shows extreme oscillations in contrast to the simulations in which PID action exhibits stick-slip cycling only at steady-state.

As mentioned in the section 4.3.1.2.2, the same case with 10 Hz bandwidth PID control action is applied with the friction compensation models. The results are shown in Figure 4.25 and Figure 4.26 for the feedforward and feedback compensation cases respectively. For the feedforward compensation case, there is not much difference with and without compensations. It can be concluded from Figure 4.25 that the response time of the system decreases and the overshoot-like peak of the PID action is removed with nearly the same steady-state errors represented. Also, the system tracks the step input trajectory much smoother at the beginning of the trajectory. On the other hand, the friction models do not improve the response when thay are used in the feedback friction compensation. The PID action with static models makes the response worse with additional oscillations. The GMS model again makes the system unstable while the GMS model with filtered input has not satisfactory response due to the changing amplitude oscillations. The LuGre model is the best one; however, it represents a sudden change in position due to the velocity measurement and stick-slip actually.

Now, after the experiments are completed with the dry friction, the friction characteristic will be changed by applying some amount of grease onto the friction interface between clutch and friction disk in order to see the effects of it on the frictional behaviour and compensation.
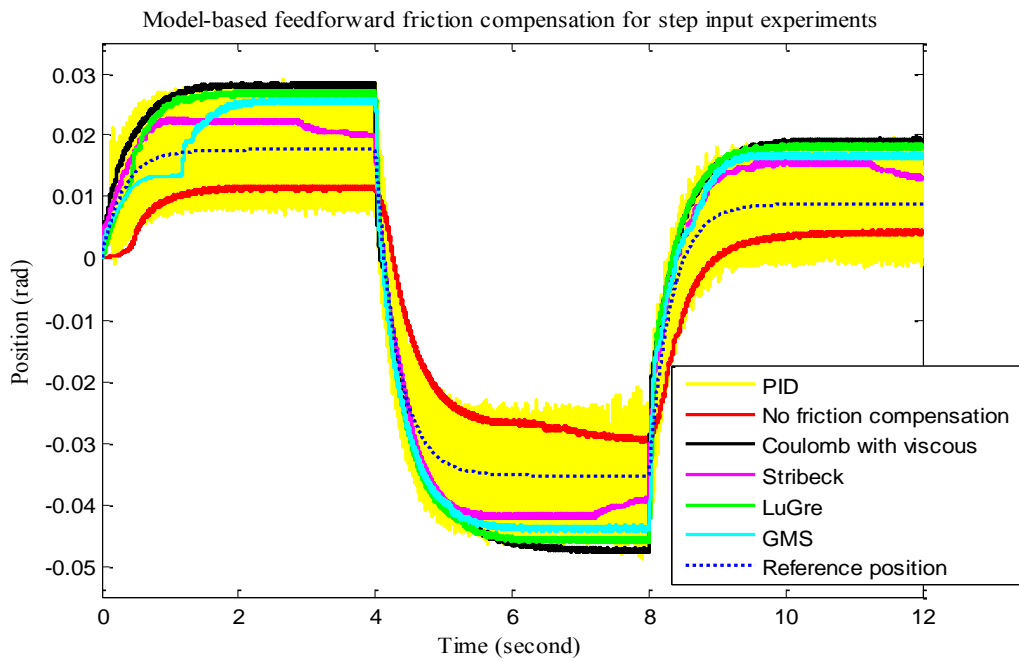
Figure 4.23. Experimental model-based feedforward friction compensation of system with dry friction in response to the step position input
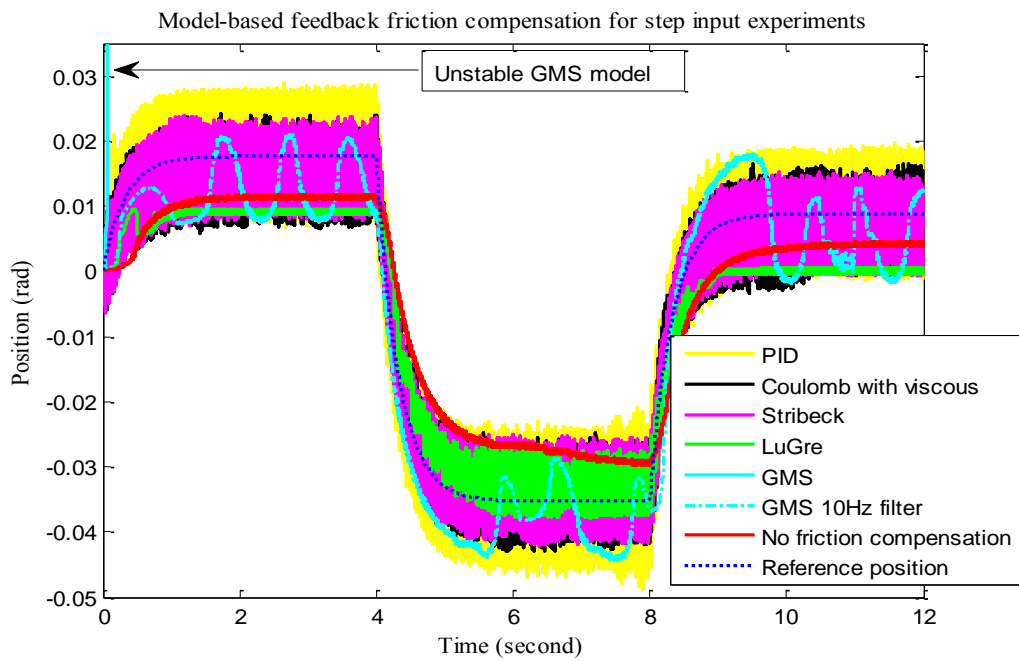
Figure 4.24. Experimental model-based feedback friction compensation of system with dry friction in response to the step position input
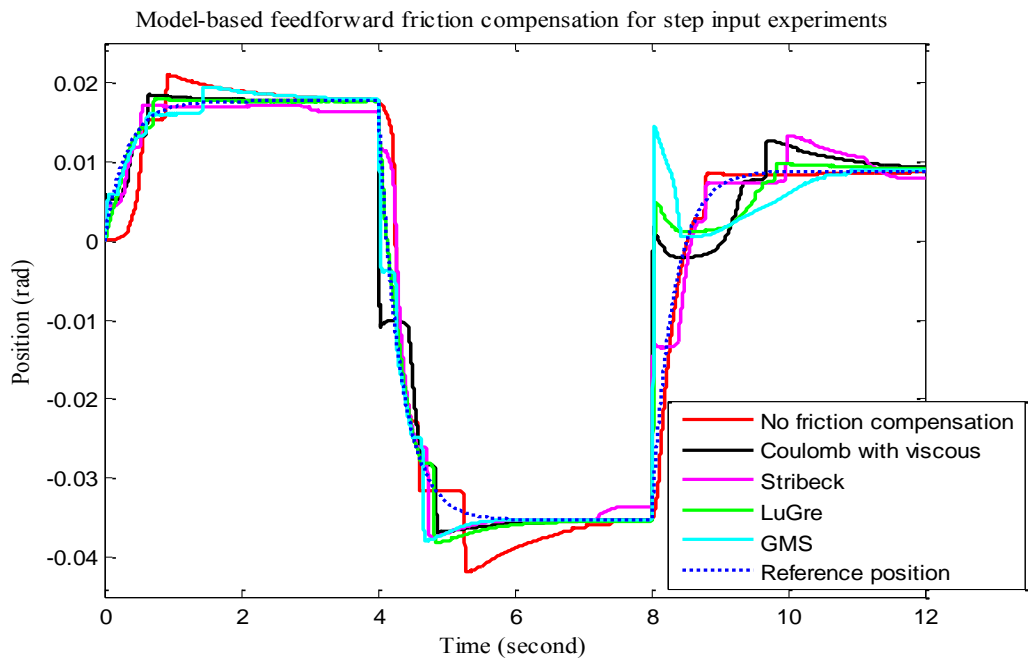
Figure 4.25. Experimental model-based feedforward friction compensation of system with dry friction in response to the step position input (PID with 10 Hz bandwidth)
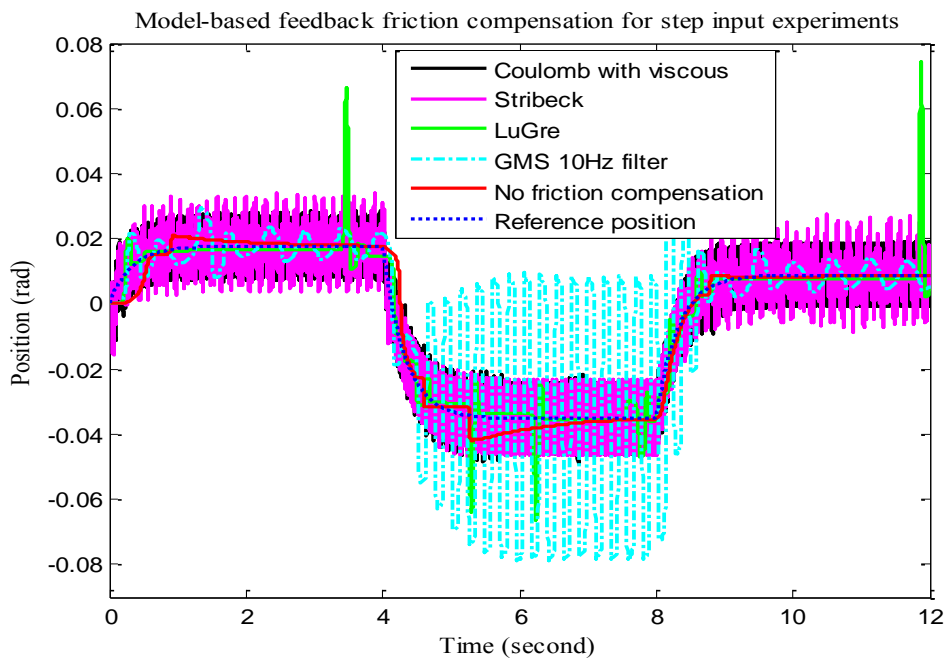

Figure 4.26. Experimental model-based feedback friction compensation of system with dry friction in response to the step position input (PID with 10 Hz bandwidth)

4.3.2 Grease-added friction case

In this case, the friction characteristic of the system is changed by adding some amount of grease onto the interface between the friction clutch and the friction disk. Since the friction clutch is dismounted while adding grease, the resulting friction level is tried to be kept as close to the one in simulations as much as possible. In this new configuration, the friction characteristic of the system again will be investigated and the parameters of the friction models will be identified. Then, the friction models with the identified parameters will be used in the friction compensation of the system with grease-added friction.

4.3.2.1 Identification of the parameters of the friction compensation models for grease-added friction case

4.3.2.1.1 Break-away torque experiments

For the identification of the break-away torque of the system, again the same procedure and open loop experiments as in the dry friction case (section 4.3.1.1.1) are applied to the system. Here, since the break-away torque of the system is again highly position-dependent, the measurements are done with the angle interval of 10˚ through 360˚ revolution of the shaft. Apart from the previous one, the experiments are done both in the positive and negative velocity directions, and the results are shown in Figure 4.27 and Figure 4.28, respectively. From these figures, the trend of the break-away torques obtained from both the motor current and torque sensor measurements can be seen.

Since the purpose here is again the compensation of the total friction, the break-away torques obtained from motor current for positive and negative velocity directions will be used in sliding region curve identification. Furthermore, although the break-away torque changes with position, the average value of it will be used in the sliding curve identification in order not to further complicate the friction identification and compensation processes, and due to the changing characteristic of friction in time.
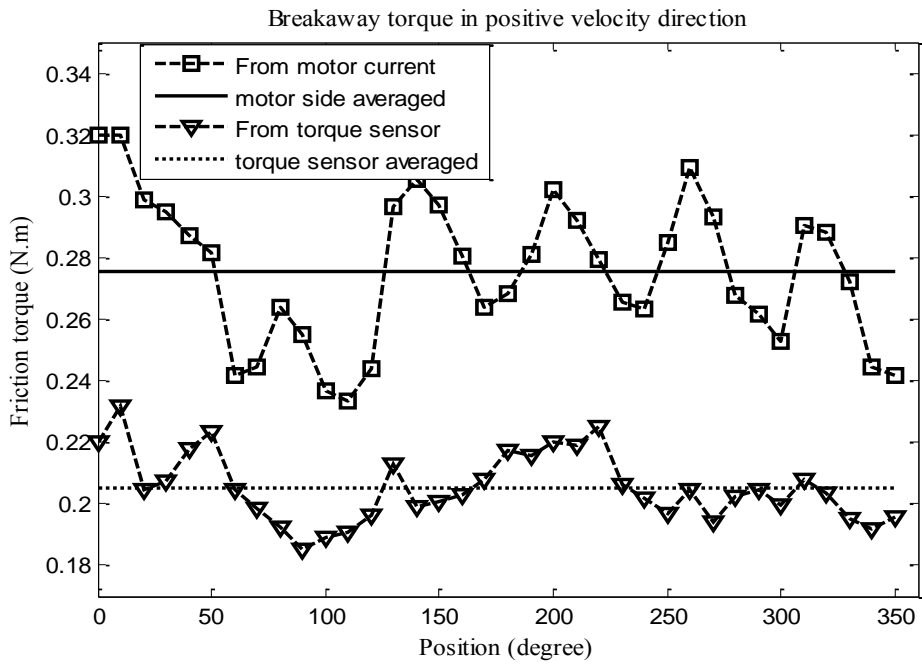
Figure 4.27. Break-away torque measurements both from the motor and torque sensor in positive velocity direction for grease-added friction case
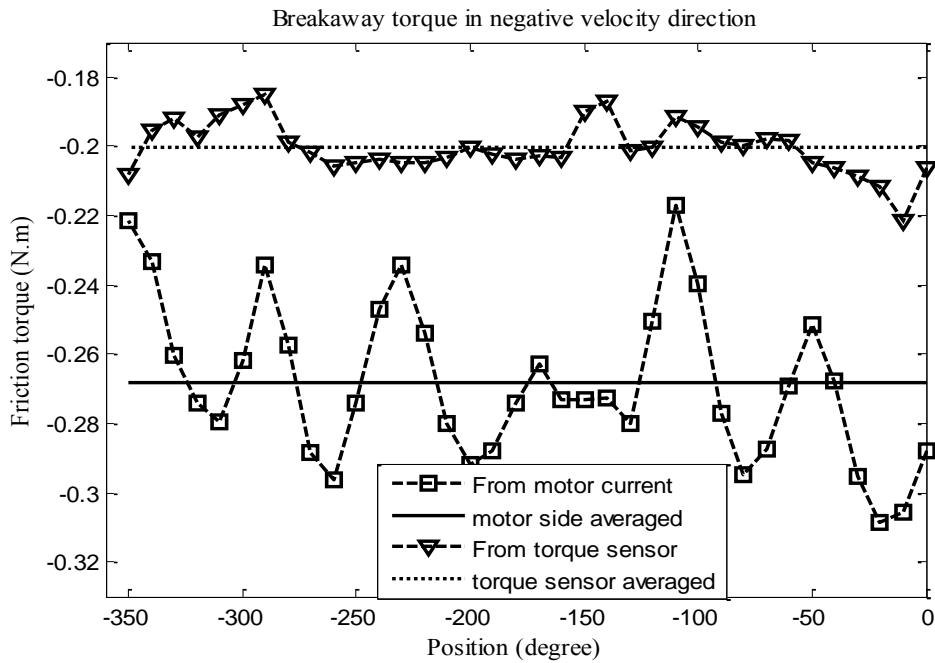
Figure 4.28. Break-away torque measurements both from the motor and torque sensor in negative velocity direction for grease-added friction case

124

4.3.2.1.2 Sliding region experiments

For the identification of this new friction characteristic, the same experiments, inputs and controllers as in the previous friction case (section 4.3.1.1.2) are applied to the system. During the experiments, the ramp position input is given to the system with the constant velocity ranges given in equation (4.3). Through the experiments, these velocities are applied to the system both in the positive and negative directions starting from the greatest one.

$$\dot{\theta} = (25; 20; 15; 10; 5; 3; 2; 1.9; 1.8; 1.6; 1.4; 1.2; 1.1; 1.0; 0.95; 0.9; 0.8; 0.7; 0.6; \\ 0.5; 0.4; 0.3; 0.2; 0.1; 0.08; 0.06; 0.04; 0.02; 0.01; 0.005) \quad (rad/s) \tag{4.3}$$

In order to see the position dependency of the friction torque, the filtered torque sensor data for some positive and negative constant velocity experiments are demonstrated in Figure 4.29 and Figure 4.30 with the transients removed for the first 20°-angle interval. If one examines both of these figures, the maximum peak to peak deviation in friction torque can be seen to be 0.07 N.m.
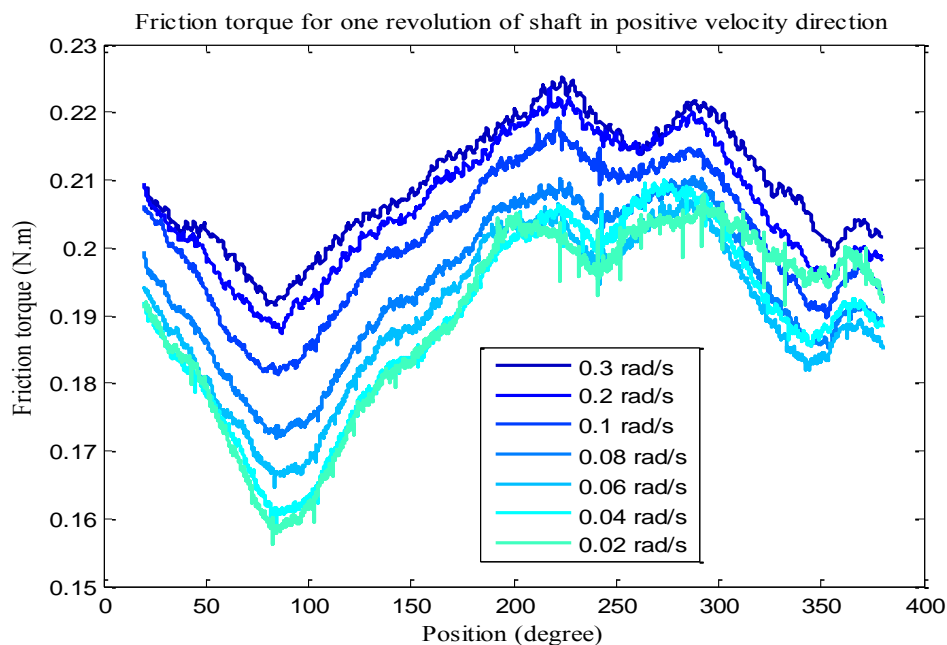
Figure 4.29. Position dependent friction torque for some positive velocities for grease-added friction case
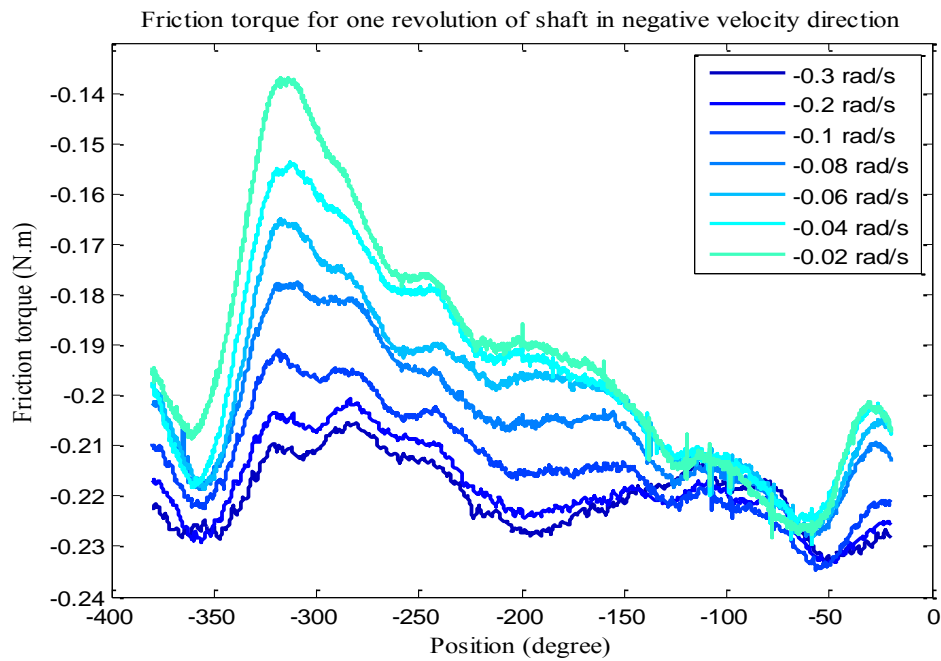
Figure 4.30. Position dependent friction torque for some negative velocities for grease-added friction case

For the compensation of the total friction, again the motor torque measurements are used for identification. The average of the measured motor torque through one full rotation of the shaft in any constant velocity given in (4.3) is considered to be the friction torque in that velocity. As a comparison, the friction torque measurements from motor and torque sensor for the 0.3 rad/s constant velocity is given in Figure 4.31. One can see from this figure that the shapes of the torques follow nearly the same path.

Different from the dry friction case, the time dependency of friction is examined here and illustrated in Figure 4.32. The 0.3 rad/s constant velocity experiments are done with 30 minutes intervals, and the change in filtered torque sensor data with time is drawn according to the position. It can be inferred from this figure that the shape of the friction curve is almost kept while the amplitude is changing in time.

126
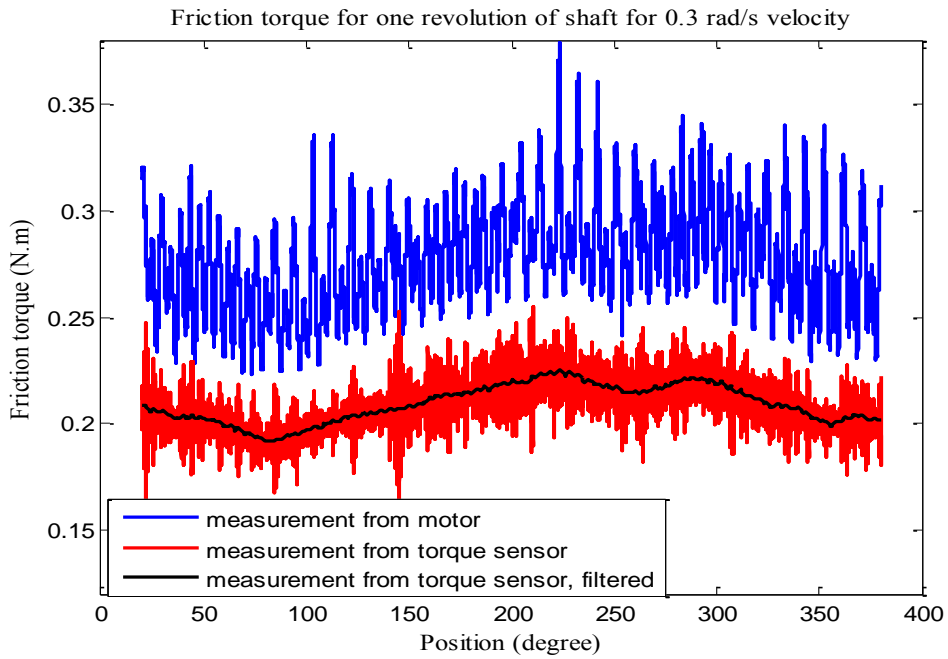
Figure 4.31. Friction torque from the motor current and torque sensor for grease-added friction case
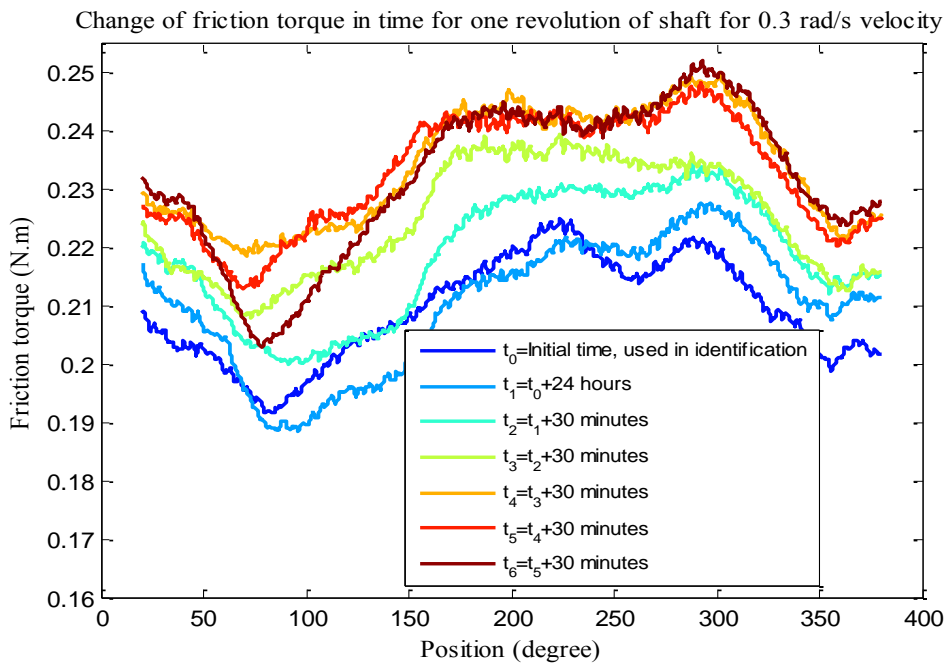
Figure 4.32. Time dependency of friction

Now, since the friction is highly time dependent and position dependent, the use of different identified parameters for the positive and negative velocity directions of motion in the friction compensation of the system is not very crucial. Instead of this, the average sliding curve is fitted and used in compensation by using the friction torques from both the positive and negative velocity regions together. In this respect, the negative velocities and corresponding friction torques are carried to the positive velocity region in order to evaluate the friction torques from positive and negative velocity directions together. This can be seen from Figure 4.33.
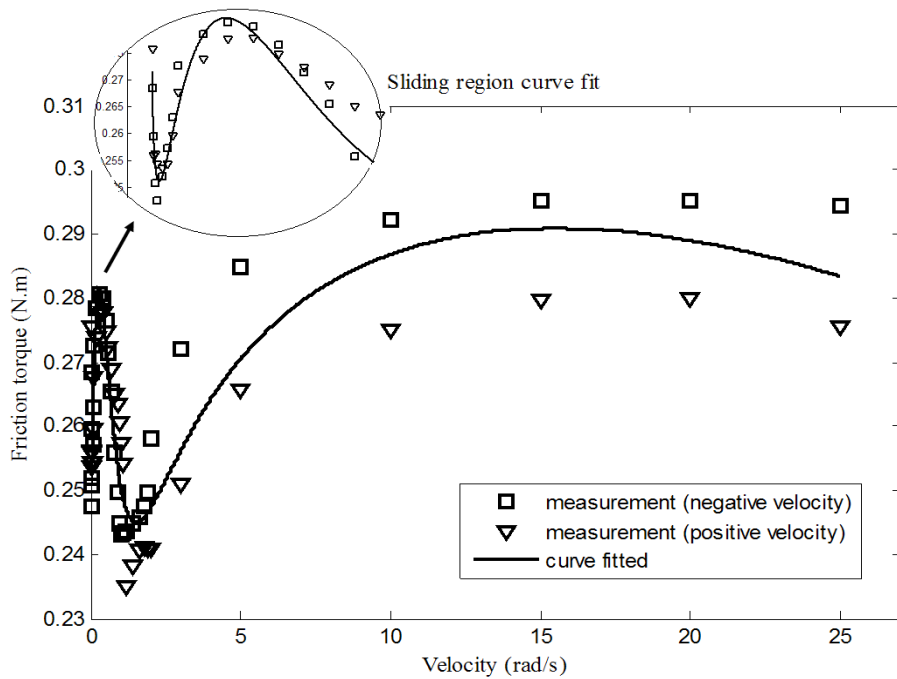
Figure 4.33. Sliding region average curve fit to the measurements in positive and negative velocity directions for grease-added friction case

As can be seen from Figure 4.33, the steady-state curve of friction given in equation (2.6) is not suitable for the fit to the measurement data. For the direct-drive systems, the new, more flexible equations for the Stribeck effect and viscous friction are given in [29] in order to obtain a better fit to the measured data. These equations are combined, and the new steady-state curve of friction in sliding region, i.e. $s_1(v)$, is obtained here as in equation (4.4) below.

128

$$s_1(v) = \text{sgn}(v)(\alpha_0 + \alpha_1 e^{-(\frac{v}{v_1})sign(v)} + \alpha_2(1 - e^{-(\frac{v}{v_2})sign(v)}) + F_v|v| + F_{v2} v^2) \quad (4.4)$$

In this equation, $\alpha_0 + \alpha_1$, $\alpha_0 + \alpha_2$, F_v, and F_{v2} stand for the static friction level, Coulomb friction level, coefficients of the linear and nonlinear viscous friction, respectively whereas v_1 and v_2 represent the different Stribeck velocities.

In our case, the measurements include two regions of Stribeck effect (decreasing friction with increasing velocity). Although the equation in (4.4) models this behaviour, it remains insufficient to fit to the measurement data here, especially for the first Stribeck effect region. Hence, the formulation in (4.4) is changed for adaptation, and the modified curve of friction in sliding region, i.e. $s_m(v)$, is obtained as given in (4.5). Then, the equation in (4.5) is used for the identification of the sliding region parameters of the friction models in the grease-added friction case as an alternative to the equation (2.6).

$$s_m(v) = \text{sgn}(v)(\beta_0 + \beta_1 e^{-\left|\frac{v}{v_1}\right|^{\beta_3}} + \beta_2(1 - e^{-\left|\frac{v}{v_2}\right|^{\beta_4}}) + F_v\left|v\right| + F_{v2}\left|v\right|^{\beta_5}) \quad (4.5)$$

In this equation, $\beta_0 + \beta_1$ represents the Static friction level, $\beta_0 + \beta_2$ represents the Coulomb friction level and F_v is known as the linear viscous friction coefficient. There is no specific meaning of the other parameters; however, they can be interpreted as follows: v_1, v_2 are used for the different Stribeck velocities, β_3, β_4 are used for the different Stribeck shape factors, and F_{v2} and β_5 are the coefficient and shape factor for the nonlinear viscous friction, respectively. According to the equation (4.5), the sliding region curve fit is demonstrated in Figure 4.33 and the identified parameters are given in Table 10.

In Figure 4.34, the friction torque measurements from the motor side and torque sensor are shown for positive and negative velocity directions. In contrast to the dry friction case, the torques from motor and torque sensor have the same trend both in the positive and negative velocity directions. Moreover, there is again a nearly constant amplitude difference between the motor and torque sensor measurements. This is due to the bearings between the torque sensor side and motor side, and can be explained by Coulomb with viscous friction again.

Another conclusion which can be inferred from Figure 4.34 is that the usage of grease in the friction interface induces the Stribeck effect or makes it more detectable. This result actually agrees with the [29]. Furthermore, the friction torque curves obtained from the motor current data have become more symmetric for the positive and negative velocity directions in contrast to the dry friction case.
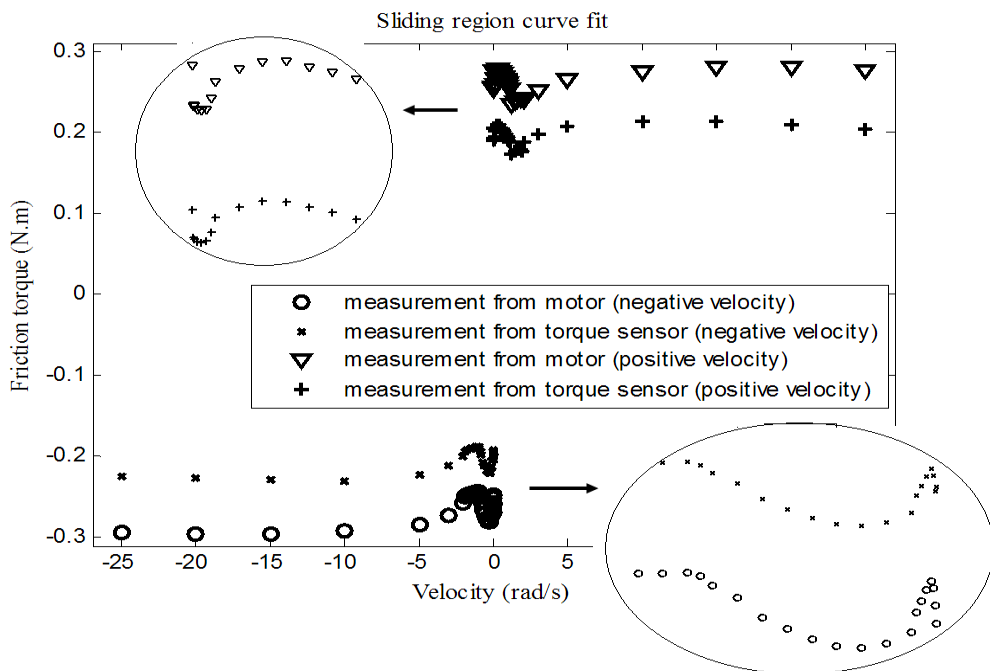
Figure 4.34. Sliding region measurements from the motor current and torque sensor in positive and negative velocity directions for grease-added friction case

4.3.2.1.3 Pre-sliding region experiments

The hysteresis curve identification in this case is performed following the same experiments in section 4.3.1.1.3. A sinusoidal input torque whose amplitude is smaller than the average break-away torque and given in equation (4.6) is applied to the open loop system. The measured hysteresis curve is shown in Figure 4.36.

$$\dot{\theta} = 0.13\sin(0.1x2\pi t) \qquad (rad/s) \qquad (4.6)$$

The parameter identification is done again by considering only the 2nd cycle of input due to the transient included in the hysteresis curve representation of the GMS model. For the identification of hysteresis curve, 3, 4 and 5-element GMS models are tried to be fitted and compared. The results of the curve fit for the 2nd cycle only are shown in Figure 4.35. According to the Figure 4.35, 3, 4 and 5-element GMS models do not have a valuable difference among each other in representing the measured hysteresis curve. Thus, the usage of 3-element GMS model is sufficient enough for the modelling of hysteresis curve and will be used in the friction compensation experiments in further sections. In this respect, the 3-element hysteresis curve fit and measured hysteresis curve are shown in Figure 4.36 for the whole cycle of input.

According to the identification, the pre-sliding region hysteresis curve parameters of the GMS model are given in Table 10.
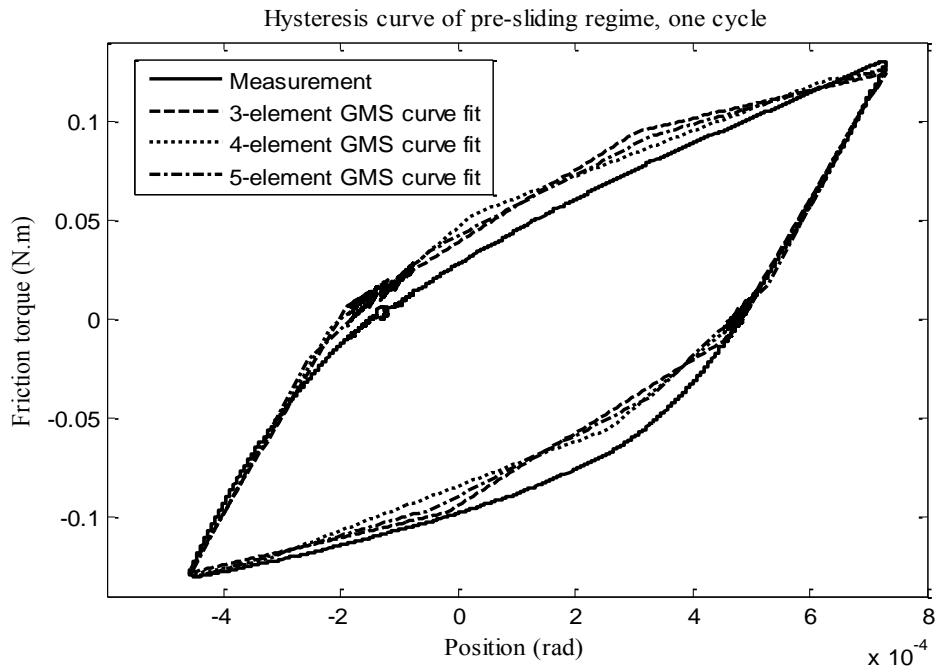
Figure 4.35. Measured and identified hysteresis curves for the 2nd cycle of input for grease-added friction case
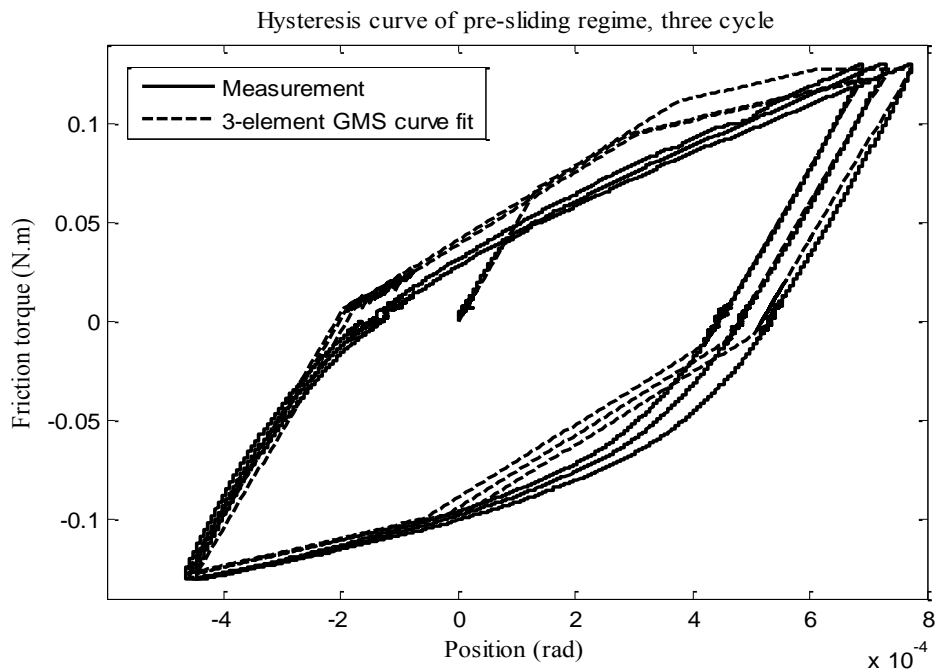
Figure 4.36. Measured and identified hysteresis curves for grease-added friction case

4.3.2.1.4 Identification of the dynamic parameters of the LuGre model

The two dynamic parameters of the LuGre friction model, i.e. σ_0 and σ_1, are determined as described in section 4.3.1.1.4 for the case of grease-added friction. An open loop experiment is done by applying a sinusoidal torque input of amplitude 0.35 N.m and frequency 1 Hz. The resulting position response of the open loop system is again not highly repeatable. Thus, the best choice will be tried to be done between the measured and simulated responses in identification.
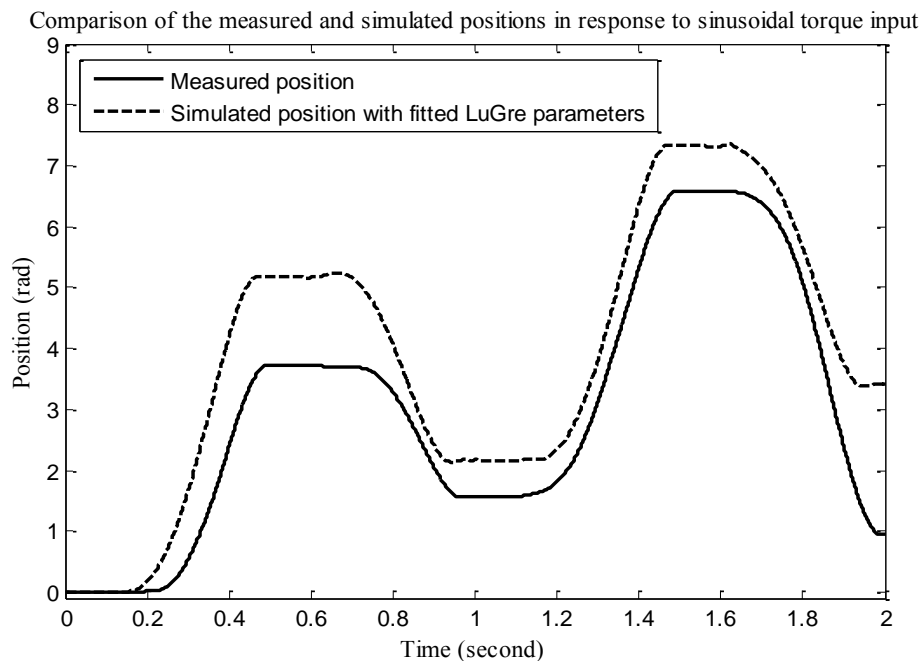
Figure 4.37. Comparison of the measured and simulated positions of the open loop system for grease-added friction case

In contrast to the dry friction case, the sliding region parameters identified separately for the positive and negative velocity directions are used in the LuGre friction model while simulating the system response. Accordingly, the drift in the position of the open loop system can now be seen in the simulated response as in the real case. Again the identification process is done by using the MATLAB$^{\circledR}$ SIMULINK$^{\circledR}$ Response Optimization tool as in section 4.3.1.1.4. Regarding these conditions, the comparison of the measured response of the real system and the

simulated response of the system model including the identified LuGre model as the actual friction is demonstrated in Figure 4.37.

Note that the identified dynamic parameters of the LuGre model are given in Table 10.

4.3.2.1.5 *Identification of the attraction parameter of the GMS model*

As mentioned before, the attraction parameter C directly affects the hysteresis behavior in sliding region. The Stribeck effect has been seen in this grease-added friction case in contrast to the dry friction case. Hence, it is possible to see the hysteresis behavior in sliding region of friction. However, the highly position dependent structure of the friction in the system prevents us to obtain a hysteresis behaviour measurement which is worth to identify. Thus, the attraction parameter will be manually tuned as in section 4.3.1.1.5.
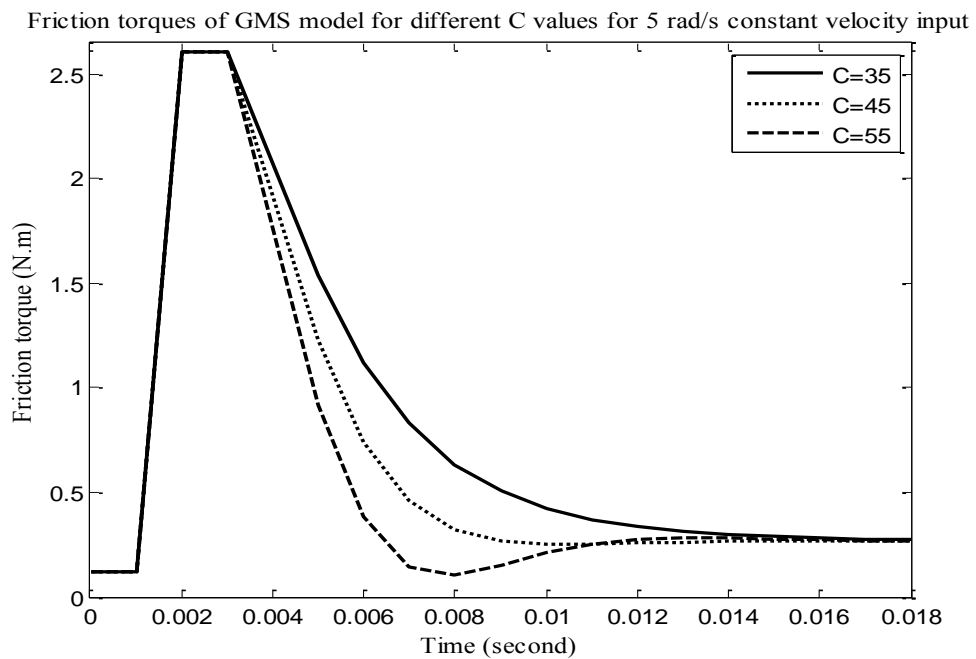
Figure 4.38. Comparison of the GMS friction model responses to the 5 rad/s constant velocity for different C values for grease-added friction case

According to the same procedure in section 4.3.1.1.5, the responses of the GMS friction model with the identified parameters to the 5 rad/s constant velocity input are shown in Figure 4.38 for different attraction parameter values. The C parameter value causing the GMS model to give the first response without overshoot is clear from the Figure 4.38. This value is thought to be the identified value of the attraction parameter and given in Table 10.

Table 10. Identified parameters of the friction compensation models for the case of grease-added friction

Pre-sliding region parameters			Sliding region parameters		
Parameter	Value	Unit	Parameter	Value	Unit
Stribeck friction model			β_0	80.7454	N·m
k	3.5×10^4	N·m·s/rad	β_1	-80.4742	N·m
LuGre friction model			β_2	-80.5930	N·m
σ_0	85	N·m/rad	β_3	0.7884	-
σ_1	0.7875	N·m·s/rad	β_4	0.7871	-
-	-	-	β_5	0.3768	-
-	-	-	v_1	0.1755	rad/s
-	-	-	v_2	0.1758	rad/s
-	-	-	F_v	-0.0054	N·m·s/rad
-	-	-	F_{v2}	0.0791	N·m·s$^{0.38}$/rad
GMS friction model					
k_1	315.0885	N·m/rad	α_1	0.1567	-
k_2	69.7325	N·m/rad	α_2	0.4222	-
k_3	113.2177	N·m/rad	α_3	0.4211	-
-	-	-	C	35	N·m/s

4.3.2.2 Experimental results of the friction compensation of the closed loop system with grease-added friction

As in the dry friction case, the results of the model-based friction compensation techniques will be presented here. In this respect, the responses will be investigated and compared to each other. Here, the real friction characteristic in sliding region does not totally correspond to the one in simulations in terms of the amplitudes. However, since the structure (shape) of the friction in sliding region is similar to the one assumed in simulations, more realistic comparisons can be made between the experimental results and simulated responses in terms of the trend of the responses in contrast to the previous dry friction case. In all of the experiments conducted, the parameters of the linear PD and PID control actions used will be the same as the ones in simulations in Chapter 3. In addition to the control strategies used in simulations in Chapter 3, a PID control strategy will be applied to the experimental set-up together with the friction compensation terms in order to see the effectiveness of the model-based friction compensation techniques more clearly. Furthermore, an integration time step of 10^{-3} seconds is selected to be used in all experiments for the grease-added friction case.

4.3.2.2.1 Response to the low-velocity sinusoidal position input

As in the section 4.3.1.2.1, the compensation results of the system in the low-velocity region will be investigated. Note that the experimental results with the same PD control action as in the simulations are highly oscillatory and the system tracks the input trajectory even only with the PD control action without any compensation term by making extreme chattering. The plots showing these behaviours are given in Figure 7.2 and Figure 7.3 in Appendix. In order to see the responses more clearly and make a comparison with the simulations, the bandwidth of the PD control action is decreased to 25 Hz, and experiments are performed with this new controller. The results of these new experiments are given in Figure 4.39 and Figure 4.40. As one can see, the PD control action can not follow the input trajectory alone.

According to the feedforward friction compensation in Figure 4.39, the dynamic models track the input profile much better than the static models although

there is some undesired tracking errors which can be improved by increasing the bandwidth of the PD control action. As expected, the Stribeck model compensation gives better response than the Coulomb with viscous model since the Stribeck effect exists now in the system. Note that the LuGre model gives the smoother response than the GMS model although the GMS friction model represents the sticking region more precisely. As in the simulation results in Figure 3.21, Figure 3.27, and Figure 3.33, the dynamic models follow the input trajectory closer than the static models, and the Stribeck model gives better response than the Coulomb with viscous model. The stick-slip behaviour at the peak of the trajectory in simulations is also seen in experimental results.

For the feedback friction compensation given in Figure 4.40, the responses follow the input, but with high amplitude oscillations. Here, the Coulomb with viscous model and the Stribeck model give closer responses having lower oscillation amplitudes than the LuGre model. Except from this, the GMS model makes the system unstable after some oscillations. Although the response of the GMS model with the filtered input is non-oscillatory, it is undesirable since the response includes stick-slip behaviour and tracking error. In these experiments, the oscillations of the LuGre model as compared to the static models do not correspond to the simulations in Figure 3.22, Figure 3.28, and Figure 3.34. Moreover, the GMS model does not represent a smooth and good response as in the simulations. These oscillations can be unfortunately the result of the velocity measurement and stability issues of the feedback friction compensation.
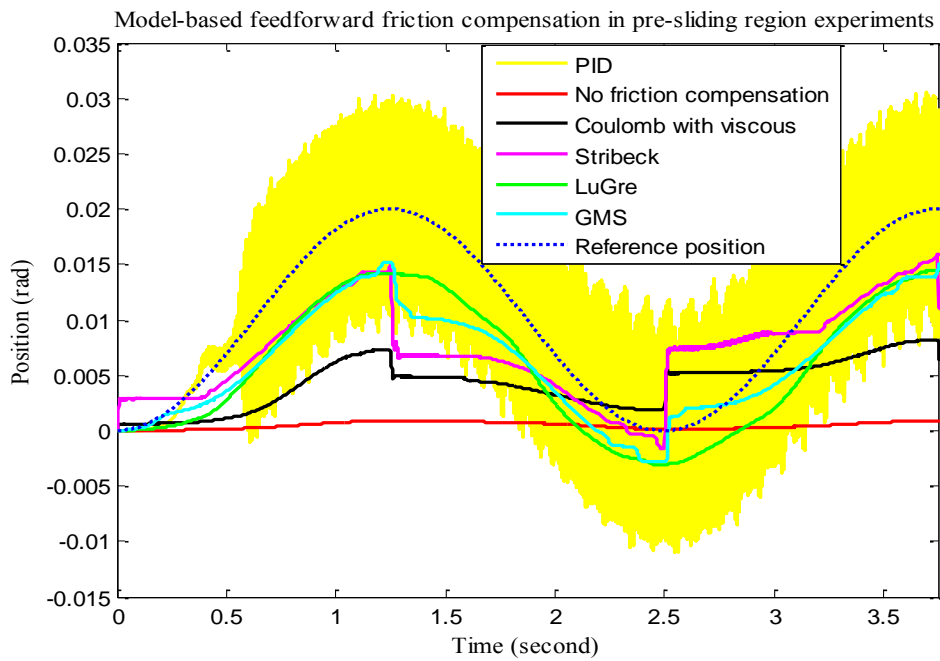
Figure 4.39. Experimental model-based feedforward friction compensation of system with grease-added friction in response to the low-velocity sinusoidal position input
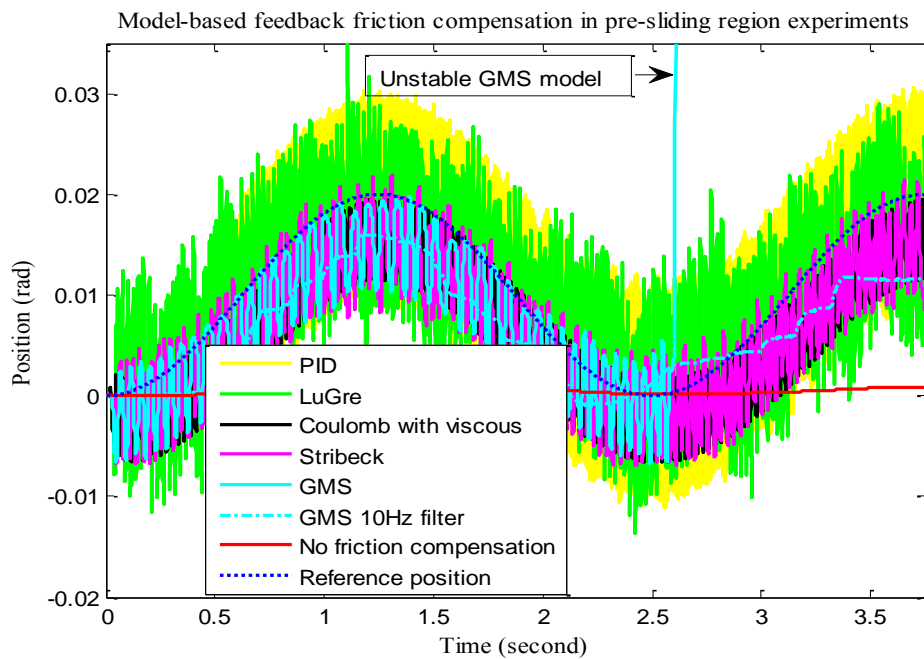
Figure 4.40. Experimental model-based feedback friction compensation of system with grease-added friction in response to the low-velocity sinusoidal position input

Note that the response of the system with the PID action with the same bandwidth as the PD control; that is 25 Hz, is also shown in Figure 4.39 and Figure 4.40. As this result is examined, it is seen that it deviates from the simulations in terms of the trend. The response follows the trajectory in a highly oscillatory manner and does not reflect a stick-slip behaviour as in the simulations although the 36 Hz bandwidth of the PID control action in the simulations is decreased to the 25 Hz. This means that the gain of the PID (bandwidth) is still too high to see a non-oscillatory response, and its response is actually worse than the use of the PD action with friction compensation models.

As done in the sections 4.3.1.2.2 and 4.3.1.2.3, the system is run under the 10 Hz bandwidth PID control action with and without the friction compensation terms in order to see the change in response for this sticking region dominant trajectory. In this respect, the model-based feedforward and feedback compensation results of the system with the PID controller are given in Figure 4.41 and Figure 4.42. As one can see from the feedforward compensation case, the response of the pure PID is not good enough. The addition of the friction compensation models except Stribeck model improves the tracking behaviour. Especially, the addition of the LuGre model makes the tracking much closer to the input trajectory, and removes the stick-slip behaviour of the PID control action without any compensation term and with other compensation terms near zero velocity regions. For the feedback compensation case, the system becomes highly oscillatory although all responses follow the trajectory. In reality, this is not a desired response characteristic.
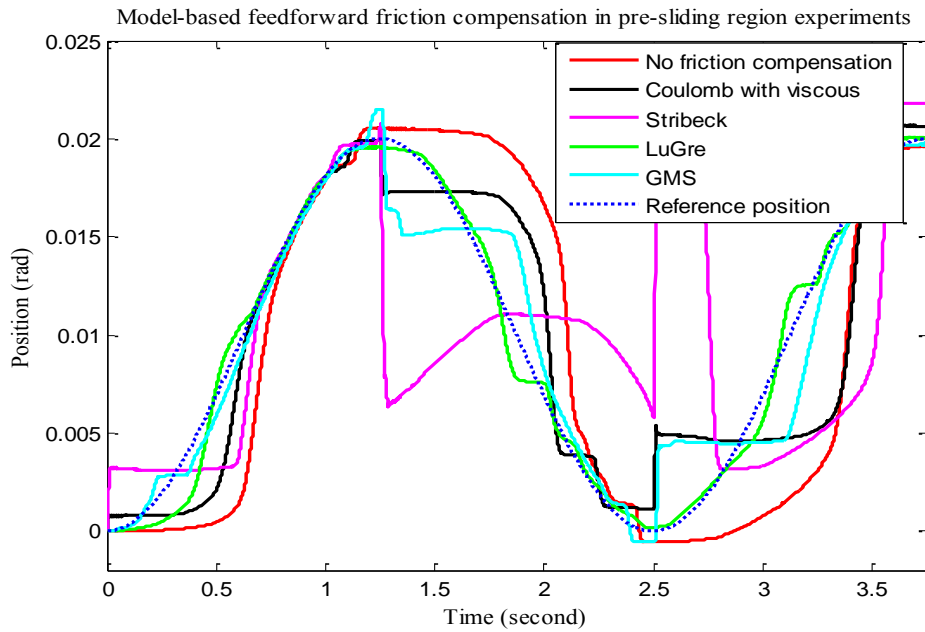
Figure 4.41. Experimental model-based feedforward friction compensation of system with grease-added friction in response to the low-velocity sinusoidal position input (PID with 10 Hz bandwidth)
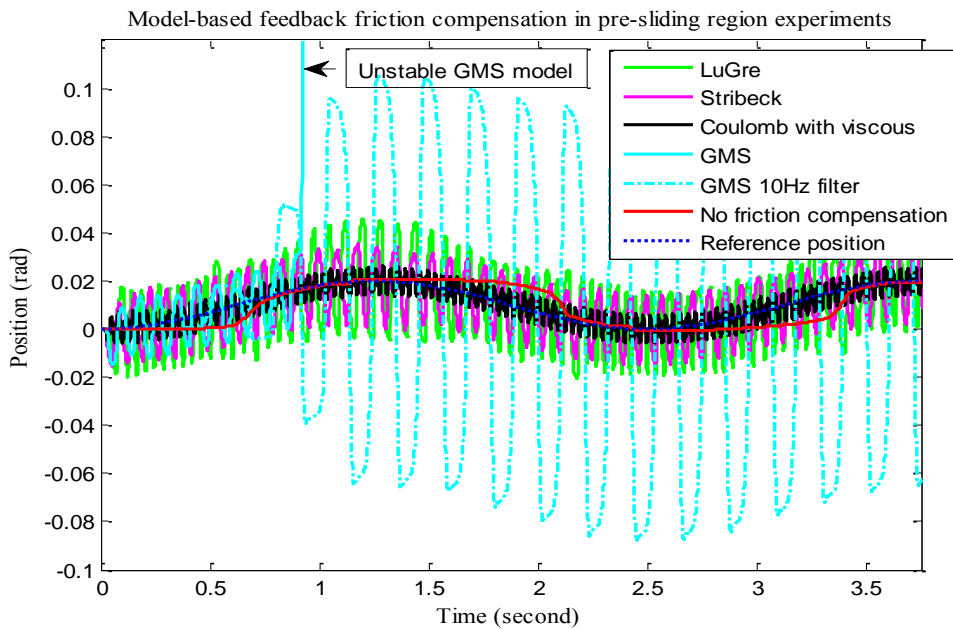

Figure 4.42. Experimental model-based feedback friction compensation of system with grease-added friction in response to the low-velocity sinusoidal position input (PID with 10 Hz bandwidth)

4.3.2.2.2 *Response to the high-velocity sinusoidal position input*

As in the previous friction case in section 4.3.1.2.2, the model-based feedforward and feedback friction compensation results of the system with grease-added friction are given in Figure 4.43 and Figure 4.44, respectively. In both of the responses, the PD control action without any friction compensation term shows the same stick-slip behaviour near zero velocity regions as expected from the simulations.

In the feedforward friction compensation shown in Figure 4.43, all models except Coulomb with viscous model follow the input trajectory with approximately the same accuracy near non-zero velocity regions, and also all models show the stick-slip behaviour near the zero velocity region as investigated in simulations in Figure 3.23, Figure 3.29, and Figure 3.35. However, the dynamic models give better tracking results near zero velocity regions. Since the friction structure in the system is highly position dependent, the stick-slip like behaviour exists at non-zero velocity regions in experiments different from the simulations.

In Figure 4.44, which demonstrates the feedback friction compensation results, all responses exhibit oscillations. The Coulomb with viscous model, Stribeck model and LuGre model give the similar degree of accuracy with the Coulomb with viscous model having the lower amplitude, higher frequency chatterring than the others. The GMS model makes the system unstable, and the GMS model with filtered input gives response including stick-slip oscillations. Although no response is satisfactory, the GMS model can be considered to give the best response with small frequency and amplitude oscillations. On the other hand, the experimental results show extremely unexpected oscillations as compared to the simulations in Figure 3.24, Figure 3.30, and Figure 3.36. Especially, the dynamic models and the Coulomb with viscous friction model do not give smooth response as expected.
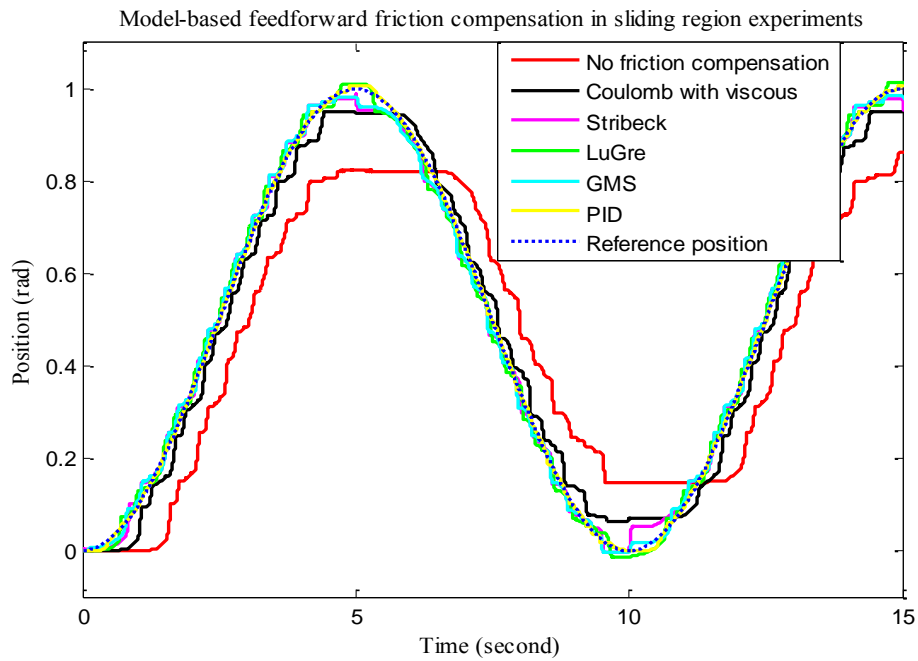
Figure 4.43. Experimental model-based feedforward friction compensation of system with grease-added friction in response to the high-velocity sinusoidal position input
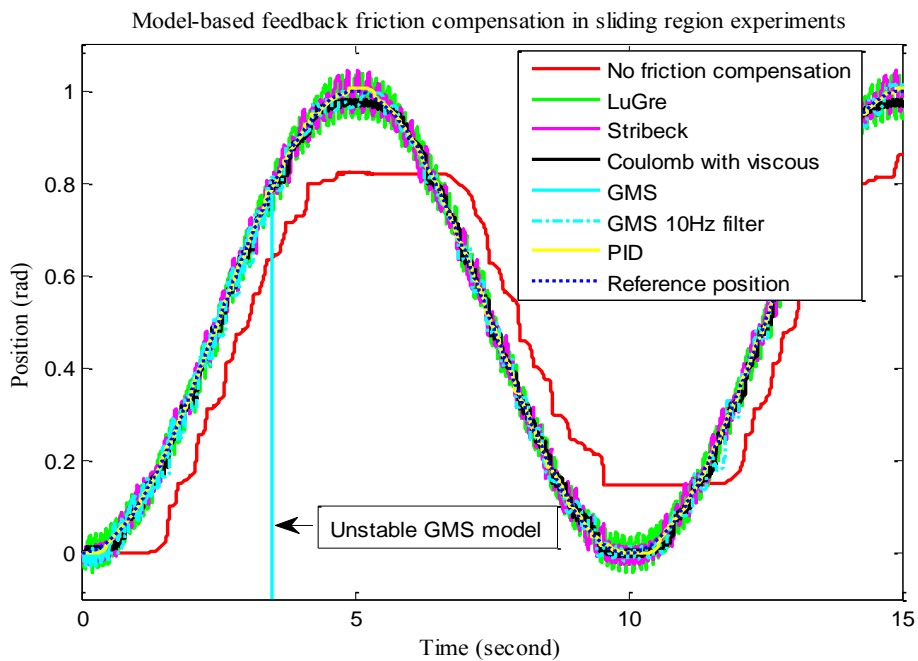
Figure 4.44. Experimental model-based feedback friction compensation of system with grease-added friction in response to the high-velocity sinusoidal position input

As the Figure 4.43 is examined, it is seen that the responses of the PID control action and the PD action with friction compensation models are similar to each other in most of the trajectory as expected from the simulations. However, the PD control with dynamic models give much closer response to the PID action near zero velocity regions, especially the PD with LuGre model compensation. Moreover, the extreme stick-slip like behaviour of the compensation models at non-zero velocities are due to position dependent friction which is compensated by the PID control action to some extent.

The 10 Hz bandwidth PID control action with and without compensation models is also applied here to see the performance of the system near zero velocity regions. In this respect, the responses of the system with only PID control action, and PID control action with feedforward and feedback friction compensation terms are shown in Figure 4.45 and Figure 4.47. According to the feedforward compensation, addition of the friction models to the PID control action except Stribeck model improves the response near zero velocity regions. Especially the LuGre model makes the response much closer to the input trajectory near zero velocity regions by providing smoother transition from stick to slip. These situations are demonstrated more clearly in Figure 4.46 by enlarging the responses near a zero velocity region. On the other hand, the responses are all oscillatory in the feedback compensation case. Here, the Coulomb with viscous model gives the best response with smallest chattering although all models can follow the trend of the input trajectory.
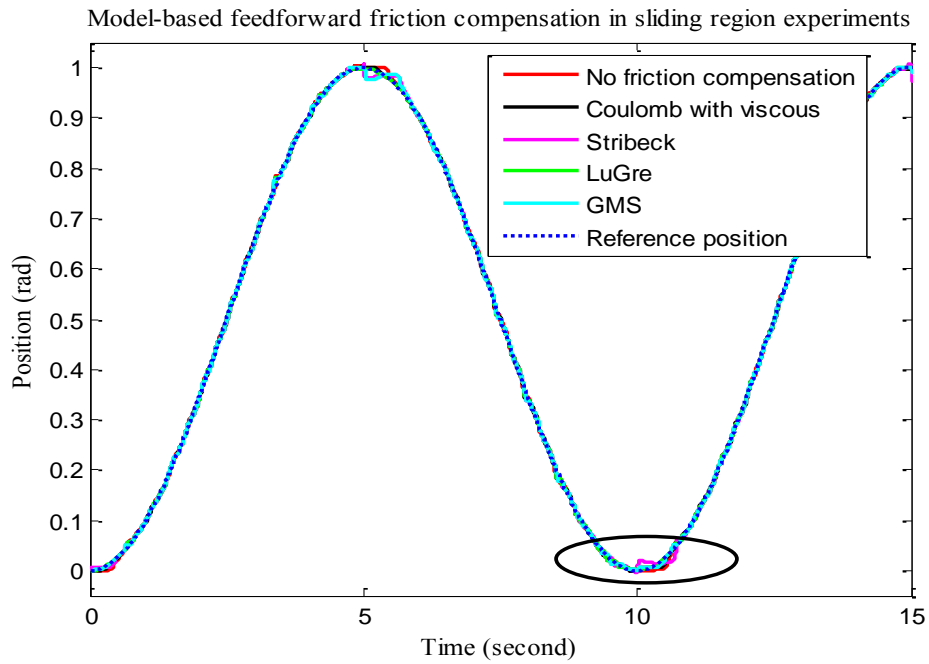
Figure 4.45. Experimental model-based feedforward friction compensation of system with grease-added friction in response to the high-velocity sinusoidal position input (PID with 10 Hz bandwidth)
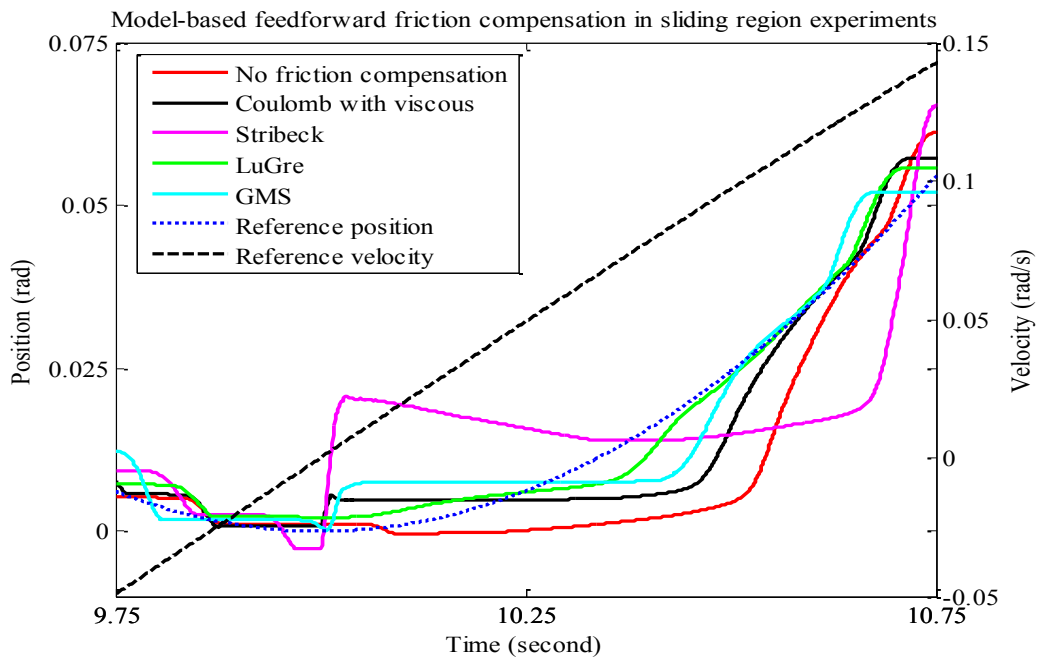

Figure 4.46. Enlarged graph of the marked region of Figure 4.45
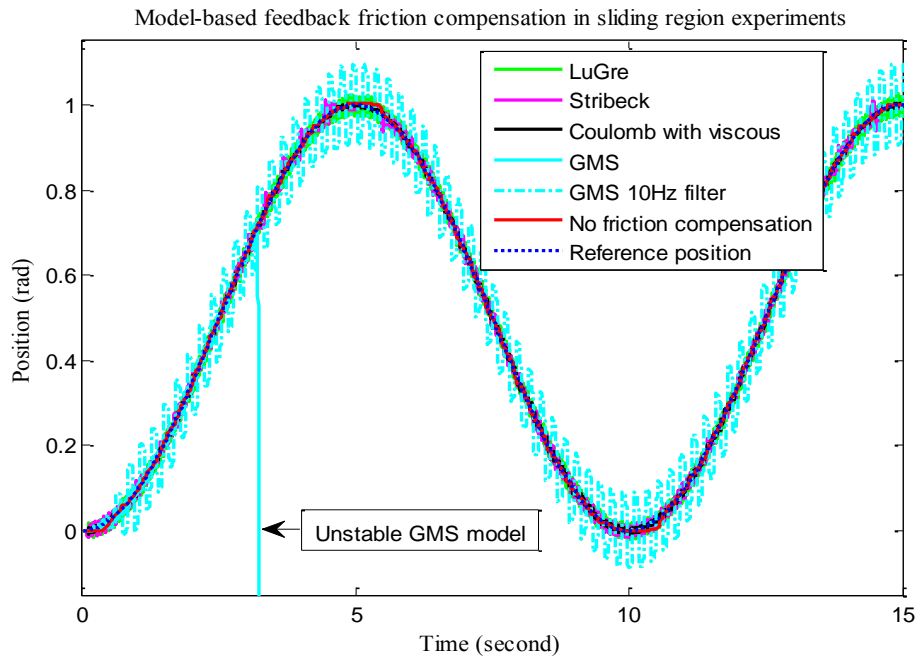
Figure 4.47. Experimental model-based feedback friction compensation of system
with grease-added friction in response to the high-velocity sinusoidal position input
(PID with 10 Hz bandwidth)

4.3.2.2.3 *Response to the step position input*

For the step position input, the experimental results with the same PD
controller as in the simulations are given in Figure 7.4 and Figure 7.5 in Appendix.
Due to the same problem mentioned in section 4.3.2.2.1, the bandwidth of the PD
controller is decreased to 25 Hz. According to this new control parameter, the results
of the model-based feedforward and feedback friction compensations are given in
Figure 4.48 and Figure 4.49, respectively. Note that the PD control action alone
cannot follow the trajectory.

As can be seen from Figure 4.48 that the Stribeck model and dynamic friction
models follow the step input with nearly the same accuracy and steady-state errors
better than the Coulomb with viscous model. However, the Stribeck model cannot
keep the accuracy and the response becomes worse at the end of the trajectory. As
compared to the simulations in Figure 3.25, Figure 3.31, and Figure 3.37, these

experimental results show similarity with the simulations in general, but especially with the case of undercompensation of friction in Figure 3.31.

On the other hand, the feedback friction compensation results in Figure 4.49 emphasize that both the static models and LuGre model track the step input with extreme oscillations. Moreover, the amplitude of oscillations of static models is lower than the one in LuGre model whereas they are comparable in themselves. Again, the GMS model makes the system unstable after some oscillatory tracking while the GMS model with filtered input gives a smooth response with steady-state error. In comparison with the simulation results in Figure 3.26, Figure 3.32, and Figure 3.38, the experimental results of the LuGre model give unexpected oscillatory behaviour instead of the smooth response whereas the static models show the expected oscillatory characteristic. Additionally, the smooth response of the GMS model with filtered input corresponds to the simulations to some extent (at steady-state), especially to the case of undercompensation of friction in Figure 3.32.

Again it is seen from the response in Figure 4.48 that the 25 Hz bandwidth PID controller exhibits highly oscillatory behaviour in contrast to the simulations which include stick-slip behaviour at steady-state. Actually, the gains of the PID control action are too high in order to obtain a smooth response.

The results of the experiments similar to the ones in previous sections with the 10 Hz bandwidth PID control action with and without the friction compensation terms are shown in Figure 4.50 and Figure 4.51. According to the feedforward friction compensation in Figure 4.50, there is not a valuable difference in responses. Actually, the steady-state errors are approximately the same for a pure PID and PID with any friction compensation term. The only improvement is that the response time to reach the steady-state is lower for the PID with dynamic friction models than the pure PID case. This condition is valid for Coulomb with viscous model from time to time, and addition of the Stribeck model makes the steady-state error worse. For the feedback compensation case in Figure 4.51, all models follow the input trajectory, but with undesirable, high frequency oscillations in comparison to the much smoother response of the PID control action without any compensation term.
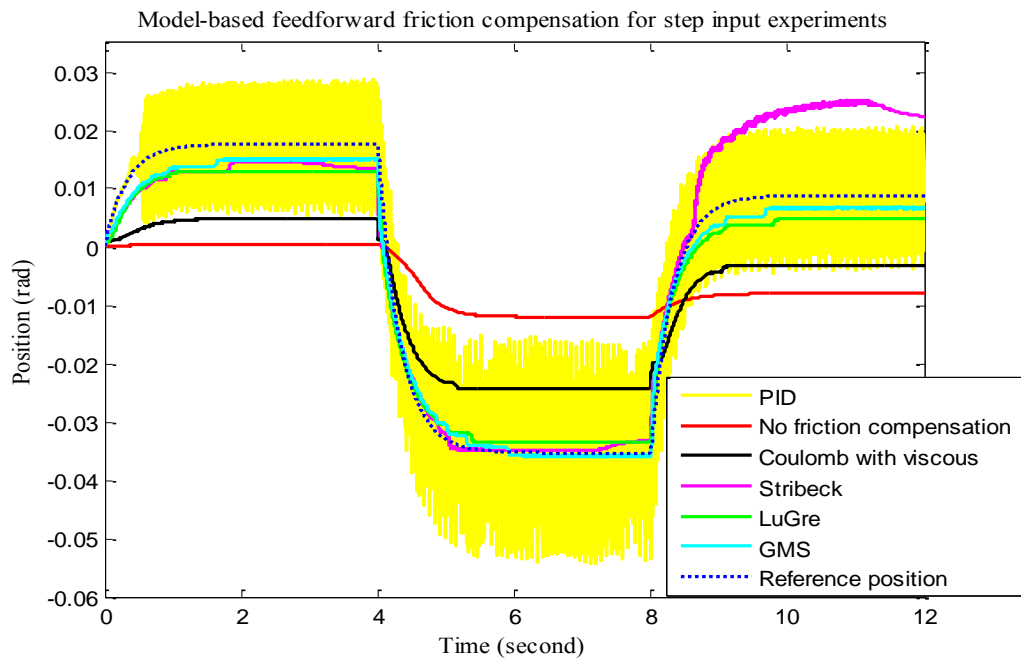
Figure 4.48. Experimental model-based feedforward friction compensation of system with grease-added friction in response to the step position input
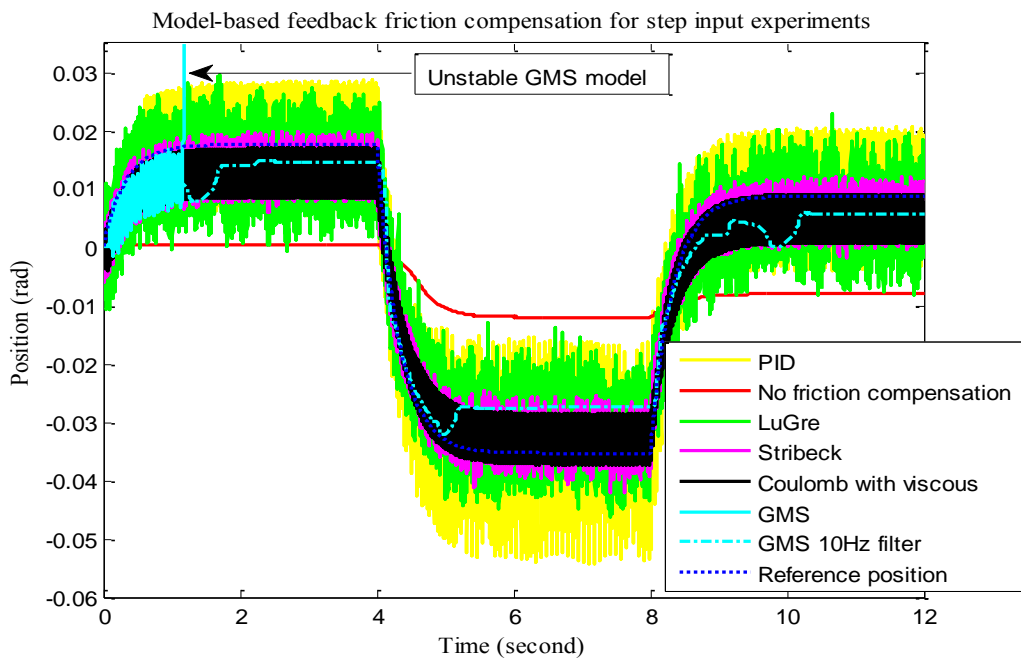
Figure 4.49. Experimental model-based feedback friction compensation of system with grease-added friction in response to the step position input
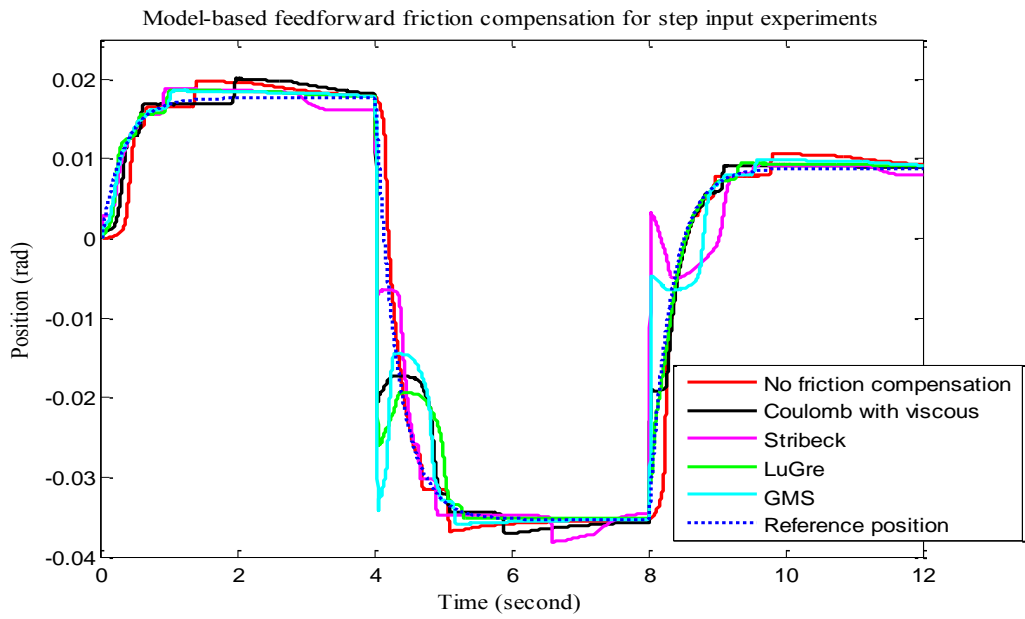
Figure 4.50. Experimental model-based feedforward friction compensation of system with grease-added friction in response to the step position input (PID with 10 Hz bandwidth)
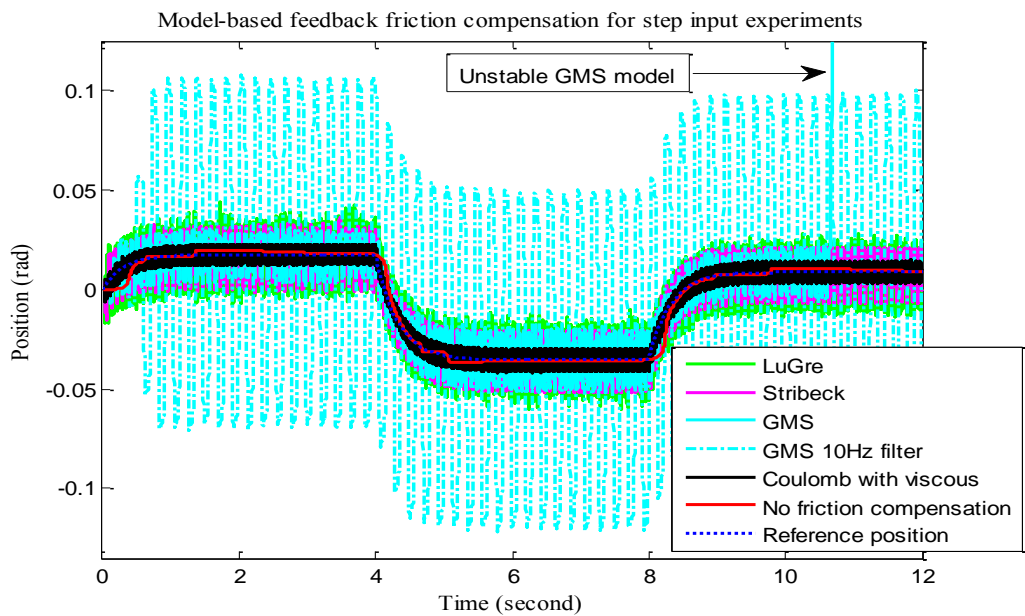
Figure 4.51. Experimental model-based feedback friction compensation of system with grease-added friction in response to the step position input (PID with 10 Hz bandwidth)

4.4 Repeatability analysis

In order to verify the accuracy of the experimental results and strengthen the comments made on these results, the experiments should be done more than one by keeping the environmental conditions as close as possible. In this study, a case is selected and some experiments are repeated on this case instead of doing the experiments in all input and friction cases. In this respect, the grease-added friction case with the low-velocity sinusoidal position input is selected as a sample one among other cases, and only the PID control action with and without the model-based feedforward friction compensation terms is applied to the system. During the system run, the experiments are repeated five times for each friction compensation technique with a time interval of ten minutes between each experiment. The results of these repeatability experiments together with the results used in this thesis are given in Figure 4.52, Figure 4.53, Figure 4.54, Figure 4.55, and Figure 4.56 for the different friction compensation models added to the PID control action. As can be shown from these figures, the results for each friction compensation model are close to each other and keep the shape of the response curves.
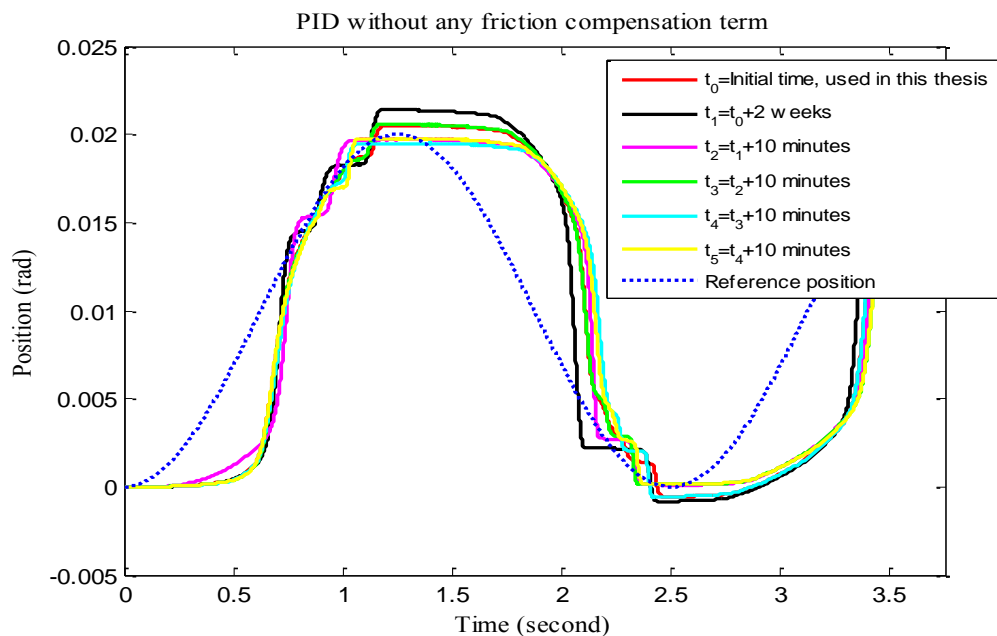
Figure 4.52. Repeatability analysis for the system with the PID control action without any friction compensation term
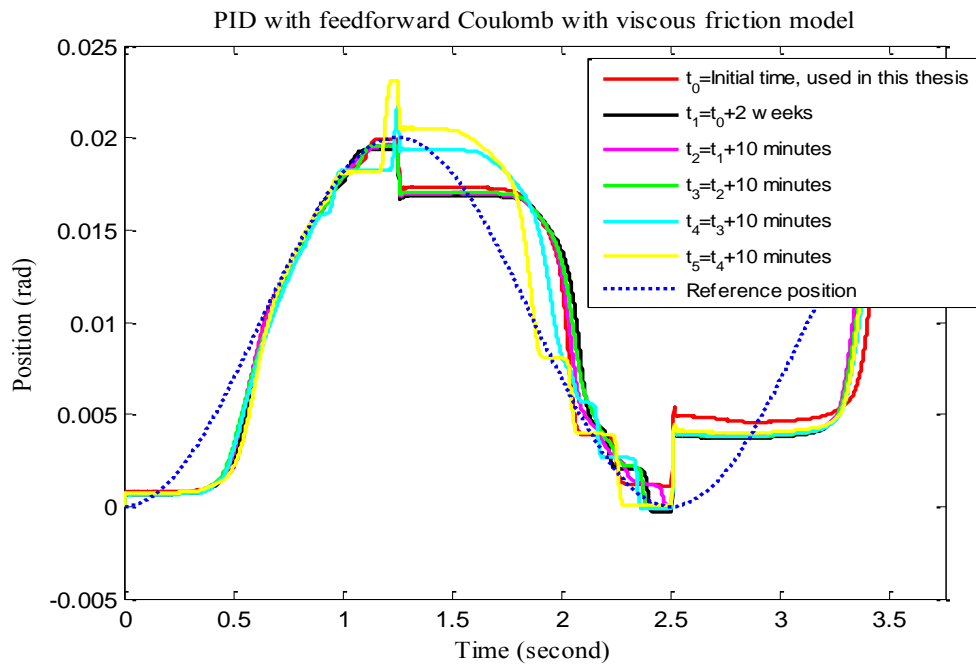
Figure 4.53. Repeatability analysis for the system with the PID control action with feedforward Coulomb with viscous friction model
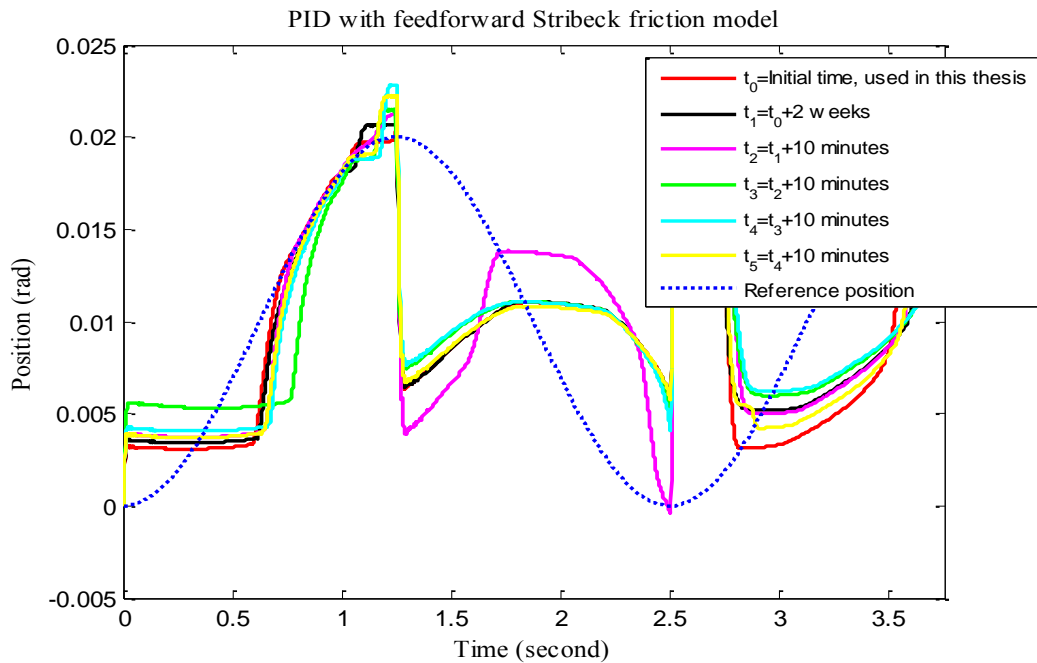
Figure 4.54. Repeatability analysis for the system with the PID control action with feedforward Stribeck friction model
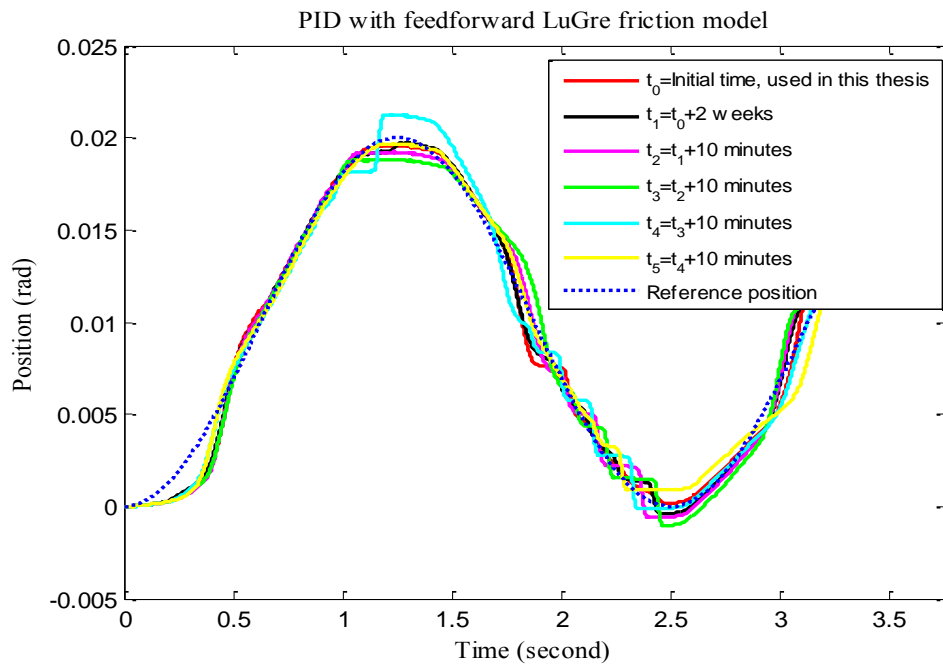
Figure 4.55. Repeatability analysis for the system with the PID control action with feedforward LuGre friction model
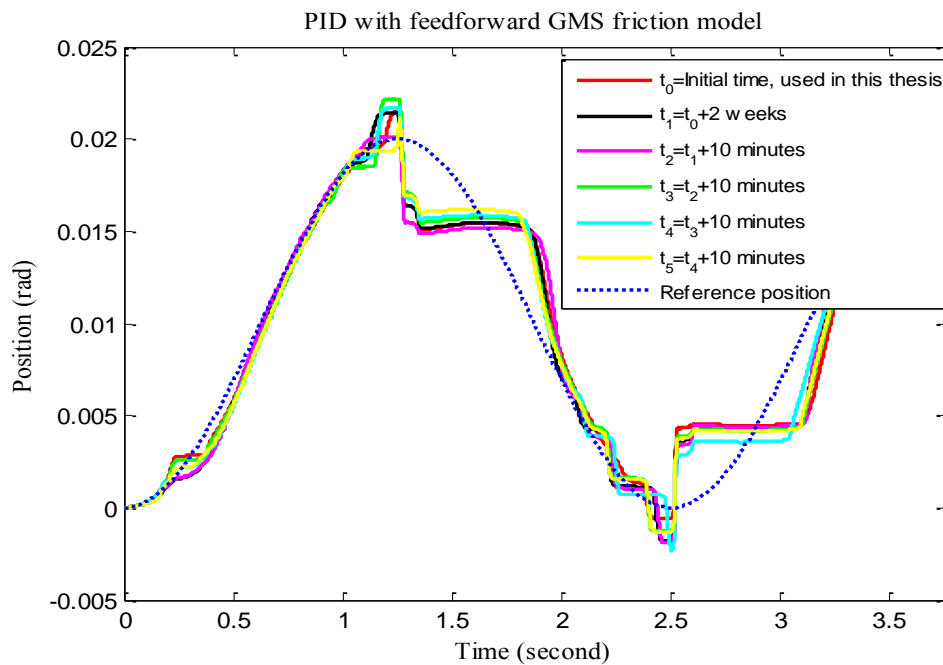
Figure 4.56. Repeatability analysis for the system with the PID control action with feedforward GMS friction model

4.5   Analysis of the flexibility effects in the system

Recall that the system is assumed to be a 1-DOF system and the angular position of the shaft (assuming rigid) is controlled under the effect of friction. For the purpose of precise position control, friction is identified in both the pre-sliding and sliding regions. Especially the pre-sliding region of friction includes the angular position measurements in the order of 10^{-4} radians. Thus, the angular deflections in the shaft should be examined in order to reach the accuracy of the position control of the free end of the shaft due to the assumption of the rigidness of the system. For this purpose, some critical dimensions of the experimental set-up are given in Figure 7.1 in Appendix.

The angular position of the free end of the shaft is affected by the elasticity of the shaft part between the encoder and friction disk (main friction torque application point). By using the information given for the shaft in Table 8 and the distance between the encoder and friction disk given in Figure 7.1, the stiffness of the shaft is found as 396 N·m/rad. Note that the level of angular position measurements in the pre-sliding region experiments of dry friction case shown in Figure 4.12 is in the order of 10^{-4} radians when the maximum torque of 0.18 N·m is applied. On the other hand, the level of static angular deflection in the shaft is calculated as 7.46×10^{-4} radians by using the stiffness value and the break-away torque value of the motor given in Table 9. In this calculation, it is remained in the reliable side by using the motor torque data instead of the torque sensor measurement data for the critical part of the shaft and assuming a static deflection although the position control is dynamic. Then, the position level in the pre-sliding region experiment of the dry friction case demonstrated in Figure 4.12 is comparable to the angular deflection of the shaft. Hence, it can be concluded that the pre-sliding region identification of friction actually includes data both from the friction torque and elasticity of the shaft, and the angular position of the free end of the shaft is different from the encoder measurement in the order of the calculated static twist level of 7.46×10^{-4} radians. However, this value is 3.73% of the maximum value of the low-velocity sinusoidal position input used in the experiments, and can be neglected for the control purpose.

By the same procedure, the static angular deflection in the shaft is calculated as 6.85×10^{-4} radians for the grease-added friction case using the stiffness value of the shaft and the break-away torque value of the motor given in Table 10 in this time. Again, the static angular deflection in the shaft is comparable to the position level in the pre-sliding region experiment of the grease-added friction case depicted in Figure 4.36. Thus, it can be said that the results of the dry friction case are also valid for the grease-added friction case. However, more accurate analysis can be made if the dynamic angular deflections are considered.

In addition to the elasticity of the shaft, the coupling between the motor and shaft has torsional elasticity that is very high. The level of static angular deflection in the coupling is calculated as 1.7×10^{-5} and 1.5×10^{-5} radians for the dry and grease-added friction cases respectively by using the stiffness value of the coupling given in Table 8 and the break-away torque values of the motor given in Table 9 and Table 10. These values are very small compared to the shaft deflections, and it can be considered that the encoder measurements on the shaft near motor rotor is the angular position of the motor rotor. Here, the deflection values in the coupling are about 0.08% of the maximum value of the low-velocity sinusoidal position input used in the experiments, and can be neglected for the control purpose as in the shaft deflection case. Then, it can be concluded that the 1-DOF system assumption is valid within the frequency range of interest.
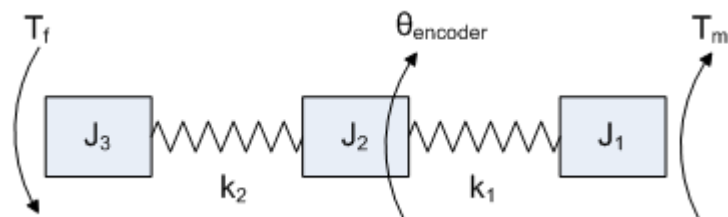
Figure 4.57. Elastic model of the system for a flexibility analysis

In Figure 4.57, a 3-DOF elastic model of the system is shown. Here, J_1 represents the total inertia of the motor rotor and half of the coupling, J_2 is the total inertia of the half of the coupling, encoder rotor and the part of the shaft between the friction disk and coupling, and J_3 is the total inertia of the remaining part of the shaft, friction clutch and the auxiliary part used. On the other hand, k_1 stands for the torsional stiffness of the coupling while k_2 exhibits the torsional stiffness of the shaft part between the encoder and friction disk. Additionally, T_m, T_f and $\theta_{encoder}$ represent the motor torque, friction torque and position measurement of the encoder, respectively.

According to the Figure 4.57, the first three undamped modes of the system are approximately found to be at 0 Hz, 270 Hz, and 2750 Hz. However, according to the Figure 4.58 and Figure 4.59, which show the power spectral density graphs of some experimental results exhibiting oscillations, the systems with the PD and PID control actions have resonances near 330 Hz and 300 Hz respectively, which are very close to the theoretical elastic mode at 270 Hz. It is known that damping shifts the resonance frequency to higher values. Thus, it can be concluded that the high frequency oscillations in some responses in the feedforward and feedback compensation cases are triggered by this elastic mode. Recall that, the sampling frequency of the systems with the PD and PID controllers used in the experiments is 1000 Hz, which allows the controllers to give output signals upto 500 Hz due to the discretization. Then, it can be considered that the sampling frequency of 1000 Hz does not constitute a problem for the stability of the system because it is higher enough than the maximum chosen bandwidth of the closed loop systems, which is 35 Hz. However, the controllers are capable of exciting the elastic modes of the system below 500 Hz since they do not vanish as the frequency increases. Then, the high frequency oscillations in some responses can be explained with the coupling between the controllers and compliance of the system.
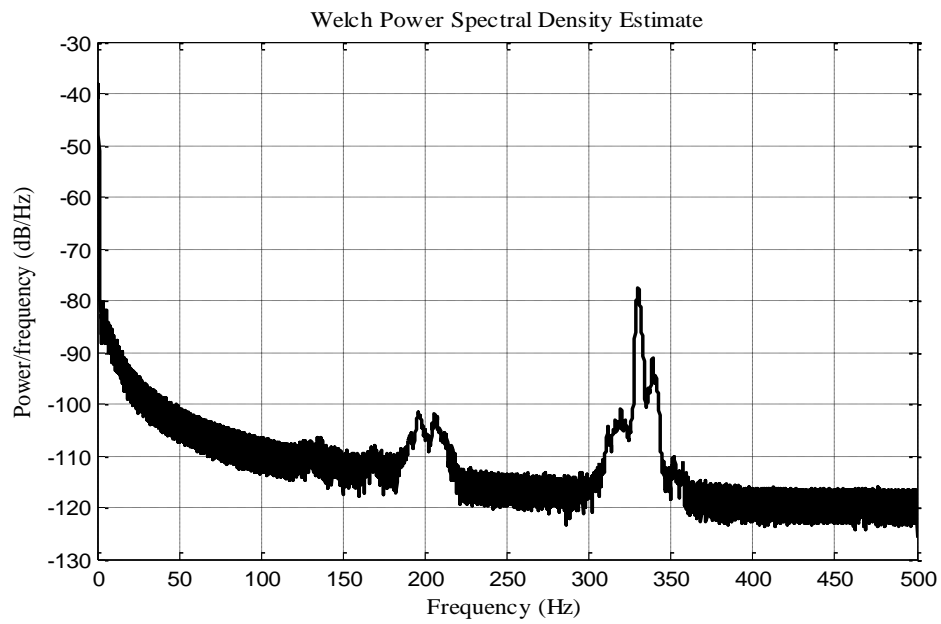
Figure 4.58. Power spectral density graph of the system with PD controller with 36 Hz bandwidth (Analysis of the response to the low-velocity sinusoidal position input for the dry friction case)
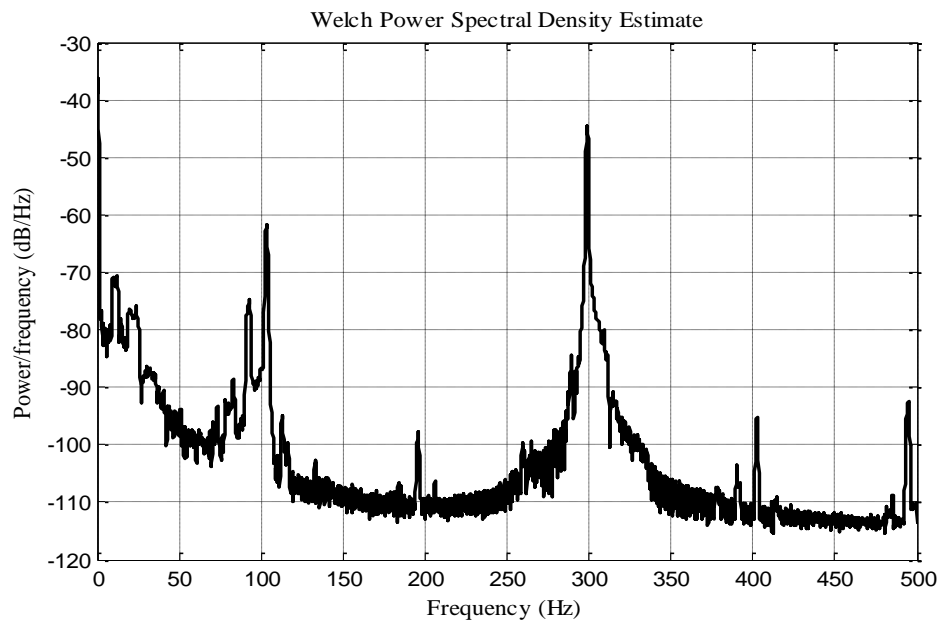
Figure 4.59. Power spectral density graph of the system with PID controller with 25 Hz bandwidth (Analysis of the response to the low-velocity sinusoidal position input for the grease-added friction case)

CHAPTER 5

DISCUSSION AND CONCLUSION

5.1 Summary and comments on the results

In this thesis, modelling, identification and compensation of friction in a control system are studied in order to obtain a satisfactory system response under the effect of friction. In this respect, a rotary 1-DOF mechanical system is considered. The system model built is simulated in computer environment, and an experimental set-up is established with the aim of the precise position control. For the compensation of the nonlinear frictional effects, only the model-based fixed parameter friction compensation approaches are considered.

In order to reach this level, firstly a general information about the friction phenomenon acquired by experiments during the few decades is given. After the common properties of friction phenomenon are described comprehensively, different friction models are introduced. These friction models are seperated into two groups in literature as static and dynamic friction models, and this seperation is done according to the inclusion of the different amount of experimental findings by the friction models in imitating the real frictional behaviour. While introducing the static and dynamic friction models, only the models which are commonly used in the control area are examined in detail. In this respect, the mathematical and/or differential formulations of these models are given, and the different aspects of them are mentioned.

After that, the modelling activities required for the simulation of the system are done. Firstly, the differential equation of the open loop system (plant) with friction is derived and its model is built in MATLAB® SIMULINK® environment. Then, the control algorithm required for the closed loop position control of the

system with friction is designed. This control algorithm is composed of two parts which are linear and nonlinear. The classical proportional with derivative (PD) feedback control action is used in the linear part of the control law while the friction models described previously are used in the nonlinear part of the control law in order to estimate the actual friction in the system and produce a signal that counteracts the actual friction instantaneously. In this respect, four friction models, two of which are static models and others are dynamic models, are used for the purpose of friction compensation and position control of the system. These compensation models are the Coulomb with viscous static friction model, Stribeck static friction model, LuGre dynamic friction model and the Generalized Maxwell-Slip dynamic friction model. Additionally, the actual friction in the system is modelled by the GMS friction model with higher elements than the GMS friction model used in the compensation.

Throughout the simulations, both model-based fixed parameter feedforward and feedback friction compensation techniques are applied to the system using the aforementioned four friction models. On the other hand, three different inputs are applied for the position tracking task of the closed loop system as given below:

- Low-velocity sinusoidal position input
- High-velocity sinusoidal position input
- Step position input

Note that the position and velocity ranges of these three inputs are different from each other. Since each input makes the system move in different dominant friction regions, it is aimed that the effectiveness of the model-based friction compensation approaches can be seen under the different dominant friction characteristics of the system. Additionally, all of these compensation methods and inputs are simulated under the three different cases of actual friction in order to see the performance of the fixed parameter friction compensation techniques under the effects of friction changing in time. These actual friction cases are given as follows:

- Nominal actual friction case

- Positively-perturbed actual friction case (undercompensation of friction)

- Negatively-perturbed actual friction case (overcompensation of friction)

While doing the simulations mentioned above, the same control parameters are used in all of them in order to make comparisons fairly. Additionally, the system is simulated with the linear PID control action alone, i.e. without any friction compensation term, for comparison with the approach of using the PD control action with friction compensation terms.

According to the simulations performed on the systems with different levels of actual friction and with different applied input trajectories, the systems with the dynamic friction compensation models generally give much better and smoother results than the systems with the static models. Especially, the system with the GMS friction compensation model gives responses which have least tracking error and non-oscillatory behaviour in response to the sinusoidal trajectories in the use of feedback compensation approach. Note that the GMS friction model is the only compensation model that does not represent oscillations in response to the sinusoidal trajectories in all feedback compensation cases. Actually, these results are expected since the actual friction in the system is also modelled by the GMS model. In most of the cases, the system with the LuGre friction compensation model follows the one with the GMS model in all input trajectories in terms of the tracking error and smoothness. For the static models, the system with the Stribeck friction model gives similar or better responses than the system with the Coulomb with viscous friction model in response to the sinusoidal trajectories in the feedforward compensation cases. In the feedback compensation; however, the system with the Coulomb with viscous friction model usually exhibits less oscillatory and better results than the one with the Stribeck friction model in all input cases although the Stribeck model represents the sliding region of friction more accurately as compared to the GMS model of actual friction.

If the results are seperated based on the input trajectories which emphasize the different dominant regions of friction, the following results can be obtained in general:

- For the low-velocity sinusoidal position trajectory, the GMS, LuGre, and the Stribeck model give similar results better than the Coulomb with viscous model in the case of feedforward compensation. For the feedback case, the accuracy order is followed by the GMS, LuGre, Coulomb with viscous and the Stribeck models respectively, except the case of increased actual friction. Here, the PID control action has a stick-slip behaviour throughout the trajectory due to the integral gain although it follows the trend of the input trajectory.

- For the high-velocity sinusoidal position trajectory, all models give relatively same accuracy in the feedforward case whereas in the feedback compensation case, the GMS is the best, the LuGre and Coulomb with viscous model give similar results with low oscillations near zero velocity regions and follow the GMS model, and the Stribeck model gives the worst results due to the high oscillations in the negative velocity directions. Here, the PID control action follows the trajectory, but with a stick-slip behaviour near zero velocity regions due to the integral gain.

- For the step position trajectory, in the feedforward compensation, the GMS, LuGre, and the Stribeck models give similar results better than the Coulomb with viscous model only for the case of positively-perturbed actual friction in terms of the steady-state errors. In other cases, the Coulomb with viscous model is better. For the feedback compensation case, the accuracy order is usually as follows: The GMS, LuGre, Coulomb with viscous, and the Stribeck models respectively, and both of the static models are oscillatory while the dynamic models are non-oscillatory. Here, the PID control action has a stick-slip behaviour at steady-state although it follows the trend of the input trajectory.

As a result, it can be concluded in general that the GMS model gives the best responses both in the feedforward and feedback friction compensation cases. On the other hand, the Coulomb with viscous model usually gives the worst responses in the feedforward friction compensation cases whereas the Stribeck model gives the worst responses in the feedback friction compensation cases. For the simulations where the PID control action is used, the system frequently represents a stick-slip behaviour at low-velocity regions where the effects of the pre-sliding region of friction dominate, and loses its smoothness.

After the simulations are completed, the experimental set-up and studies performed in order to see the accuracy of the simulations and friction compensation models in reality are mentioned. In this respect, firstly the experimental set-up is described. In brief, this set-up is a 1-DOF, direct-drive, rotary mechanical system same as in the simulations. Then, the identification of the system inertia and the parameters of the friction models is performed for the two different friction adjustments as case studies. By using the identified parameters, the system is run seperately in these two different friction cases for the purpose of accurate positioning and for looking at the performances of the model-based fixed parameter feedforward and feedback friction compensation approaches in real conditions. Finally, a repeatability analysis is done for an experimental case chosen as a sample in order to see the accuracy of some experimental results and comments made on these results, and a simple flexibility analysis of the system is given.

For the first case study, the friction in the clutch-disk interface is purely dry friction and the viscosity is only coming from the bearings in the system. During the friction identification experiments, it is seen that the friction in the system is highly position dependent. Because of this, the friction characteristic of the system, i.e. the break-away torques and the friction in constant velocities, has highly oscillatory behaviour through the $360°$ rotation of the shaft. Hence, the experiments are performed under this uniformity condition and the friction level slightly different from the simulations. However, the same PD and PID control actions as in the simulations are used as linear feedback controllers in position tracking experiments. Moreover, since the aim is the compensation of the total friction in the system, the

friction identification is done using the motor current data instead of the torque sensor measurements. However, it is seen during the friction identification experiments that there is nearly a constant difference between the motor current and torque sensor measurements, which can be respresented by the Coulomb with viscous friction model. Thus, it is concluded that the friction torque due to the bearings in the system can be modelled by the Coulomb with viscous friction model in general. Another result of the friction identification experiment is that the Static friction level in the system comes lower than the Coulomb friction level and no Stribeck effect is present in the system for this dry friction case. Then, this statement together with the aforementioned experimental conditions suggests that the comparison between the experiments and simulations can be done only for the trend of the responses.

According to the results of the experiments with dry friction, the system with dynamic compensation models gives much better and less oscillatory responses than the one with static models in response to the sinusoidal trajectories. The addition of the compensation models to the PD and PID control actions generally improves the responses, especially near zero velocity regions with the addition of the dynamic models. For the step position input; however, the addition of the compensation models does not change the responses of the pure PD action and even pure PID action in a valuable manner. In all input trajectories except the high-velocity sinusoidal one, the model-based feedback compensation approaches of all models make the system responses oscillatory or increase the oscillation level in comparison to the usage of the pure PD or PID action. Generally, the dynamic models and static models give similar responses between themselves, and cannot be seperated much from each other in terms of the accuracy. As a final note, the GMS model-based feedback compensation generally makes the system unstable and it is proposed that it should be used with some filters on the input signal in order to obtain a stable response. As far as the pure PID control is considered, it gives an extremely oscillatory responses whose amplitudes are higher than the PD control action with friction compensation terms in contrast to the simulations due to the high bandwidth of the PID control action and nonlinearity of the system.

As the responses are compared in terms of the input trajectories, the following results can be inferred:

- For the low-velocity sinusoidal position trajectory, the systems with the GMS and LuGre dynamic friction compensation models give similar, better and more continuous-like tracking results in the feedforward compensation approaches in comparison to the Stribeck and Coulomb with viscous static friction models, which inturn give similar results between each other. For the feedback case, the static models again give similar responses with higher oscillations than the dynamic models although they follow the input trajectory. Here, the LuGre model can be said to give the best result with lower oscillations. On the other hand, the PID action is extremely oscillatory due to the high bandwidth and worse than the other compensations although it follows the input trajectory. As compared to the simulations, it can be said that not much correspondence exists except that the dynamic models give better results.

- For the high-velocity sinusoidal position trajectory, the GMS and LuGre dynamic friction models give similar, non-oscillatory and much smoother responses near zero velocity regions in comparison to the Coulomb with viscous and Stribeck static friction models in both the feedforward and feedback compensation cases. Furthermore, addition of the compensation models to the PD action improves the tracking in a valuable manner. Here, the use of the pure PID action gives a similar response to the case where PD action with dynamic models is used. Additionaly, when the compensation models are added to the PID action with 10 Hz bandwidth, it is seen that only the usage of the dynamic models smoothens the responses near zero velocity regions as compared to the pure PID in the feedforward compensation. As compared to the simulations, the results are generally as expected.

- For the step position trajectory, addition of the friction compensation models to the PD control action cannot give a satisfactory responses and a valuable performance increase in the feedforward compensation case. However, the

order of accuracy is as follows: the Stribeck, GMS, LuGre and Coulomb with viscous models. For the feedback compensation, all models give oscillatory responses which are actually not good enough as compared to the pure PD action. Again the usage of the pure PID action makes the system highly oscillatory, which is worse than the other compensations although it follows the input trajectory. In this case, the simulations and experimental results do not correspond to each other actually. On the other hand, for the experiments with 10 Hz bandwidth PID control action, the addition of the feedforward friction compensation terms does not change the response crucially. Only the response time to reach the steady-state value decreases slightly while the steady-state error is kept almost the same. In the feedback compensation case, all models make the system response worse. Only the system with LuGre dynamic friction model does not exhibit oscillations; however, it represents unexpected and sudden, glitch-like changes in position, which are undesirable.

For the second case study, the friction characteristic of the system is changed by adding grease into the friction clutch-disk interface. This addition does not change the position dependent structure of the friction; however, it causes a considerable change in the sliding region characteristic of friction. It induces two different Stribeck effect-like behaviours in constant velocity friction curve. In this respect, friction identification experiments show that the static friction level becomes higher than the Coulomb level, i.e. the Stribeck effect is detectable in this case. Although the friction characteristic becomes much similar to the one in simulations in terms of the shape of the steady-state curve of the friction in sliding region, the friction torque level is not close enough to the simulations in terms of the amplitude, and actually smaller than the simulations. Thus, the comparison between the experiments and simulations can be done regarding only the trend of the responses as in the previous friction case.

According to the experiments with grease-added friction, the system with dynamic friction compensation models gives much better tracking results than the

static models in response to the sinusoidal trajectories as in the dry friction case. Although addition of the feedforward compensation terms of all models improves the responses in comparison to the pure PD and PID actions, especially the LuGre model-based feedforward compensation makes the responses smoother near zero velocity regions. In contrast to the feedforward compensation, the feedback compensation approaches of all models make the system responses oscillatory and worse when added to the pure PD and PID actions, and especially the LuGre model exhibits higher oscillations than the static models, which is different from the dry friction case and simulations unexpectedly. For the step input case, addition of the feedforward friction compensation models to the PD action improves the response in contrast to the dry friction case while the compensation terms do not affect the response of the pure PID in a satisfactory manner when added. Unfortunately, the GMS model-based feedback compensation generally makes the system unstable as in the dry friction case, and it is again proposed that it should be used with some filters on the input signal. On the other hand, the PID control with the same bandwidth as the PD action gives oscillatory responses with higher amplitudes than the PD control with compensation models for low-velocity sinusoidal and step position trajectories. This situation does not correspond to the simulations and is again due to the high bandwidth of the PID action and nonlinearity of the system. As all of the cases are considered, the results of the feedforward compensation approaches show a similarity with the simulations to some extent whereas the feedback compensations do not exhibit this similarity.

According to the input trajectories, the following results can be concluded specifically:

- For the low-velocity sinusoidal position trajectory, the LuGre model definitely gives the best and smooth results near zero velocity regions as compared to the others in the feedforward compensation case. The GMS, Stribeck, and Coulomb with viscous model follow it in terms of the tracking accuracy. For the feedback compensation case, all models make the system response highly oscillatory except the GMS model. However, the tracking of

the GMS model is undesirable due to the stick-slip behaviour it induces. Again, the use of the pure PID action with the same bandwidth as the PD action causes the system to have responses with high amplitude oscillations, which is worse than the use of the PD action with friction compensation terms. On the other hand, tracking is not satisfactory for the 10 Hz bandwidth pure PID control action. In this case, only the addition of the LuGre model-based feedforward friction compensation term makes the system response much closer to the sinusoidal input trend and highly smoothens the response near zero velocity regions as compared to the pure PID control action.

- For the high-velocity sinusoidal position trajectory, the responses of the system with PD control action with dynamic compensation models added are slightly better than the one with static models in the feedforward compensation case. However, the response of the system with the LuGre compensation model again is the best one. For the feedback compensation case, responses of all models are oscillatory except the GMS model, which inturn exhibits stick-slip like oscillations throughout the trajectory. In response to this trajectory in which viscous friction dominates, the pure PID action with the same bandwidth as the PD control action gives smoother results than the PD action with friction compensation models at non-zero velocity regions while they give similar results near zero velocity regions. On the other hand, the advantage of the use of the dynamic friction models is perfectly seen near zero velocity regions when the friction compensation terms are added to the 10 Hz bandwidth PID control action. Especially, addition of the LuGre model-based feedforward friction compensation term removes the stick-slip behaviour near zero velocity regions in the response of the pure PID action as in the previous case. Here, the GMS and the Coulomb with viscous model do the same task, but not as good as the LuGre model.

- For the step position trajectory, addition of the dynamic model-based feedforward friction compensation terms to the PD control action improves the responses by decreasing the steady-state errors as compared to the pure PD control action. Actually the system with the GMS friction model gives the

best response, then the LuGre, Stribeck and Coulomb with viscous models follow it respectively. For the feedback friction compensation case, all models cause oscillations except the GMS model with filtered input, which has smooth response with unsatisfactory steady-state error. On the other hand, the system with the pure PID action whose bandwidth is the same as the PD action has an undesirable response with high oscillations. When a PID control with 10 Hz bandwidth is used with the friction compensation terms, it is seen that the responses do not change in a satisfactory manner in comparison to the pure PID control action. However, lower response time to reach the steady-state value is the only improvement and is obtained with the addition of the dynamic model-based feedforward friction compensation terms to the PID control action.

In conclusion, addition of the model-based fixed parameter friction compensation terms to the PD and PID linear control actions generally improves the responses in a satisfactory manner, thus its usage is proposed. On the other hand, the use of the fixed parameter feedforward friction compensation approaches is suggested instead of the feedback friction compensation techniques since the feedback compensation cases of all friction models cause oscillatory responses in almost all experiments performed. Hence, it can be inferred that the fixed parameter feedback friction compensation methods suffer from the stability issues and a stability analysis should be made if they are decided to be used in friction compensation. Furthermore, the use of the dynamic friction models instead of the static friction models is proposed for the friction compensation tasks when the low-velocity motions dominantly exist in the system. Recall that the system with dynamic friction compensation models exhibits better tracking results than the static models at the low-velocity regions in experiments. Otherwise, both dynamic and static models can be used with similar degree of accuracy of the system response, especially where the velocity of the motion is relatively higher and the viscous friction dominates. Finally, the LuGre model-based friction compensations, especially in the feedforward compensation case and at the low-velocity regions, give better tracking

results in the case of grease-added friction whereas the seperation between the use of the LuGre and GMS dynamic friction models cannot actually be done in the dry friction case due to the similar responses obtained in the experiments. This condition can be due to the highly position dependent characteristic of the friction in the system, and the elimination of this situation can be done by improving the mechanical assembly firstly. On the other hand, it can be concluded from the experiments that the Stribeck static friction model can be used instead of the Coulomb with viscous static friction model for the cases where the static friction level is higher than the Coulomb friction level.

As far as the linear control parts are considered, the PD action with compensation terms added can be used for the friction compensation of a system with the similar degree of accuracy of the pure PID control action. However, if the PID control action is already used in the system, addition of the dynamic model-based feedforward friction compensation terms makes the system response better, especially at the regions of low-velocity motions.

5.2 Future works

In this study, the cogging effect in the motor is definitely effective since the experimental set-up is a direct-drive system without any reduction element. Thus, the cogging and frictional effects are actually identified together in the experimental works as if the combined effects presented the total friction in the system. In this respect, as a first future work, the cogging effect can be modelled and compensated in some manner seperated from the frictional effects in order to represent only the frictional effects with the friction models.

Friction in the system is highly position dependent and time dependent due to the mechanical assembly of the set-up and environmental conditions. In this respect, the friction identification is done by averaging the measured data, and the corresponding mean value is used in the compensation tasks. Therefore, the experimental friction compensations done here actually include both the undercompensation and overcompensation of friction. If the position dependency can be approximated with some mathematical expressions instead, and added to the

friction models, more accurate friction modelling and much better compensation results will be obtained definitely. As a result, the simpler and lower bandwidth linear feedback controllers can also be used in a control system. Of course, this situation is out of the scope of this thesis and another future work to be done.

As an alternative way to the modelling of position dependency and another future work, the parameters of the friction models can be made time dependent and estimated on-line in order to deal with adaptively the time and position dependent characteristic of friction in the system. Note that this adaptation requires a careful derivation of an adaptive control law as well as an extensive stability analysis. However, the resulting adaptive control law, which is usually used with the model-based feedback friction compensation terms, is expected to improve the performance of the system since improvements are seen in [2], [6], [7], [8], [9], [10], [11], [14], [15], [23], [24], [25].

A more specific future work can be done on the GMS friction model. In most of the feedback friction compensation experiments in this thesis, the use of the GMS friction model makes the system unstable in contrast to the other friction models. In this respect, a stability analysis should be done for the GMS model-based feedback friction compensation, and the reasons of the instability results obtained in this thesis should be understood.

As an another future work, the simulation studies of the system with friction compensation terms can be improved and done more accurately if the position and time dependent effects of friction are included in the system model. As a further improvement, the quantization effect can be added to the feedback signal coming from the position output of the system, i.e. measurement signal, as well as the noise effect, which can be added to the control input signal, i.e. motor current signal, in simulating the system.

REFERENCES

[1]   Swevers, J., Al-Bender, F., Ganseman, C. G., and Prajogo, T., "*An integrated friction model structure with improved presliding behavior for accurate friction compensation*", IEEE Transactions on Automatic Control, Vol. 45, No. 4, pp. 675-686, April 2000.

[2]   Ge, S. S., Lee, T. H., and Ren, S. X., "*Adaptive friction compensation of servo mechanisms*", International Journal of Systems Science, Vol. 32, No. 4, pp. 523-532, 2001.

[3]   Van Seters, N., *Compensation of friction in the flight simulator stick using an adaptive friction compensator*, University of Twente, 2001.

[4]   Tjahjowidodo, T., Al-Bender, F., Brussel, H. V., and Symens, W., "*Friction characterization and compensation in electro-mechanical systems*", Journal of Sound and Vibration 308, pp. 632-646, 2007.

[5]   Márton, L. and Lantos, B., "*Identification and model-based compensation of Striebeck friction*", Acta Polytechnica Hungarica, Vol. 3, No. 3, pp. 45-58, 2006.

[6]   Márton, L., "*Friction model for low velocities. Proprieties and applications*", Fourth International Workshop on Robot Motion and Control, pp. 333-338, June 17-20, 2004.

[7]   Márton, L. and Lantos, B., "*Friction model for adaptive compensation*", Proceedings of the 11th Mediterranean Conference on Control and Automation (MED2003), Rhodes: IEEE, pp. 1-5, 2003.

[8]   Márton, L. and Lantos, B., "*Modeling, identification, and compensation of stick-slip friction*", IEEE Transactions on Industrial Electronics, Vol. 54, No. 1, pp 511-521, February 2007.

169

[9]   Márton, L. and Lantos, B., "*Friction modelling and robust adaptive compensation*", IFAC, 2005.

[10]   Tan, K. K., Huang, S. N., and Lee, T. H., "*Adaptive friction compensation with time-delay friction model*", Proceedings of the 4th World Congress on Intelligent Control and Automation, Shanghai, P. R. China, June 10-14, 2002.

[11]   Song, G., Cai, L., Wang, Y., and Longman, R. W., "*A sliding-mode based smooth adaptive robust controller for friction compensation*", International Journal of Robust and Nonlinear Control, No. 8, pp. 725-739, 1998.

[12]   Makkar, C., Dixon, W. E., Sawyer, W. G., and Hu, G., "*A new continuously differentiable friction model for control systems design*", Proceedings of the 2005 IEEE/ASME, International Conference on Advanced Intelligent Mechatronics, Monterey, California, USA, pp. 600-605, July 24-28, 2005.

[13]   Canudas de Wit, C., Olsson, H., Åström, K. J., and Lischinsky, P., "*A new model for control of systems with friction*", IEEE Transactions on Automatic Control, Vol. 40, No. 3, pp. 419-425, March 1995.

[14]   Canudas De Wit, C. and Lischinsky, P., "*Adaptive friction compensation with partially known dynamic friction model*", International Journal of Adaptive Control and Signal Processing, Vol. 11, pp. 65-80, 1997.

[15]   Olsson, H., Åström, K. J., Canudas de Wit, C., Gäfvert, M., and Lischinsky, P., "*Friction models and friction compensation*", 1997.

[16]   Lampaert, V., Swevers, J., and Al-Bender, F., "*Modification of the Leuven integrated friction model structure*", IEEE Transactions on Automatic Control, Vol. 47, No. 4, pp. 683-687, April 2002.

[17]   Iurian, C., Ikhouane, F., Rodellar, J., and Griñó, R., *Identification of a system with dry friction*, Work Report, Institut d'Organització i Control de Sistemes Industrials, Universitat Politècnica de Catalunya, Setembre 2005.

[18]   Lampaert, V., Swevers, J., and Al-Bender, F., "*Experimental comparison of different friction models for accurate low-velocity tracking*", Proceedings of

the 10th Mediterranean Conference on Control and Automation (MED2002), Lisbon, Portugal, July 9-12, 2002.

[19]   Lampaert, V., Al-Bender, F., and Swevers, J., "*A Generalized Maxwell-Slip friction model appropriate for control purposes*", PhysCon 2003, St. Petersburg, Russia, 2003.

[20]   Al-Bender, F., Lampaert, V., and Swevers, J., "*The Generalized Maxwell-Slip model: A novel model for friction simulation and compensation*", IEEE Transactions on Automatic Control, Vol. 50, No. 11, pp. 1883-1887, November 2005.

[21]   Lampaert, V., Swevers, J., and Al-Bender, F., "*Comparison of model and non-model based friction compensation techniques in the neighbourhood of pre-sliding friction*", Proceedings of the 2004 American Control Conference, Boston, Massachusetts, pp. 1121-1126, June 30-July 2, 2004.

[22]   Tjahjowidodo, T., Al-Bender, F., Brussel, H. V., "*Friction identification and compensation in a DC motor*", IFAC, 2005.

[23]   Nilkhamhang, I. and Sano, A., "*Adaptive compensation of dynamic friction using a linearized GMS model*", International Control Conference, Glasgow, Scotland, August 2006.

[24]   Nilkhamhang, I. and Sano, A., "*Adaptive compensation of a linearly-parameterized GMS friction model with parameter projection*", Proceedings of the 45th IEEE Conference on Decision & Control, San Diego, CA, USA, December 13-15, 2006.

[25]   Nilkhamhang, I. and Sano, A., "*Model-based adaptive friction compensation for accurate position control*", Proceedings of the 47th IEEE Conference on Decision & Control, Cancun, Mexico, December 9-11, 2008.

[26]   Casanova, C. C., De Pieri, E. R., Moreno, U. F., Castelan, E. B., "*Friction compensation in flexible joints robot with GMS model: Identification, control and experimental results*", Proceedings of the 17th World Congress, The International Federation of Automatic Control, Seoul, Korea, July 6-11, 2008.

[27] Baykara, B., Özgören, M. K., and Özkan, B., *"Notable friction models used in the investigation of dynamic systems" (in Turkish)*, The Proceedings of the 14th National Machine Theory Symposium (UMTS2009), Middle East Technical University North Cyprus Campus, North Cyprus Turkish Republic, July 2-4, 2009.

[28] Ogata, K., *Modern Control Engineering*, Fourth Edition, New Jersey, Prentice Hall, 2002.

[29] Żabiński, T. and Turnau, A., *"Compensation of friction in robotic arms and slide tables"*, IFAC, 2005.

APPENDIX
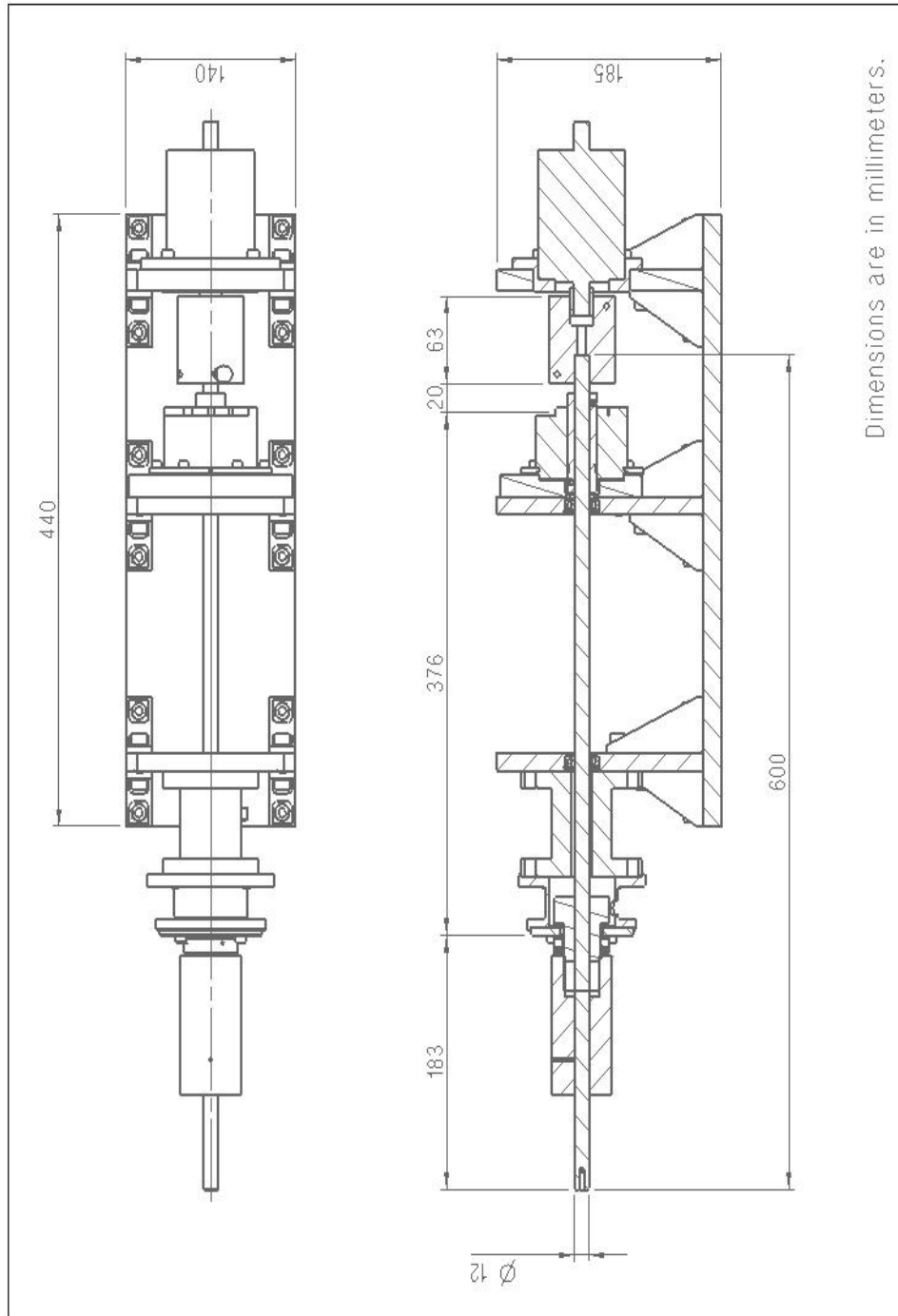
Figure 7.1. Critical dimensions of the experimental set-up
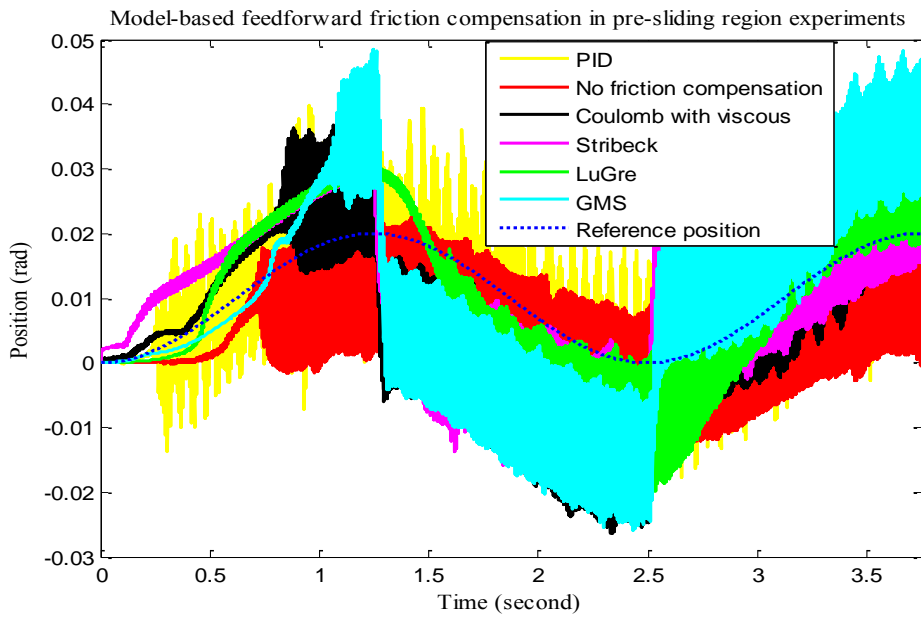
Figure 7.2. Experimental model-based feedforward friction compensation of system with grease-added friction in response to the low-velocity sinusoidal position input (PD with 36 Hz bandwidth same as in the simulations)
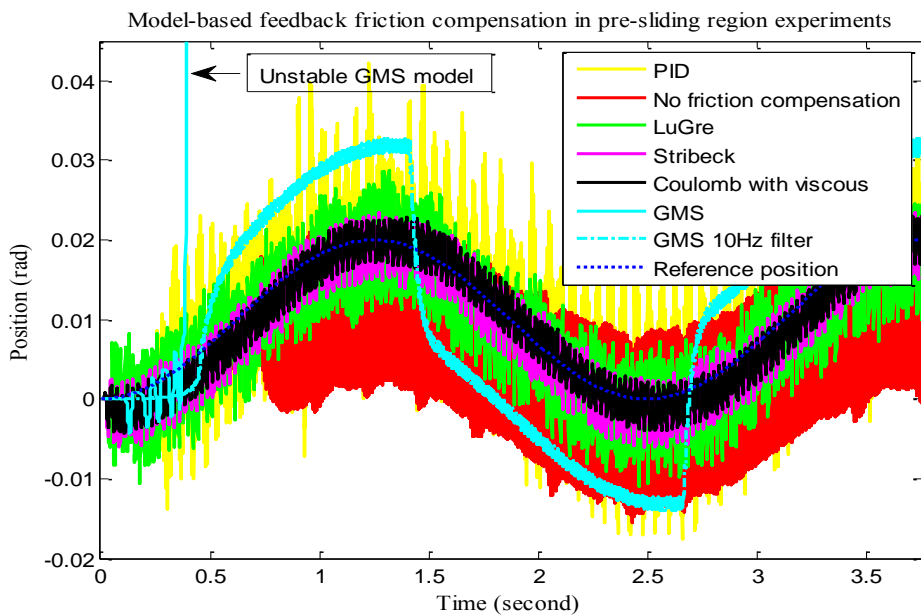

Figure 7.3. Experimental model-based feedback friction compensation of system with grease-added friction in response to the low-velocity sinusoidal position input (PD with 36 Hz bandwidth same as in the simulations)
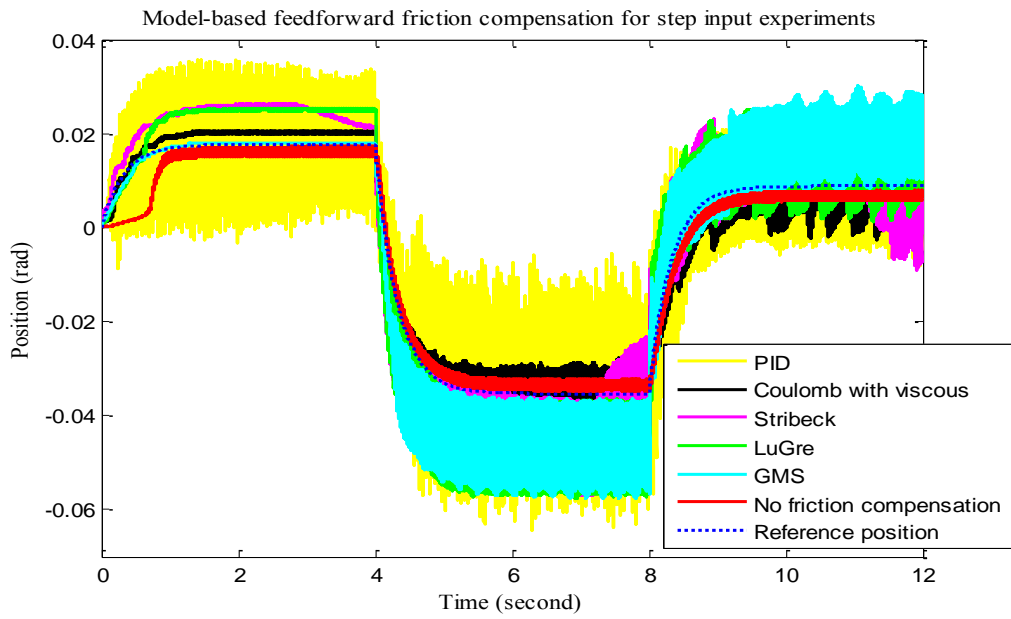
Figure 7.4. Experimental model-based feedforward friction compensation of system with grease-added friction in response to the step position input (PD with 35 Hz bandwidth same as in the simulations)
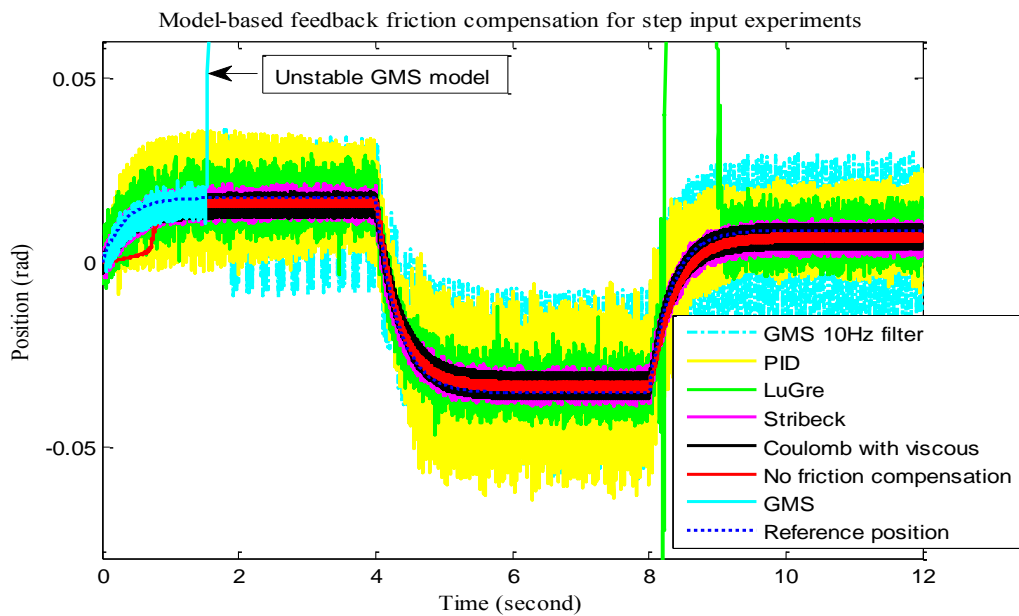

Figure 7.5. Experimental model-based feedback friction compensation of system with grease-added friction in response to the step position input (PD with 35 Hz bandwidth same as in the simulations)